Department of Civil and Environmental Engineering

University of Strathclyde

Colloidal Silica Grout for the Formation of Hydraulic Barriers: An Investigation of the Hydro-Mechanical and Gelling Behaviour

A Thesis presented for the Degree of Doctor of Philosophy

by

Christopher Shi Kiu Wong

August 2021

Glasgow, United Kingdom

Declaration

This thesis is the result of the author's original research. It has been composed by the author and has not been previously submitted for examination which has led to the award of a degree.

Signed: 

Christopher Shi Kiu Wong

Date: 25 August 2021

Publications

Pedrotti, M., Wong, C., El Mountassir, G., Renshaw, J. C. & Lunn, R. J. 2020. Desiccation behaviour of colloidal silica grouted sand: A new material for the creation of near surface hydraulic barriers. Engineering Geology, 270, 105579.

Wong, C., Pedrotti, M., El Mountassir, G. & Lunn, R. J. 2018. A study on the mechanical interaction between soil and colloidal silica gel for ground improvement. Engineering Geology, 243, 84-100.

Pedrotti, M., Wong, C., El Mountassir, G. & Lunn, R. J. 2017. An analytical model for the control of silica grout penetration in natural groundwater systems. Tunnelling and Underground Space Technology, 70, 105-113.

Acknowledgements

My supervisor Dr Gráinne El Mountassir I am sincerely grateful for your guidance, wisdom, and patience. Without your support this work would not be possible.

I would also like to thank Prof. Rebecca J. Lunn and Dr. Matteo Pedrotti your insight and knowledge has been invaluable.

Lastly, I would like to thank my parents and sisters for their continued support.

In Memory of

Jordan Voice

Jack Gow

Contents

Chapter 1. Introduction

1.1. Background

Hazardous waste sources such as heavy metals, chemical substances, gases, asbestos, and radioactive substances situated in the subsurface due to historical urban and industrial activities have contributed to a considerable legacy of contaminated sites both in the UK and worldwide. It is estimate that in England and Wales there is potentially 300,000 ha across 325,000 sites of contaminated land (Environment Agency, 2005). Furthermore, the numbers of potentially contaminated sites may increase from future closures and decommissioning of sites across various industries such as nuclear facilities (NDA, 2016). Contamination and its implications cannot be avoided; thus, remediation of contaminated waste sites and improvements to current technologies can provide global environmental benefits (Rivett et al., 2002).

The Sellafield site located in northwest England is regarded to be one of "the most hazardous places in Europe" (McKie, 2009). With the most hazardous facilities including four legacy ponds, silos that hold large quantities of nuclear material, and stores housing the UK plutonium inventory. The Nuclear Decommissioning Authority (NDA) estimate costs of £121 billion for the completion of decommissioning work at the Sellafield site by 2120 (NAO, 2018). Statutory guidelines by DEFRA (2012) outline the legal obligations to minimise the risk posed to both humans and the environment from land contamination. In addition, specific industrial licence regulators state requirements of redundancy in the case of leakages (i.e. secondary containment systems) (ONR, 2016).

Assessment of contaminated land and appropriate remediation method can be examined by considering three key factors: hazard, pathway, and receptor. The relationship between the three factors is known as pollutant linkage and can be used to determine risks (Angel et al., 2005, DEFRA, 2012). Remediation strategies adopted to minimise or control risks in contaminated land scenario typically comprise three main techniques: hazard reduction (e.g. removal or treatment of the contaminant), pathway modification (e.g containment

barrier prevent contact between receptor and hazard), or receptor control (e.g modify the location or nature of the receptor). However, it is usually very difficult to modify receptor behaviour (i.e. humans/biological receptors). Therefore, remediation technologies generally fall into two categories: (i) hazard reduction and (ii) pathway modification.

Hazard reduction methods include pump and treat, sparging, and venting. These methods can be implemented to remove and treat contaminated groundwater and volatile compounds. However, contaminants may still remain *in situ* sorbed onto soil particles. Permeable reactive barriers may also be used as an engineered treatment zone placed to remediate contaminated groundwater as it flows through utilising the mechanism of sorption, oxidation/reduction, precipitation, fixation, and biodegradation. Several other methods also exist including electro-remediation and phytoremediation treatment, these techniques can typically be applied both in-situ and ex-situ. (Nathanail et al., 2007, DEFRA, 2010, Angel et al., 2005).

A common strategy for pathway modification is excavation and disposal, the main advantage is that it removes the contaminated soils and breaks the contaminant pathway. However, high costs with transporting and handling of waste, in addition to on site restrictions of operational structures or services are driving the development of alternative remediation strategies (SEPA, 2017). Hydraulic containment is another method of pathway modification utilising pumping to lower the water table to isolate contamination. However, the use of pumps to achieve hydraulic containment can be expensive due to the need for long-term intervention and monitoring. Physical containment barriers use low permeability barriers constructed in the subsurface to inhibit contaminant transport by controlling ground water flow (Persoff et al., 1998, Mulligan et al., 2001). For sites, with very large volumes of contamination or contamination beneath remaining buildings containment may be the only practical option. The advantage of physical containment systems is that they can be widely applied to sites with a range of different contaminants.

1.2. Research objectives

The aim of this thesis is to investigate the performance of colloidal silica grout, as a geomaterial for deployment in the construction of hydraulic barriers. To achieve this aim, the objectives of this research were to:

- Determine the soil water retention behaviour of colloidal silica and colloidal silica grouted soils, given that for *in situ* application variations to the water table may result in variable saturation conditions.
- Determine the hydro-mechanical behaviour (1D compression and shearing behaviour) of colloidal silica gel and colloidal silica grouted soils under different curing times and curing conditions using industry standard geotechnical tests.
- Determine the influence of pH, electrolyte concentration and temperature on the gelling behaviour of colloidal silica, in order, to design controllable gel times considering *in-situ* environmental conditions.

1.3. Outline of thesis

This thesis has been organised into the following chapters:

Chapter 2 Review of grout materials and colloidal silica behaviour: presents an overview of grouting techniques and materials, including cementitious and chemical grouts. The previous work investigating colloidal silica, chemistry, structure, and applications are discussed.

Chapter 3 Soil water retention behaviour of colloidal silica grout: presents a brief introduction of unsaturated soil mechanics. Experimental results investigating the unsaturated behaviour of soils specimens mixed with colloidal silica grouted of subjected to drying and wetting cycles.

Chapter 4 Hydromechanical behaviour of colloidal silica grout: presents the compression and shearing behaviour of colloidal silica grout and colloidal silica grouted containing sand and kaolin clay. Additionally, the hydraulic behaviour of colloidal silica and soil & colloidal silica specimens is investigated.

Chapter 5 Gelation behaviour of colloidal silica grout: presents the gel state and gel time behaviour of colloidal silica-based grouts. Factors based on grout composition were investigated considering: accelerator concentration, electrolyte valency, molar mass, and silica concentration. Furthermore, environmental factors influencing grout gelation behaviour of pH, temperature, and the presence of sand and clays were considered.

Chapter 6 Conclusions and recommendations highlights the main findings of this thesis and discusses implications for its deployment in practice and gives recommendations for future work.

1.4. Research contribution

The results of this thesis have been published into a series of papers published in peer-review journals. The papers included in each results chapter are as follows:

Chapter 3

Pedrotti, M., Wong, C., El Mountassir, G., Renshaw, J. C. & Lunn, R. J. 2020. Desiccation behaviour of colloidal silica grouted sand: A new material for the creation of near surface hydraulic barriers. Engineering Geology, 270, 105579.

Chapter 4

Wong, C., Pedrotti, M., El Mountassir, G. & Lunn, R. J. 2018. A study on the mechanical interaction between soil and colloidal silica gel for ground improvement. Engineering Geology, 243, 84-100.

Chapter 5

Pedrotti, M., Wong, C., El Mountassir, G. & Lunn, R. J. 2017. An analytical model for the control of silica grout penetration in natural groundwater systems. Tunnelling and Underground Space Technology, 70, 105-113.

Chapter 2. Review of grout materials and colloidal silica behaviour

This chapter presents an overview of grouting techniques and an overview of literature relating to grouting materials and colloidal silica. Firstly, technologies for creating in-situ ground barriers and current grouting materials are discussed. Secondly, an overview of the behaviour of colloidal silica is presented including its gelling behaviour, hydraulic and mechanical performance and its suitability for deployment in ground engineering applications

2.1. Grouting

2.1.1. Grouting techniques

Grouting is a technique in which a grout fluid is injected under pressure into voids, fissures, crevices or cavities in a soil or rock formation to improve engineering performance. Grouting may be carried out specifically to increase stiffness and strength and or reduce ground permeability (Nonveiller, 1989). Grouting is used in a range of applications in the field of civil engineering including: to reduce the permeability of formations under the foundations of structures to control seepage; to increase the strength of material around underground excavations and structures; to fill voids between rocks and tunnel linings; and groundwater control on contaminated sites. In modern civil engineering, grouting has attracted increasing attention globally and significant advancements have been made in including the development of new grout materials (e.g. chemical grouts, environmental friendly grout mixes, and low viscosity grouts) and new injection systems (e.g. horizontal injection, permeation grouting, and compensation grouting) (Warner, 2004, Granata et al., 2015, Li et al., 2016, Atangana Njock et al., 2018).

Materials injected by the grouting process penetrate void spaces of soils and rocks, later setting or hardening, increasing strength, and lowering the permeability of the soil or rock. Specifications for grouting procedures are outlined in BS EN 12715 (BSI, 2000). Grout penetration depends on several factors including hydraulic conductivity of the ground, porosity and size of pores/fissures, grout viscosity, injection pressure. Figure 2-1 illustrates different grouting techniques used in soils and rocks including jet grouting, compaction grouting, fissure grouting, and permeation grouting.

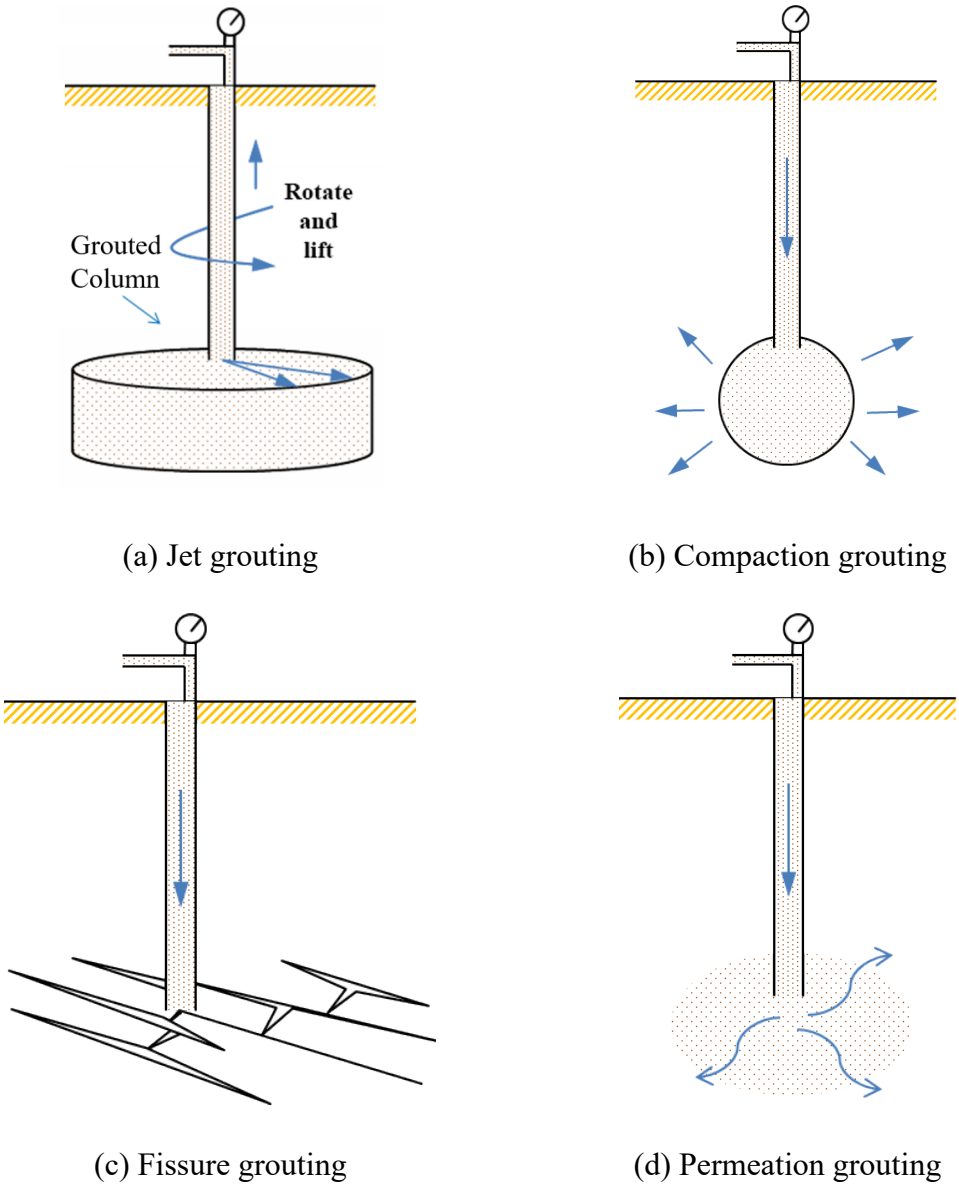

(a) Jet grouting

(b) Compaction grouting

(c) Fissure grouting

(d) Permeation grouting

Figure 2-1 Basic modes of grouting

Jet grouting was conceived in the 1970s and is a grouting technique in which soil and grout are hydraulically mixed *in-situ*. High velocity fluid jets of grout, (also water and air) are pumped into the soil, breaking it up and mixing it simultaneously with the grout to form grouted soil. Jet grouting can be used for a range of applications including supporting the excavation of existing structures, enabling adjacent excavation of deeper structures and groundwater control. Dependant on the in-situ soil conditions the grouted soil erodibility and strength can vary. The injection process is a bottom-up procedure. Attached to the end of a drill stem the grout monitor is flushed to the bottom of the treatment zone. Subsequently, high velocity fluid jets of grout are pumped through the side of the monitor. Whilst the jet grout erodes and mixes the in-situ soil, the drill stem and monitor are rotated and raised (Hussin, 2013). The impact of the jet grouting installation inevitably results in the disturbance of the surrounding ground, that impacts the state of stress and strain in the soils (Wang et al., 2013).

Compaction grouting was first developed in the 1950s as a remedial measure for the amendment of building settlement. Low mobility aggregate grouts are injected into soils creating columns of overlapping grout bulbs in the subsurface by a phased injection process. In granular soils, compaction grouting can be used to increase soil density in a process known as densification. Densification increases the relative density of the treated soil reducing contractive behaviour of soils improving bearing capacity and reducing settlement and liquefaction potential (Spencer et al., 2007, Miller and Roycroft, 2004).

Fissure grouting is typically performed to reduce the hydraulic conductivity of a rock volume by injection of grout into joints and fissures in the rock forming a grout curtain. The process of fissure grouting is the filling or partly filling of fissures in a rock. As part of the grout injection cycle hydraulic factures maybe created to enabled further grout penetration. Fissure grouting is commonly deployed in mining, dam engineering and tunnelling (Rawlings, 2000).

Permeation grouting is a technique in which a grout material is injected to fill soil pores without causing significant movement of the soil. Grouts are initially fluid but harden over time in the soil pore spaces. Permeation grouting is suitable in the formation of permanent or temporary cut-off barriers through the injection of particulate or chemical grouts. In addition to groundwater control, permeation grouting also increases the soil density, providing improved load-bearing capacity of soils, and can be used to stabilise

excavations (Woodward, 2005). Suitability of grouts and grout penetration is dependent on several factors including soil type, pore size and hydraulic conductivity, grout type, grout viscosity, and injection pressure.

2.1.2. Grouting materials

The selection of the appropriate grout material to be injected depends on the application purpose and properties of the treatment area. Bruce et al. (1997) outlined four basic classification categories of grouting materials recognized within the grouting industry. A simple four group distinction was drawn between particulate grouts (Binghamian); colloidal solutions (evolutive Newtonian); pure solutions (non-evolutive solutions), and miscellaneous grouts.

1. Particulate (cementitious) grouts that behave as a Bingham fluid (figure 2-2a and 2-2b).
2. Colloidal solution, evolutive grouts with behaviours related to Newtonian fluids in which viscosity progressively increases with time figure 2-2a and Figure 2-2c.
3. Pure solution, non-evolutive grouts with behaviours related to Newtonian fluids in which viscosity is constant until a controllable setting period (Figure 2-2c).
4. Miscellaneous, materials not otherwise included in categories 1 to 3.

Figure 2-2a shows Bingham and Newtonian fluid behaviour. For a Bingham fluid, a minimum yield stress is required to be exceed in order to induce flow. In a Newtonian fluid, the shear stress, that is the force required to move a fluid is constant, regardless of the shear rate, thus can be described by viscosity (Figure 2-2a). Both viscosity and *apparent* viscosity is commonly used in the description of flow in a Bingham and Newtonian fluid. Viscosity refers to a fluid's resistance to flow being the proportional constant relating the shear resistance in a fluid to the velocity gradient. The term *apparent* viscosity is used because the viscosity of a non-Newtonian fluid will change at different shear rates, thus *apparent* viscosity is defined as the relationship between shear stress at a given shear rate (Warner, 2004). The outlined categories distinguished grout materials by rheological performance reflecting the work of earlier authors, including Cambefort (1977), Association Française des Travaux en (1991), and Karol (2003).

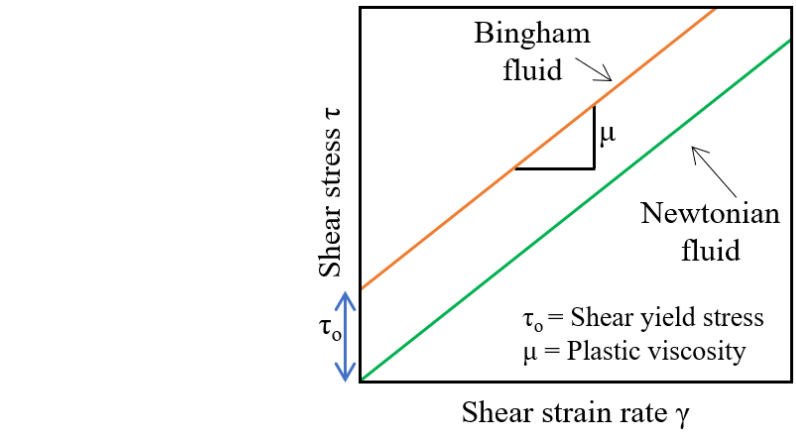

(a) Bingham and Newtonian behaviour

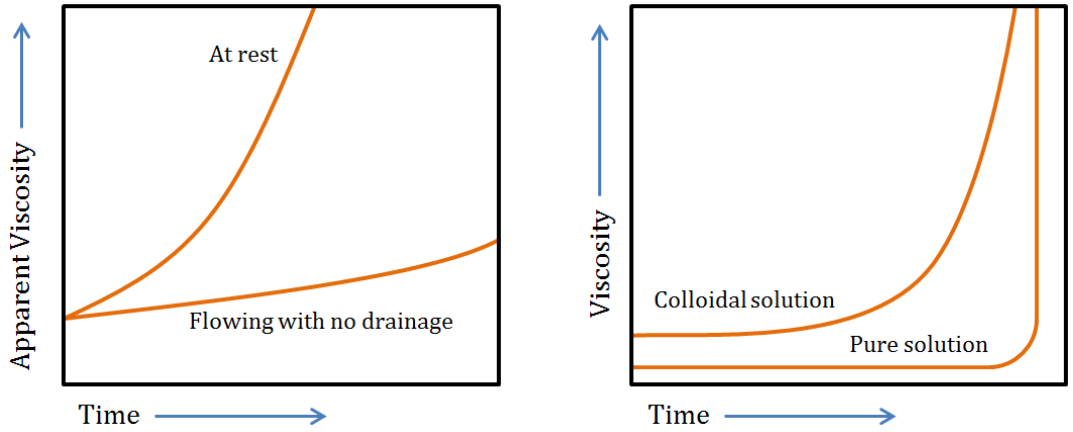

(b) Bingham fluid (c) Newtonian fluid

Figure 2-2 Rheological behaviour of typical grouts (Mongilardi and Tornaghi, 1986)

Figure 2-2a and 2-2b presents the typical rheological behaviour of Bingham fluids (Category 1). This category comprises mixtures of water and cement alongside the addition of other additives and particulate solids such as clay, or sands. The flow of particulate type grouts is dependent on both viscosity and cohesion (Lombardi, 1985, Gallagher, 2000). Grout materials in category 1 have both cohesion and an increase in viscosity with time. Depending on the composition, grouts in this category may either be stable, meaning they exhibit minimal bleeding (separation of water and grout particles) or unstable when left at rest.

Solution type grouts (Categories 2 & 3) generally behave as Newtonian fluids (see Figure 2-2a and 2-2c). Colloidal solutions such as colloidal silica or sodium silicate are evolutive, increasing in viscosity gradually over time (category 2). Pure solutions such as resin as

shown in figure 2-2c are non-evolutive with viscosity remaining constant until just before gelling (category 3).

The rheological property of category 3 grouts together with their low initial viscosity enables permeation into fine soils such as silty sands (k 10^{-5} m/s). Category 4 comprises grouts typically used infrequently and only in specific application requiring special performance characteristics (e.g. Hot bitumens grout for rapid setting for water control; Water-reactive hydrophilic polyurethane grout, and Precipitation grouts) (Bruce et al., 1997, Warner, 2004, Li et al., 2015).

The main practical difference between chemical and particulate grouts is the function of penetrability. For chemical grouts, penetrability is a function of solution viscosity. For particulate grouts the extent of penetration is also dependent on viscosity; however, particle size is the main limiting factor (Karol, 2003, U.S. Army Corp of Engineers, 1995).

2.1.3. Particulate (cementitious) grouts

Particulate cementitious grouts are the most commonly used grout for ground improvement and the creation of hydraulic barriers. The most commonly used particulate grout is Portland cement. Portland cement is a processed mixture of mineral solids pulverized, fired, and ground into a fine solid dust. Typically the grain size of cement grouts are: Portland cement grouts (d_{95} < 128 μm), Microfine cements (d_{95} < 20 μm), and Ultrafine cements (d_{95} < 12 μm) (Zebovitz et al., 1989, Truex et al., 2011). Cementitious grouts behave as Bingham fluids, consequently, the yield strength of the material must be overcome before it starts to flow; however, flow stops if the shear stress applied is lower than the material yield stress (Funehag and Gustafson, 2008). Due to the required high injection pressures, cement grouts are not typically injected in the first 10 m below ground, due to the potential for ground heave.

In cement grout as noted by Tomiolo (1982) stability refers to the capacity of a grout to maintain its characteristics during the grouting process without increasing density or sedimentation. Under the action of gravity, suspended particles may settle resulting in grout bleeding (separation of water from the grout). For a stable cement grout, minimal sedimentation due to gravity occurs. However, unstable cement grout mixtures readily form flocs or pressure filtrate leading to anisotropic characteristics in grouted soils. As such, it is possible for grouted areas to consist of high residual permeability in the

horizontal direction and low residual permeability in the vertical direction arise (Helal and Krizek, 1992).

2.1.4. Chemical grouts

Chemical grouts were developed to overcome the particle size limitations of conventional Portland cement grouts to grout soils with finer grain size distributions. The most widely used chemical grouts are sodium silicates or resin based stable aqueous solutions with low viscosities similar to water. As such these grouts can be injected at lower injection pressures than cement based grouts (Gallagher et al., 2013). As a result, chemical grouts do not have the same potential to create ground heave and therefore have the significant benefit that they can be applied in near surface soils. Chemical grouts initially behave as fluids (with low viscosity) and after a predetermined time, the chemical grouts react to form a solid.

2.1.5. Grout penetrability

Shown in figure 2-3 is the penetrability of various grouts including cement, chemical, resin in relation to soil grain size (Karol, 2003). The penetrability of grouts in rock fissure is principally dependent on particle size; whereas, the ability of a grout to permeate in soil is influenced by both particle size and grout rheology.

Cement rheology can be controlled by variations to the water/cement ratio and addition of additives, e.g. superplasticisers. Lombardi (1985) noted that cohesion largely controls the maximum distance a cement grout can penetrate, whilst viscosity governs the flow rate and injection time required. Traditional Portland cement can be used to grout gravel; however, the particle size of Portland cement restricts its use in sands. Ordinary Portland cement grouts are considered to be ineffective for permeation grouting of medium and fine-grained sands, along with soils with significant fine content due to jamming/packing of cement particles at pore throats (Zebovitz et al., 1989).

Chemical grouts can be used to grout fine and medium sands as well as silts (Maher et al., 1994). Conservatively, in terms of permeability, grouts with viscosity less than 2 cP such as polyacrylamides can typically be pumped into soils with permeabilities $\geq 10^{-4}$ cm/s. All grouts typically have difficulty penetrating unfractured soils with a silt fraction exceeding 20% of the total (Karol, 2003).

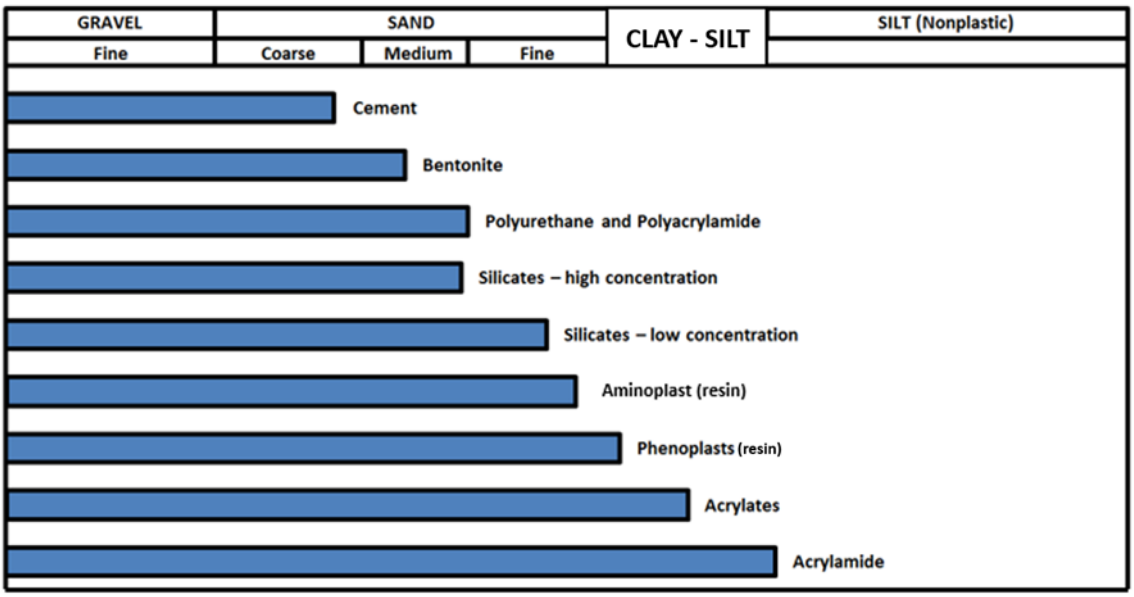

Figure 2-3 Penetrability of various grouts (Karol, 2003).

2.1.6. Material selection

When determining the type of grout to use for a particular application there are chemical and mechanical behaviours that require evaluation. Common grout parameters that are used for a basis to determine suitability are viscosity, durability, strength, safety, availability, and cost (U.S. Army Corp of Engineers, 1995). The consideration of viscosity has been previous discussed in section 2.1.2. Durability is the ability of grouts to withstand exposure in-situ over time to hostile conditions without impacting the engineering behaviour of the grout (i.e. strength or permeability). Exposure to hostile conditions may arise because of variable environmental conditions such as cycles of wetting and drying or freezing and thawing. Grouted soils must provide sufficient strength to meet their intended function. The placement of grouts may occur below the water table. Consequently, the strength of the saturated grouted material may be lower than that of a dry specimen. Safety related concerns of toxic or hazardous grouting materials include both potential environmental impacts and the potential of hazardous exposure for workforces involved. Safety issues can influence application and material handling procedures. Material availability can vary dependant on geographical location of the site, technological developments, and regulatory changes. For a given application grout availability must be sufficient to fulfil the intended purpose. Lastly, costs consideration for grout selection in addition to the material cost include other factors such as labour and equipment (U.S. Army Corp of Engineers, 1995, Hemphill, 2012).

Table 2-1 provides a general outline of grout properties and various factors of consideration. Traditional cementitious grouts are the least expensive option and there is hundreds of years of experience of their application in industry in a range of different contexts. However, cementitious grouts require high injection pressures due to their cohesion and high viscosity, limiting their application near-surface due to ground disturbance generation. Furthermore, their large particle size generally inhibits penetration into pore spaces of <50 μm (Karol, 2003). Chemical grouts, on the other hand, can penetrate smaller pore spaces and have a much lower viscosity than cement grouts. Conversely, however, they can be expensive, and potentially toxic due to complex chemistries of the material practice. As such, apprehensions from limited material experience and understanding has hindered the uptake of chemical grouts in practice.

Table 2-1 Ranking of grout properties (U.S. Army Corp of Engineers, 1995, Gallagher, 2000)

Type	Penetration in Grouted Units	Durability	Ease of Application	Potential Toxicity	Flammability of Materials	Relative Costs
Cement-based grouts	L	H	M	L	N	L
Silicates	H	M	H	L	N	L
Acrylates	H	M	H	M	L	H
Lignins	H	M	H	H	L	H
Urethanes	M	H	M	H	H	H
Resins	L	H	M	H	M	H
Colloidal Silica	H	M	H	L	N	M

N = non-flammable; L = low; M = moderate; H = high

Colloidal silica is a silica-based chemical grout with several favourable characteristics over other grouting materials. In contrast to other chemical materials, silica-based grouts provide favourable penetration, durability and could be easily applied for the construction

of hydraulic ground barriers with low toxicity concerns. For ground barrier applications colloidal silica is an attractive material as it has a low viscosity enabling the material to easily penetrate pore spaces in fine-grained soils (Yossapol and Meegoda, 2001, Whang, 1995).

2.2. Colloidal silica

Colloidal silica has been used in a range of industrial applications including catalyst production, ceramic glazing agent, coating materials, textiles, and paper treatment since the 1940s (Bird, 1941). Successive improvements in the production process of stable colloidal silica at higher concentrations in the 1970s greatly increased commercial availability and usage (Bergna and Roberts, 2005).

Colloidal silica, also known as silica sol, is a stable aqueous suspension of silica (SiO_2) nanoparticles in a liquid typically water. If the liquid is water, the dispersion is identified as an aquasol or hydrosol (Iler, 1979). The appearance of colloidal silica can vary from optically transparent to opalescent depending on the particle size and concentration of silica particles. Dilute solutions of colloidal silica are similar in density and viscosity to water. Commercial solutions are available with concentrations in the range of 15 – 40% silica (weight percentage). Colloidal silica is produced by the polymerization of silicic acid to form silica monomers by the formation of siloxane (Si-O-Si) bonds (Iler, 1979). The repeated accretion of molecules by this mechanism enables the formation of controllable uniform particle sizes. Particles are approximately spherical, uniform in size, can have particle sizes ranging from 2nm to 150nm (Persoff et al., 1999, Karol, 2003). Particles within colloidal silica solutions are sufficiently small (≤1μm) to not to be affected by gravitational forces (i.e. they do not settle out of suspension) but are sufficiently large (>1nm) to exhibit behaviour distinct from the properties of a true solution.

Colloidal silica exists as a stable low viscosity solution; the addition of a salt solution can destabilize colloidal silica to form a solid gel. A salt solution added to trigger gelling of the colloidal silica is also referred to as ‘an accelerator’. Figure 2-4 shows the viscosity behaviour of destabilized colloidal silica including two phases: an initial low viscosity phase known as the ‘induction period’ prior to the gel time, followed by a rapid increase in viscosity known as gelation until the formation of a rigid solid gel (Hunt et al., 2013).

The gel time is defined as the intersection of the tangents to the two straight line portions of the viscosity & time plot (Allison et al., 1986). The induction period and gel time of colloidal silica can be controlled either by altering the silica solution (i.e. particle size, silica concentration) or accelerator solution (i.e. concentration, or cation).

Gel times of colloidal silica can range from minutes to several months (Persoff et al., 1999, Gallagher et al., 2007b). This is of considerable interest for its application in ground engineering, where long gel times could ensure adequate grout penetration within a soil volume prior to gelling occurring. The initial low viscosity provides a grout which is relatively easy to inject (similar to injection of water) using low injection pressures. Furthermore, colloidal silica is nontoxic, biologically and chemically inert. Thus the solution will remain stable in a range of operating environments and there are minimal safety concerns associated with its use (Northcroft, 2006, Chang et al., 1994, Whang, 1995, Jurinak and Summers, 1991).

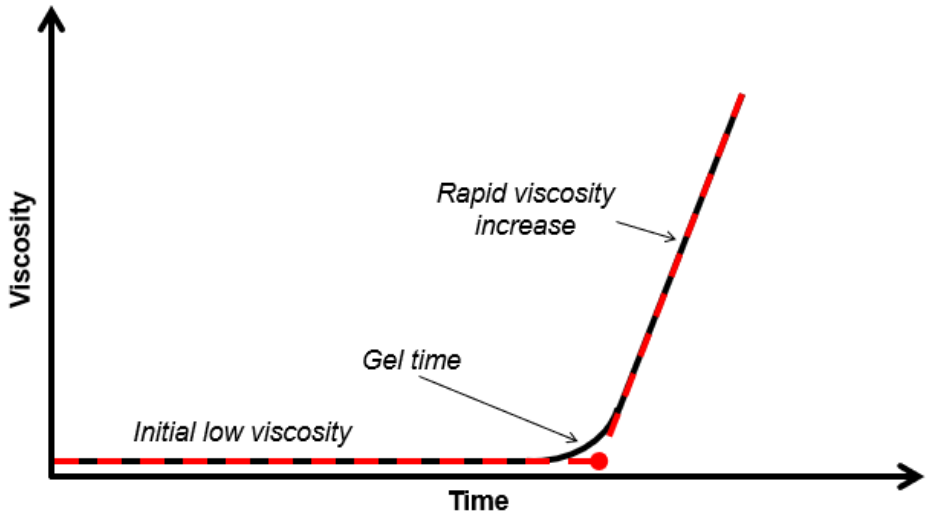

Figure 2-4 Viscosity behaviour of colloidal silica and gel time

2.2.1. Chemistry and structure of colloidal silica

Colloidal silica is made up of particles consisting of silicon atoms covalently bonded to four oxygen atoms in a tetrahedral arrangement. A two-dimensional representation of a single colloidal silica particle with both siloxane (Si-O-Si) and silanol (Si-O-H) groups, formed with oxygen or hydrogen respectively, is shown in figure 2-5; the fourth bonded oxygen atom to the silicon atoms are either above or below the plane presented in the figure. Uncombined Si-OH groups remain on the particle surface. On gelling siloxane bonds (Si-O-Si) form between particles to form a porous network (a gel) (Yossapol, 2002,

Bergna and Roberts, 2005), see figure 2-5. The simplified chemical reaction for the formation of a siloxane bond is:

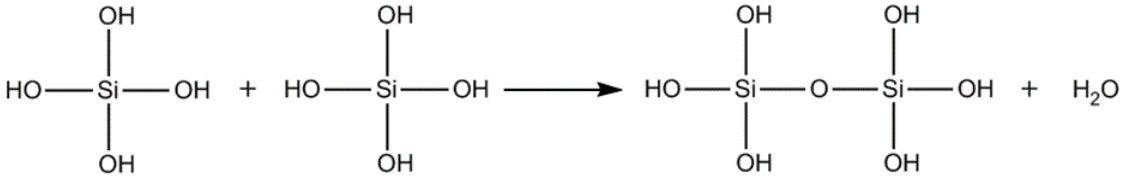

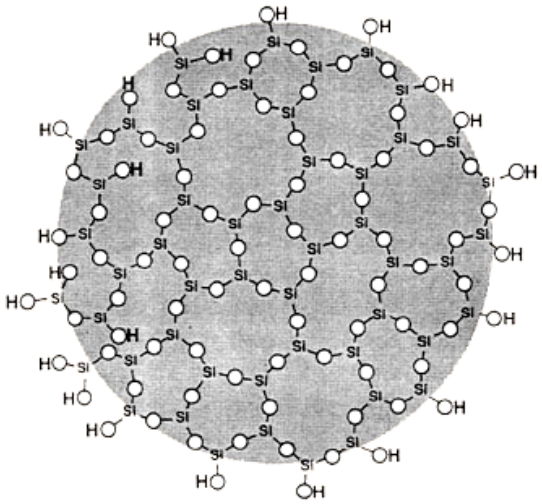

Figure 2-5 Two-dimensional representation of a dehydrated and hydroxylated colloidal silica particle (Bergna and Roberts, 2005).

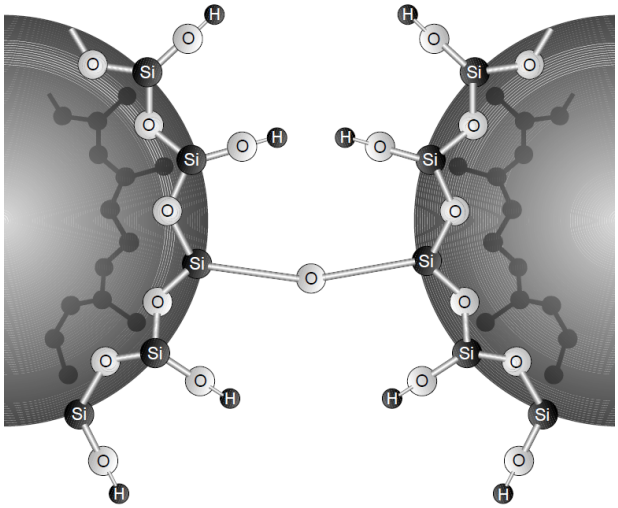

Figure 2-6 Formation of siloxane bonds as a colloidal silica particle gel (Moridis et al., 1995b).

2.2.2. Mechanism of gelling

The term aggregate is used in colloidal science to describe all the mechanisms of colloidal silica structures formed by the cohesion of colloidal particles (Bergna and Roberts, 2005). The primary mechanisms of aggregation differentiated by Iler (1979) are gelling,

coagulation, and flocculation (see figure 2-7). In gelling or gelation, the particles link together in branched chains to form a three-dimensional network filling the original volume of the sol. There is no increase in the concentration in any macroscopic region of the solution during gelling. Instead, the overall solution becomes viscous and then develops rigidity. In coagulation, particles come together linking to one another forming relatively close-packed clumps. The coagulum being more concentrated than the solution settles as a relatively dense precipitate. In flocculation, particles are linked together by bridges of the flocculation agent to form aggregates with a relatively open structure. In solutions with a high concentration of silica particles (as used in this thesis) it is not possible to differentiate between coagulation and flocculation. This thesis focuses on the formation of a gel from colloidal silica and its resulting hydraulic and mechanical behaviour and that of colloidal silica grouted soils.

The basic mechanisms in gel formation outlined by Iler (1979) considers the collision of two silica particles and the subsequent formation of siloxane bonds to bond the particles together irreversibly (see Figure 2-8). In order for two silica particles to collide they must have a sufficiently low surface charge to allow them to come into contact. Once a collision has occurred siloxane bonds can form, their formation is catalysed by the presence of OH^- (hydroxyl) ions. At the point where the two spherical particles come into contact, there is a negative radius of curvature, where the solubility of silica is zero. At this point, monomers of silica are instantly deposited, with the result that the particle grows in size (Iler, 1979).

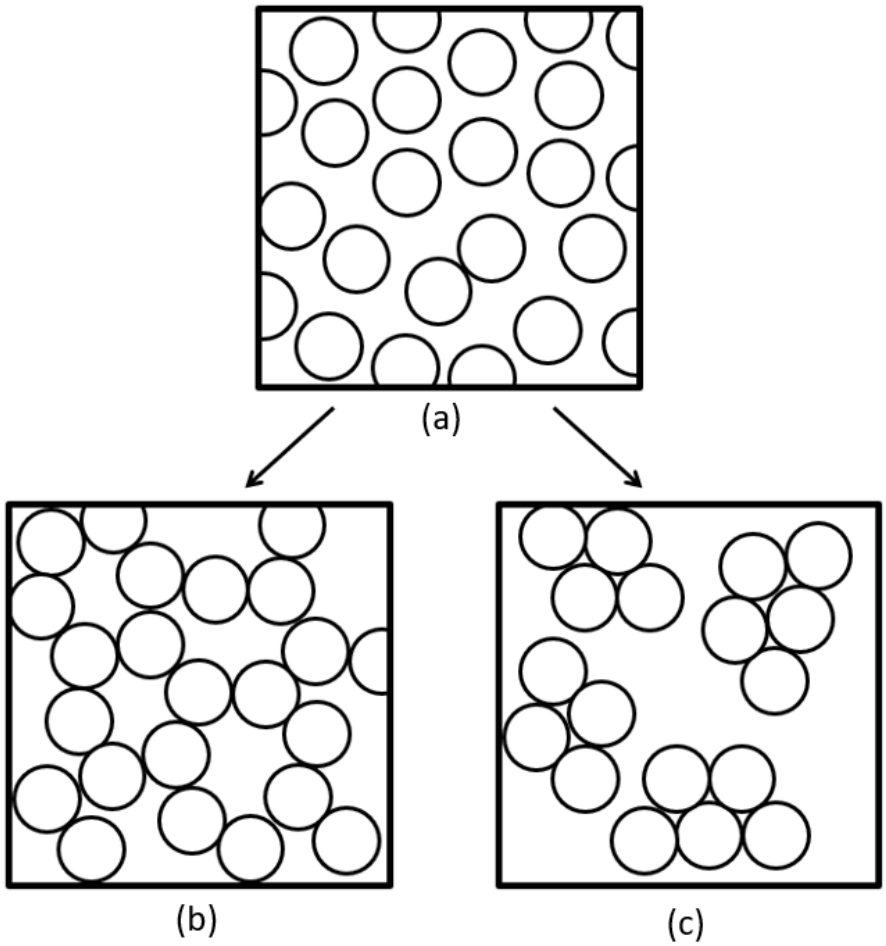

Figure 2-7 (a) Silica sol; (b) gel and (c) coagulation and flocculation (Iler, 1979)

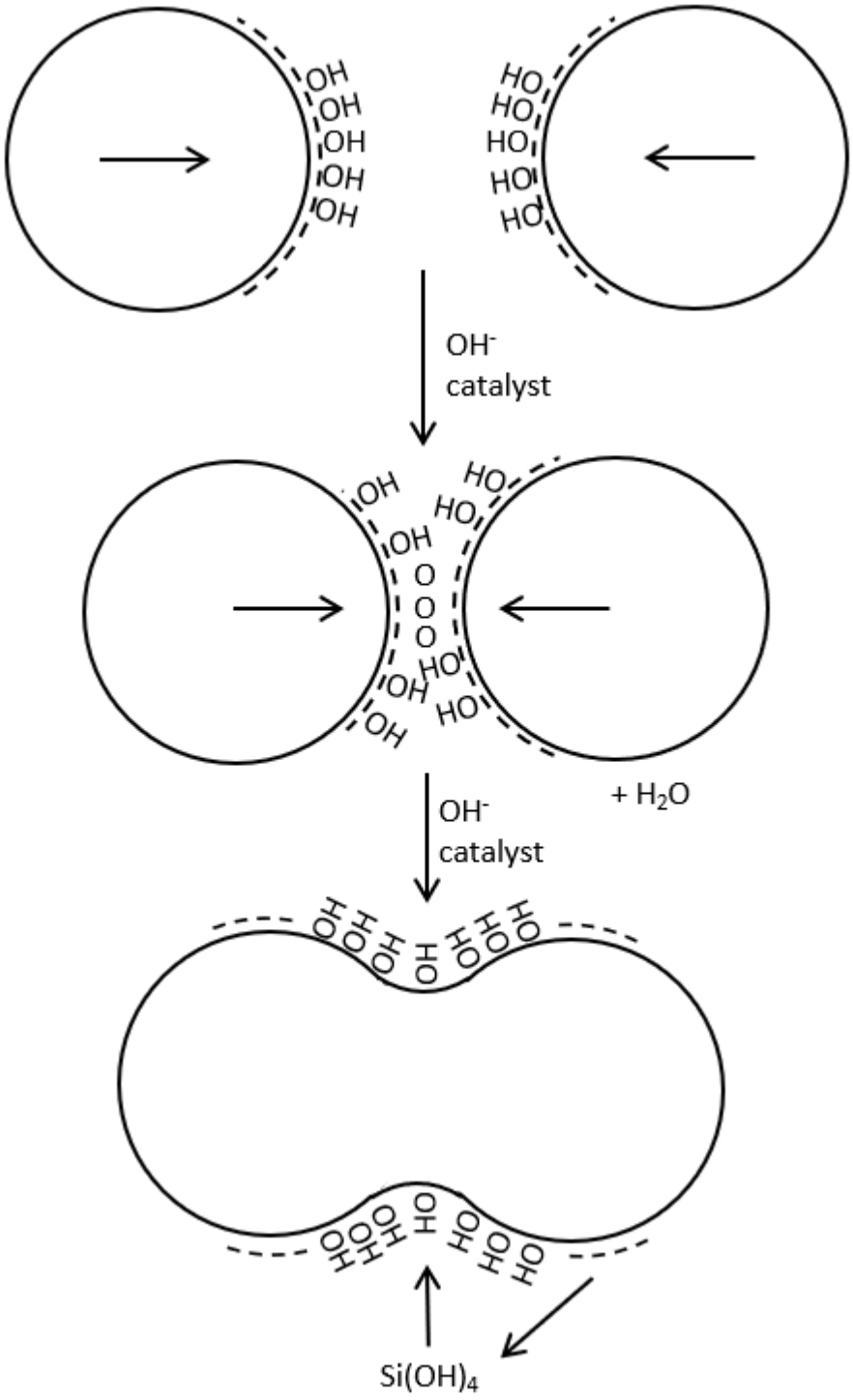

Figure 2-8 Collision and siloxane bond formation between two silica particles (Iler, 1979).

Both the rate of collisions and rate of siloxane bond formation are influenced by pH. Figure 2-9 shows the effect of pH on the gel time of colloidal silica as outlined by Iler (1979). Particle collisions are controlled by the net negative electrical charge of the silica particles. The isoelectric point of silica is close to 2, this is the point at which the particles exhibit no net electrical charge (Trompette and Clifton (2004). Above pH = 2 the particles are negatively charged and increasing the pH increases the negative electrical charge of the particles and this increases repulsion between particles therefore reducing the frequency of collisions.

As mentioned the presence of OH^- ions acts as a catalyst in the formation of the siloxane bonds. Increasing the pH increases the concentration of OH^- ions present. The higher the concentration of OH^- ions the higher the likelihood that the particles which come into contact will form siloxane bonds (i.e. polymerize). In the pH range between 3 to 5; the rate of gel formation increase is proportional to the hydroxyl ion concentration (Jurinak and Summers, 1991). Above pH 6, hydroxyl ions are available in abundance and are no longer the limiting factor for the rate of gelling. However, the rate of gelling decreases due to fewer collisions between particles because of their increasing particle charge (Iler, 1979, Risö, 2011). The range of pH with minimum gel times was approximated by Gallagher (2000) to occur in the range of pH of 5 to 7, with a distinctive increase in gel times outside of this range.

Figure 2-10 shows the increase in viscosity with time as the colloidal silica suspension undergoes gelling. This increase in viscosity can be attributed to the formation of initially short chains of microgel, these become progressively more branched and longer in size. As the fraction of microgel reaches approximately 0.5 of the total volume, the viscosity rises rapidly, this is considered to be responsible for the sharp change in viscosity at the gel time (see Figure 2-10) (Iler, 1979).

Persoff et al. (1999) developed a chart of gel state descriptions for colloidal silica from the work of Sydansk (1990) based upon visible qualitative changes that occur during the gelling process (see table 2-2).

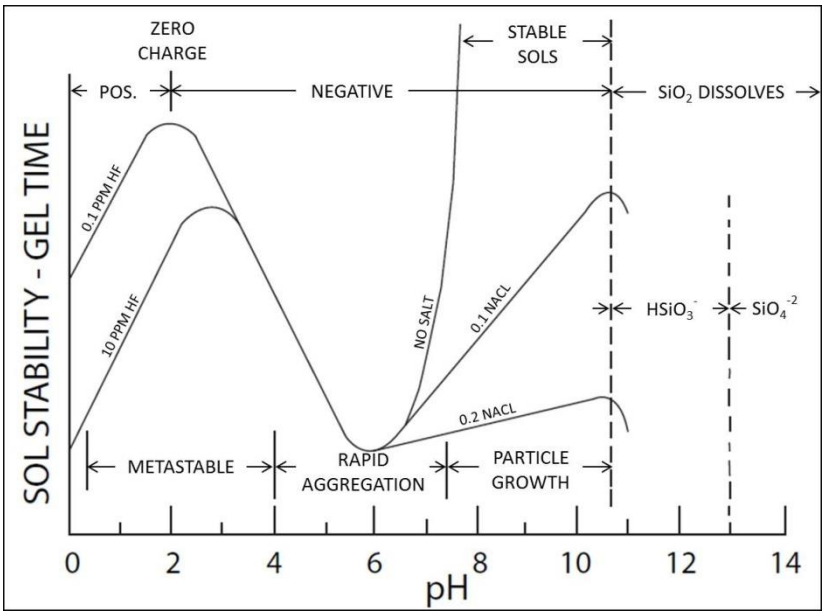

Figure 2-9 Effects of pH in colloidal silica-water system (after Iler, 1979)

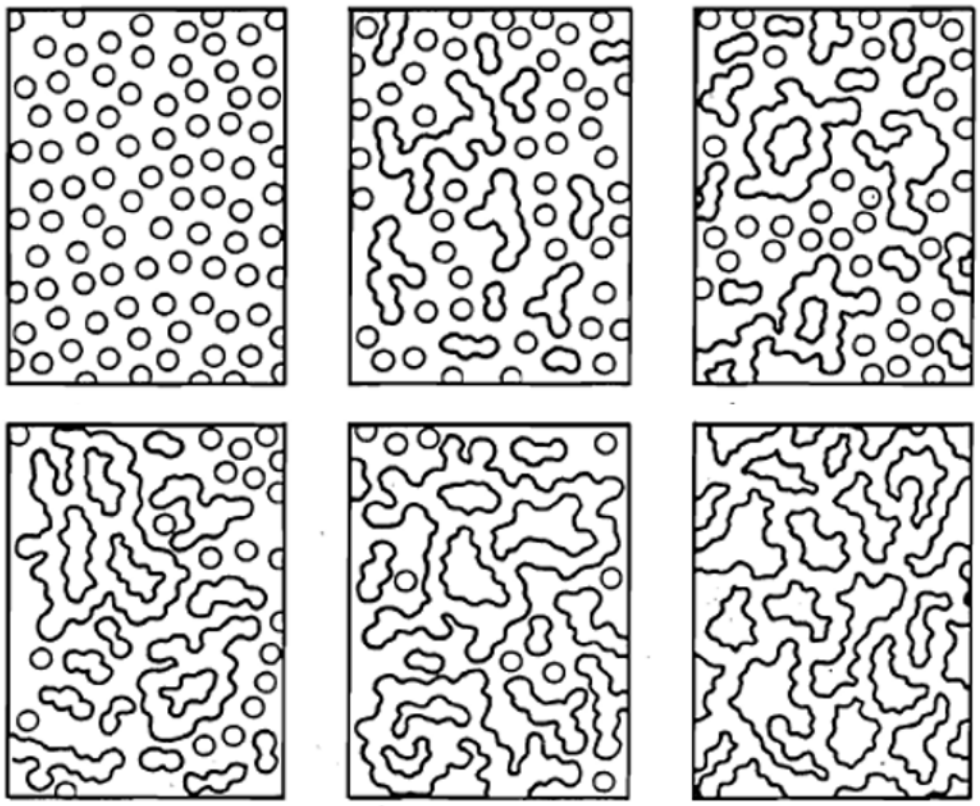

Figure 2-10 Microscopic bonding of colloidal silica particles for increasing viscosity (Iler, 1979).

Table 2-2 Jar test gel states (Persoff et al., 1999).

State	Gel state descriptions
1	No detectable gel formed. Gel appears to have same viscosity as original solution.
2	Highly flowing gel. Gel appears only slightly more viscous than original polymer.
3	Flowing gel.
4	Moderately flowing gel.
5	Barely flowing gel.
6	Highly deformable non-flowing gel.
7	Moderately deformable non-flowing gel.
8	Slightly deformable non-flowing gel.
9	Rigid gel.
10	Rigid ringing gel. Tuning-fork-like mechanical vibration can be felt.

2.2.3. Gel time control

The ability to modify and control the gel time of a grout can be critical to the success of a project (Karol, 2003). The gelation rate, and gel time can be controlled by varying factors that influence the processes of particle collisions and bond formation (Iler, 1979, Bergna and Roberts, 2005). Gelling is dependent on several factors including pH (as discussed above), silica particle size, silica concentration, temperature, and electrolyte (Conlee, 2010). For grouting applications, the most practical method to controlling gel times is to vary the electrolyte (concentration or type) added as the accelerator.

The addition of an electrolyte solution to a colloidal silica suspension increases the probability of particle-to-particle collisions occurring, reducing the overall gel time (Jurinak and Summers, 1991, Yossapol, 2002). This is in line with classical DLVO theory as developed by Derjaguin and Lanadau (1941) and Verwey and Overbeek (1948) which predicts the behaviour of colloidal suspensions based on the interaction of charged particle surfaces. The DLVO theory describes particle interactions within colloidal dispersions as a superposition of repulsive double-layer forces and an attractive dispersion (van der Waals) force. The electro-static diffuse double-layer repulsion between particles (in the case of silica where pH > 2) negatively charged can be counteracted by attractive Van der Waals forces. This can be achieved by the introduction of an electrolyte solution (an accelerator e.g. salt solution), which will dissociate into

positively charged cations and negatively charged anions, this acts to compress the electro-static diffuse double layer around the colloidal silica particles allowing the particles to approach more closely, hence increasing the frequency of collisions.

Increasing the electrolyte concentration increases the rate of collisions, resulting in a reduced gel time in line with diffuse double-layer theory. Consequently, factors that change ionic strength for example cation valency can also influence gel time. Divalent cations such as calcium have a greater effect on compressing the diffuse double layer around colloidal silica particles than monovalent cations (e.g. sodium); thus, divalent cations have a greater effect on gelation kinetics than monovalent cations. Increases to the electrolyte concentration reduce gel times up to a point. However, at very high electrolyte concentrations gels do not form, but destabilization results in a flocculated precipitate (Hunt et al., 2013). The nature of the cation in the electrolyte solution has also been shown to influence gelling behaviour independently of valency and electrolyte concentration (Trompette and Clifton, 2004; MacLachlan et al., 2013).

Although DLVO theory generally provides a good basis for the prediction of stability of colloidal suspensions (Iler, 1979, Bergna and Roberts, 2005, Baldyga et al., 2012). the stability of silica particles has been repeatedly reported to exhibit a more complex behaviour than can be explained by DLVO theory alone (Iler, 1979, Yotsumoto and Yoon, 1993). At relatively short distances (less than 10 nm), silica surfaces show large repulsive forces in aqueous solutions not predicted by DLVO theory. As a result, colloidal silica exhibits higher stability at low pH. Conversely, at high pH colloidal silica exhibits a lower stability than predicted by DLVO (Allen and Matijević, 1969). Several hypotheses have emerged to account for non-DLVO short-range repulsions arising from the presence of a gel layer (Adler et al., 2001, Kobayashi et al., 2005)

The influence of temperature on gelling is due to the kinetic phenomenon involved during aggregation, increasing the temperature increases the energy of the particles, thus increasing the frequency of collisions. As a result the influence of temperature on the rate of gelling follows an Arrhenius relationship (Hunt et al., 2013). However, it is not usually practical to control the temperature of the ground or the fluids being injected during a grouting campaign.

The influence of silica particle size and silica concentration are interrelated. The rate of gelling is proportional to the total surface area of silica for a given volume. Therefore,

increasing the silica concentration reduces gel times (Bergna and Roberts, 2005). Reducing the silica particle diameter also reduces gel times due to increasing surface area. As the specific surface area of silica is equal to the surface area /unit volume this means it is inversely proportional to the particle diameter. Therefore, for the same ratio of silica concentration to particle diameter gel times are similar (Beavers et al., 2014). In practice the commercial colloidal silica suspension used will dictate the silica particle size and the silica concentration may be varied only by diluting the colloidal suspension, thereby increasing gel times, however this will also have implications for the grout strength.

Colloidal silica solutions are stabilized during manufacturing to prevent gelling during storage and transport, either by raising the pH or by isomorphous substitution of alumina for silica on the particle surface (Conlee, 2010, Persoff et al., 1998). Adjustments of the suspension pH will change the particle surface charge; the higher the pH the more negatively charged the surface, as such the colloidal silica particles are sufficiently ionized so as to repel each other so they do not come into contact (Iler, 1979, Grace, 2007, Persoff et al., 1999).

2.3. Applications of colloidal silica

2.3.1. Petroleum industry

As an injectable fluid, the use of colloidal silica originated to divert, direct, and control fluid flow through porous media in the petroleum industry for enhanced oil recovery in the late 1980s. Colloidal silica has been injected to modify fluid flow in permeable strata and also to repair leaking well casings with limited success (Jurinak and Summers, 1991). Only one of four injection profile treatments was a success, 3 out of 4 casing repairs were successful (at least for a period of 6months) (Jurinak and Summers, 1991). One drawback highlighted was the need to use freshwater to make up the colloidal silica grout mixture (i.e. for the accelerator component) as using sea water would result in different gel times due to the existing presence of ions (Yonekura and Kaga, 1992, Jurinak and Summers, 1991).

2.3.2. Contaminated land applications

Noll et al. (1992) first demonstrated the application of colloidal silica grout for reducing permeability and contaminant immobilisation for contaminated land sites. They reported a 3 to 4 order of magnitude reduction in hydraulic conductivity for sand specimens treated

with 5% colloidal silica grout down to values in the range of 10^{-9} to 10^{-10} m/s. In addition, silica gel was found to adsorb metals from solutions, with 30% reduction of leaching of heavy metals measured from the effluent of colloidal silica treated samples than untreated samples.

Researchers at Lawrence Berkeley National Laboratory proposed the formation of subsurface barriers using viscous liquids including colloidal silica grout (Finsterle et al., 1994, Persoff et al., 1995, Apps et al., 1998). In this body of work an early concern has been the influence of soil (and in particular clay) on gelling behaviour and thus gel penetration. Moridis et al (1993) demonstrated almost immediate gelling of colloidal silica in contact with Hanford sand. Hanford is a nuclear site located in Washington in the US which is now mostly decommissioned. Moridis et al. (1995a) observed following the excavation of a field injection area that fairly uniform colloidal silica grout plumes were formed despite the soil heterogeneity, indicating that potential issues of preferential flow pathways (such as a gravel bed overlying a tight silty or clayey zone) could be overcome. In-situ permeation grouting using colloidal silica to develop a subsurface barrier was investigated at the Brookhaven National Laboratory (Moridis et al., 1999). In this field trial a barrier was constructed to prevent migration of tritium and ^{22}Na off-site which had leaked previously from the facility. The barrier was achieved by close-spacing (overlapping) bulbs of colloidal silica-grouted soils. In-situ hydraulic conductivity measurements of the barrier were in the range of 10^{-5} to 10^{-9} m/s (Moridis et al., 1999). This wide range of hydraulic conductivity was thought to be due to soil anisotropy and limited injection of colloidal silica volumes resulting in poor overlapping of bulbs.

Truex et al., (2011) in a review of grouting options for the Hanford site recommended the use of colloidal silica. However, to the author's best knowledge it has not yet been applied on the site, this is likely due to concern over grout emplacement in a heterogenous subsurface environment and difficulties in monitoring grout penetration subsurface (Truex et al., 2011).

Durmusoglu and Yavuz Corapcioglu (2000) demonstrated in laboratory experiments the formation of continuous horizontal barriers created using colloidal silica either by vertical or horizontal injection. However, these methods again relied on the overlapping of closely-spaced bulbs (injected either vertically or horizontally) of grouted soil. Given that gel times of colloidal silica can be as long as months, it is possible that greater penetration

of colloidal silica prior to gelling could be utilised in grouting campaigns, particularly in the creation of horizontal barriers, that do not rely on overlapping small bulbs (or small diameter columns) of silica grouted soils.

Persoff et al. (1995) studied the effect of Hanford soil on grout gel state (see Table 2-2). Results from tests conducted using colloidal silica in the absence and presence of soil are shown in figure 2-11. Premature gelation and decreased gel times were observed in all specimens where soil was present. Likewise, Durmusoglu and Yavuz Corapcioglu (2000) performed batch experiments and found that the gel time of the colloidal silica when passed through Vulcan sand decreased by a third. In both studies, the presence of divalent cations of calcium and magnesium adsorbed onto the soils increased the ionic strength and charge density of the colloidal silica solution. Thus, the electro-static diffuse double layer surrounding the colloidal silica particles becomes more compressed facilitating premature gelation by enabling colloids to approach each other more readily to form siloxane bonds (as discussed in section 2.2.3). Pre-flushing and soil rinsing with dilute sodium chloride (4% NaCl) solutions prior to injection prevented premature gelling by eliminating in-situ divalent cations in alkaline colloidal silica (Persoff et al., 1995).

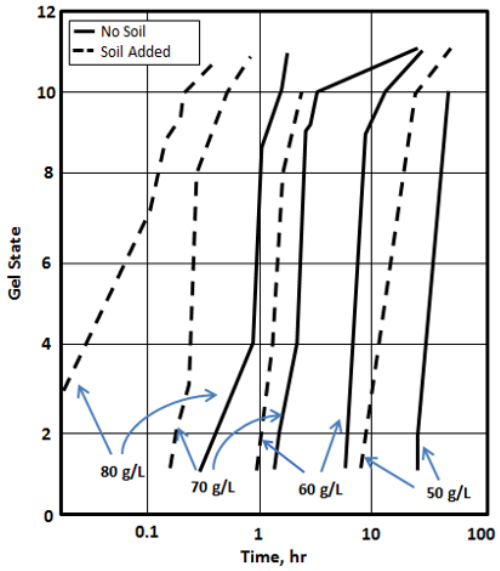

Figure 2-11 Gel states of colloidal silica with and without soil present (Persoff et al., 1995).

2.3.3. Liquefaction mitigation

Colloidal silica grouting into loose sands for liquefaction mitigation was first investigated by Gallagher (2000). In a technique called passive site remediation, colloidal silica grout was proposed as a potential stabilizer for binding sand grains because it has long controllable gel times and low viscosity. In these studies, the principal objective was to make use of groundwater flow to transport colloidal silica into soil layers to reduce their liquefaction potential. In this approach, mostly low concentration colloidal silica is adopted to allow grouts to penetrate greater distances before gelling. Gallagher and Mitchell (2002) showed that treating loose sands with a 5% colloidal silica grout increased deformation resistance to cyclic loading compared to the untreated sand specimens. Higher concentration of colloidal silica treatment further reduced strain development. Field injection trials conducted by Gallagher et al. (2007a) demonstrated that colloidal silica treatment in sands showed settlement reduction. Hamderi and Gallagher (2015) developed a 10m^3 pilot scale box model to examine the injection of dilute colloidal silica in loose sand. One challenge highlighted was the delivery of grout over the distance required without sinking of the colloidal silica. Injection rates in the pilot scale box model between 1900 and 7600 ml/min/well were identified to enable sufficient delivery. The feasibility of passive site remediation techniques using colloidal silica were shown to provide improved mechanical behaviour by stabilizing formations of loose sand to mitigate liquefaction (Gallagher and Mitchell, 2002, Gallagher et al., 2007a, Conlee et al., 2012).

2.3.4. Rock fracture grouting

For hard rock tunnelling the use of colloidal silica grout material has been proposed by several researchers (Funehag and Axelsson, 2003, Butrón et al., 2009, Hernqvist et al., 2012). Colloidal silica grout was considered favourable due to its the ability to penetrate and seal fractures where cement cannot, and its non-hazardous nature fulfilling the requirement in the application for High Level waste repository for nuclear waste (Tsuji et al., 2014). Field studies at the Äspö Hard Rock Laboratory Sweden conducted by Funehag and Fransson (2006) successfully used colloidal silica to penetrate over one metre distance into a rock fracture with a hydraulic aperture in the range of 40-50 μm. Hydraulic tests prior to grouting ranged in transmissivity of 1.2×10^{-8} to 1.5×10^{-9} m^2/s, after grouting with colloidal silica reduced transmissivity were 1.3×10^{-8} to 5.2×10^{-10} m^2/s (Funehag and Fransson, 2006). Similar field studies were conducted in Onkalo, Finland by Hollmen et al. (2013) and Kurashiki, Japan by Kobayashi et al. (2014) demonstrating colloidal silica grout injection in narrow fractured zones. Kobayashi et al. (2014) further examined the chemical stability of colloidal silica grout. Results compared the dissolution rates of silica in the grout arising from the interaction with local groundwater and deionised water. Concluding findings suggested that the local groundwater did not have an influence on the chemical stability of the hardened colloidal silica grout.

Funehag and Gustafson (2008) examined the main parameters controlling colloidal silica grouting at depth in rock fractures. Funehag and Gustafson (2008) developed analytical models for the prediction of colloidal silica penetration into a rock fracture, based on the cubic law (e.g.Witherspoon et al. (1980)). As a general rule of thumb they recommended grouting until 0.5 times the gel time in order to achieve adequate penetration of colloidal silica into rock fractures surrounding an injection borehole (Funehag and Axelsson, 2003).

2.4. Hydraulic behaviour of colloidal silica grouted soils

Colloidal silica has primarily been investigated for use in ground engineering due to its low hydraulic conductivity. Laboratory tests and field trials were conducted by Moridis et al. (1996) examining the reduction in hydraulic conductivity arising from colloidal silica grouting. Table 2-3 shows the hydraulic conductivity of colloidal silica grouted specimens by Moridis et al. (1996). Two types of laboratory specimens were prepared:

(i) specimens prepared by pouring sand into the grout (ii) injection of grouts into sand packs. Permeability reduction from 10^{-4} m/s to less than 10^{-10} m/s after colloidal silica grouting were reported in both test types. In the case of field specimens from Los Banos, observed hydraulic conductivities were reported to reflect incomplete saturation of the pore space. Moridis et al. (1996) demonstrated multiple sequential injections of grouts could overcome issues of incomplete saturation. Subsequent testing reported hydraulic conductivity measurements ranging from 1 x 10^{-5} to 3 x 10^{-7} m/s after the first injection. Following two to three injection cycles further reduction in hydraulic conductivity were reported with comparative measurements to laboratory results. Several other laboratory studies of soils grouted with colloidal silica also reported similar results in the range of 10^{-9} to 10^{-10} m/s (Noll et al., 1992, Persoff et al., 1999, Durmusoglu and Yavuz Corapcioglu, 2000, Zaluski et al., 2001).

Butrón et al. (2009) investigated the hydraulic conductivity of colloidal silica only specimens after gelling. They reported a range of hydraulic conductivity values between 10^{-8} to 10^{-11} m/s. Furthermore, they reported a continuous decrease in hydraulic conductivity with increasing vertical stress applied (as expected).

These results confirm the low hydraulic conductivity of colloidal silica gel and its ability to turn permeable soils (e.g. sands) into low permeability materials with hydraulic conductivity values which would be expected for clays, indicating its great potential for use in constructing *in-situ* hydraulic barriers via grouting.

Table 2-3 Hydraulic conductivity measurements on laboratory and field specimens of colloidal silica grouted sand (Moridis et al., 1996).

Specimen	Test type	Hydraulic gradient (-) x10^3	Hydraulic conductivity (m/s)
Hanford sand & CS	Sand added to CS	9.302	6.48×10^{-10}
		9.302	3.39×10^{-10}
		9.302	2.02×10^{-10}
Hanford sand & CS	Laboratory injection	13.953	1.03×10^{-09}
		13.953	6.33×10^{-10}
		13.953	4.60×10^{-10}
		41.86	4.20×10^{-10}
Los Banos sand & CS	Undisturbed specimens	6.977	3.96×10^{-6}
		6.977	3.07×10^{-6}
		6.977	2.59×10^{-6}
Los Banos sand & CS	Undisturbed specimens	6.977	6.02×10^{-6}
		6.977	3.63×10^{-6}
		6.977	2.85×10^{-6}

2.5. Drying behaviour of colloidal silica

Axelsson (2006) conducted a study investigating drying shrinkage behaviour of colloidal silica gels specimens over a 6-month period. The specimens were stored at 8 ^{o}C in three different relative humidities: 75%, 95%, and 100%. The results presented in Figure 2-12 showed that most of the drying shrinkage occurred between 200 to 1000 hours with a lower relative humidity resulting in more shrinkage. Expanding on the work Butrón et al. (2007) conducted further shrinkage tests storing colloidal silica gels under different relative humidities and measuring the weight change. For colloidal silica gel specimens surrounded by water, shrinkage did not occur. Evaporation and diffusion were the main two mechanism of water loss, thus cause of shrinkage within the colloidal silica gel specimens. Increasing the humidity in the surrounding environmental was shown to decrease the drying rate.

From the results of the work Axelsson (2006) and Butrón et al. (2007) the authors concluded that in tunnel rock fracture grouting the colloidal silica gel face in contact with air will partly shrink dependant on the tunnel humidity and temperature. However, assuming that groundwater will be in contact with the other side of the silica gel, diffusion

of water into the silica from the groundwater in a fracture is enough to prevent any significant shrinkage.

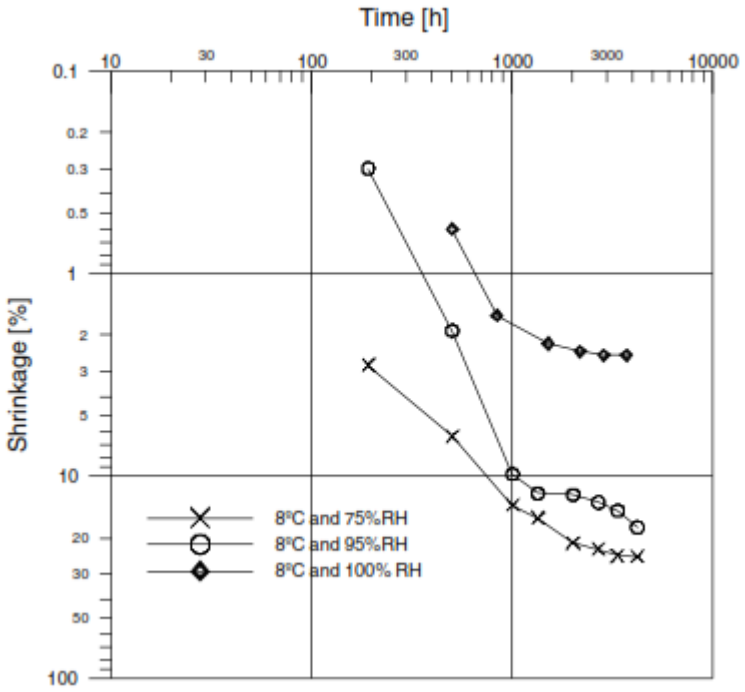

Figure 2-12 Measurements of drying shrinkage for colloidal silica gel

2.6. Mechanical performance of colloidal silica

Storage environment have been noted to influence the strength of colloidal silica (Butrón et al., 2009, Jurinak and Summers, 1991). Table 2-4 shows the results of the mechanical testing conducted over a 6-month period on aged colloidal silica specimens stored in different conditions (Axelsson, 2006). Specimens stored at lower relative humidity reported higher compressive strength development up to 12000 kPa and exhibited greater shrinkage of 25% over the test period. In contrast, specimens stored at 100% relative humidity reported compressive strength of 70 kPa and 2% shrinkage over the same test period. Colloidal silica gel specimens exhibited a general failure trend of brittle failure at lower relative humidities and ductile failure at higher relative humidities. Later work by Butrón et al. (2009) reported colloidal silica gel specimens upon gelling exhibited low initial compressive strength around a few kPa that increased with time. Depending on the storage environment, the rate of strength development can vary, at higher temperatures or lower humidity a faster increase rate occurs.

Table 2-4 Mechanical test results of aged colloidal silica specimens (Axelsson, 2006).

T (°C)/RH (%)	Shrinkage (%)			Compressive strength (kPa)			Young's modulus (MPa)		
	7 days	28 days	168 days	7 days	28 days	168 days	7 days	28 days	168 days
8/100	0	0.8	2.5	6	40	70	-	1.6	2
8/95	0.3	1.2	18	6	50	2000	-	2	210
8/75	3	6	25	4	140	12000	-	5	1700

Persoff et al. (1999) conducted unconfined compressive strength (UCS) test on sand specimens grouted with various concentrations of colloidal silica. Results of the laboratory tests recorded UCS values of 124 kPa and 417 kPa for colloidal silica concentrations of 7.4% and 27.0% respectively. Similar laboratory UCS tests on colloidal silica grouted sand specimens by Gallagher and Mitchell (2002), Liao et al. (2003), and Mollamahmutoglu and Yilmaz (2010) concluded that as the colloidal silica suspension within the grout mixture increases, the strength of the grout sand specimen would also increase.

As part of the study of colloidal silica grout for the application of liquefaction mitigation several research studies have examined the mechanical behaviour of grouting loose sands with colloidal silica grout through laboratory, centrifuge, and field tests (Gallagher, 2000, Gallagher and Mitchell, 2002, Liao et al., 2003, Gallagher et al., 2007a, Conlee et al., 2012). Across these studies the focus of mechanical behaviours was mainly considered through strain development as an indication of liquefaction. Initial studies carried out undrained cyclic triaxial tests on sand with 5-10% colloidal silica grout (Gallagher and Mitchell, 2002). Results of the cyclic stress ratio defined as the ratio of the maximum cyclic shear stress to the initial effective confining stress were used to compared specimens tested at different loading conditions (Liao et al., 2003). Gallagher and Mitchell (2002) reported grouted sand specimens with 5-10% colloidal silica required more than 100 loading cycles at cyclic stress ratio from 0.2 to 0.4 to initiate liquefaction compared to the average of 3 cycles for ungrouted sands specimens. Likewise, Liao et al. (2003) reported an increased number of loading cycles at a higher cyclic stress ratio required to initiate liquefaction for grouted sand specimens compared to ungrouted specimens. Centrifuge tests examining the dynamic loading of sand specimens grouted with 4%, 5%, and 9% colloidal silica were conducted by Conlee et al. (2012) in a 1.65 m length x 3 m width x 4.8 m height laminar box model. Eight shaking motions,

corresponding to 20 cycles of shaking with a centrifugal acceleration of approximately 15 g. Findings of the work reported ungrouted sand experienced rapid, large strains and collapsed shortly after liquefaction was triggered. Conversely, grouted sand specimens exhibited very little strain during the cyclic loading and the strains accumulated uniformly throughout loading rather than rapidly prior to collapse. In addition, ground deformations of lateral movement and settlement were progressively reduced with increased colloidal silica concentration and could be further reduced with increased injection cycles of colloidal silica (Conlee et al., 2012).

Gallagher et al. (2007a) conducted a field test grouting approximately 2 m of a 10 m thick layer of liquefiable sand with 8% colloidal silica injected under low pressures using permeation grouting techniques. Across a 9m diameter test area eight injection wells and a central extraction well was used grout the test area. Following grouting, blast-induced liquefaction resulted in a 40% reduction in settlement in a nearby untreated area.

Curing of colloidal silica gel can increase material strength by allowing additional dissolution reactions of silica from the particle surface and redeposition at the contact points to occur. The curing reaction diminishes asymptotically with time, as gels reach their ultimate strength. Laboratory results of the UCS tests for sand specimens grouted with colloidal silica at different curing times by Liao et al. (2003) reported a UCS increase from 113 kPa after 7 days to 141 kPa after 28 days (as shown in Figure 2-13). Similarly, Mollamahmutoglu and Yilmaz (2010) reported the strength of colloidal silica grouted sand specimens to increase with curing period.

These results show that colloidal silica grout can provide increased resistance to cyclic loading and compressive strength dependant on curing period and environmental conditions.

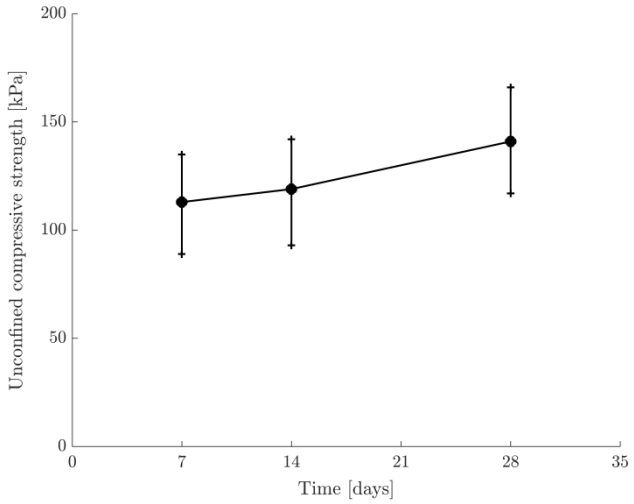

Figure 2-13 Unconfined compressive strength of colloidal silica grouted sand at different curing times (Liao et al., 2003)

2.7. Gaps in knowledge

Within the subsurface as a hydraulic ground barrier, *in-situ* conditions of colloidal silica grout may be subject to varying degrees of saturation dependant on the groundwater table level. Desiccation behaviour of soils can be a critical issue for both structural integrity and hydraulic performance of ground barriers (Ballesteros et al., 2014). Physical processes that effect desiccation of soils include drying, shrinkage, and cracking (Peron et al., 2009). Previous studies by Axelsson (2006) and Butrón et al. (2009) have shown drying shrinkage of colloidal silica gel happens when stored absent of water influencing its mechanical behaviour. Studies into the extent of desiccation in colloidal silica grout and influence of potential environmental conditions remains limited, and its soil water retention behaviour remains to be determined.

Chapter 3 investigates the soil water retention relationship for colloidal silica gel under different curing environments and for colloidal silica grouted soils (colloidal silica-sand, colloidal silica – clay and colloidal silica-sand-clay mixtures).

The mechanical and hydraulic behaviour of soils such as sands and clays are well understood as geomaterials. The behaviour of soils grouted with colloidal silica, a composite geomaterials, have been investigated largely in terms of hydraulic conductivity post-treatment, which has highlighted its attractiveness for use in hydraulic ground

barriers. Studies on the mechanical behaviour of colloidal silica and soils grouted with colloidal silica have been limited thus far to studies of the undrained behaviour (UCS tests), demonstrating its potential for use in short-term applications. Decommissioning at contaminated sites although often considered as short-term works, in the context of nuclear waste legacy sites may last up to one hundred years. Decommissioning works may introduce loading, as structures are constructed to contain existing contaminated buildings, and heavy plant is introduced on site to retrieve waste and dismantle contaminated buildings/structures. As such, soil grouted using colloidal silica to form barriers to contaminant migration may be subjected to variable loading conditions over an extended period of time. Therefore, there is a need to understand the long-term drained performance of colloidal silica grouted soils for barrier applications and other potential ground engineering applications.

Chapter 4 presents the hydro-mechanical behaviour of colloidal silica gel and colloidal silica grouted soils from 1D compression tests and direct shear tests conducted under drained conditions. The behaviour under a range of curing conditions and curing times is investigated.

For applications in the subsurface as a ground barrier, it is necessary to understand how the behaviour of colloidal silica grout is influenced by environmental conditions. This is a complex issue as the interaction of colloidal silica grout in-situ soils and groundwater chemistry may influence the gelling process, the curing process and the subsequent hydraulic and mechanical behaviour. However, much of our understanding is based upon a limited range of conditions that do not reflect the conditions which may be encountered *in-situ*. Much of the work on colloidal silica has been conducted on colloidal silica-sand mixtures. In this thesis the behaviour of colloidal silica gel alone, sand-colloidal silica, sand-clay-colloidal silica and clay-colloidal silica mixtures are investigated.

Jurinak and Summers (1991) and Lim et al. (2010) have highlighted the uncertainty regarding using colloidal silica in saline groundwater environments or using saline water (i.e. sea water) to mix up the grout. This study investigates the combined influence of pH, temperature and electrolyte concentration on colloidal silica gelling behavior, in order to better predict and control gel times in *in-situ* environments where cations are already present in the groundwater or there may be existing variations in pH. The results from a

comprehensive experimental campaign addressing this objective are presented in Chapter 5.

2.8. Conclusion

Colloidal silica grout shows great potential for use in the formation of ground barriers to inhibit fluid flow and prevent migration of contaminants in the subsurface. In order for colloidal silica grout to see widespread usage within grouting applications and in particular as a hydraulic barrier for deployment at nuclear sites, more research is required to assess the suitability of the material. This thesis focuses on the development of colloidal silica as an injectable grouting material, and investigates specifically its drying, hydro-mechanical, and gelation behaviour in order to better understand its performance under *in-situ* conditions.

Chapter 3. Soil water retention behaviour of colloidal silica grout

This chapter presents a brief introduction of unsaturated soil mechanics with a discussion pertaining to its prevalence and importance. The theory of soil suctions and its influence on the mechanical behaviour of soil under unsaturated conditions is also discussed. Features of the water retention curve are also explained in this section. Firstly, the general behaviour based on the pore size distribution of geomaterials is discussed. Secondly, the experimental drying and wetting water retention curves (WRC) of colloidal silica grouts and mixtures of soils and colloidal silica are presented and discussed in this chapter. The WRCs were determined using the chilled-mirror dew-point technique (WP4-C). Additional SEM, X-CT, and photographic image analysis were conducted to investigate the fabric of the various geomaterials tested.

3.1. Unsaturated soils

While classic soil mechanics has focused traditionally on the study of saturated soils, unsaturated soils are prevalent in the environment, for example the surface layers of natural deposits are typically unsaturated. In engineered geostructures, compacted materials are commonly used and these remain generally at least in part unsaturated in flood, road or rail embankments. The movement and removal of water in soils can occur by various physical and chemical mechanisms such as gravity, evaporation, or a change in the water table level. It is important to understand the behaviour of unsaturated soil conditions for the design and analysis of geostructures; basic differences of material nature and engineering response for soils exist depending on the saturation state (Laloui et al., 2013, Fredlund, 2014). Within a nuclear decommissioning context, near surface soil layers surrounding legacy waste containment structures are likely to be in an unsaturated condition. It is important to investigate how the injection of grouts into these soils to minimise radionuclide migration alters soil water retention behaviour in order to

understand the saturation of these treated soils in situ and their response to environmental cycles of wetting and drying.

For example, the division between the saturated capillary zone directly above the water table and the zone filled with both continuous air and water phases would be controlled by the air entry value of the treated soil.

A soil mass can usually be described as a three-phase system comprised of solid particles, a liquid phase, and a gaseous phase. The solid phase is composed of mineral aggregates and particles of all sizes forming the solid skeleton. Both the liquid and gaseous phases make up the void space in the soil (Fredlund et al., 2012). In a saturated soil by definition, all the void spaces are completely filled with liquid (usually water). In an unsaturated soil, both liquid and gas are present in the void space as illustrated in Figure 3-1. Commonly referred to as air the gas present in an unsaturated soil is a combination of air and water vapour. The composition and proportion of different phases within a soil form a multi-phase porous material of variable behaviour. It is the presences of all three phases within a geomaterial that differentiates the mechanics of unsaturated soils from classical soil mechanics.

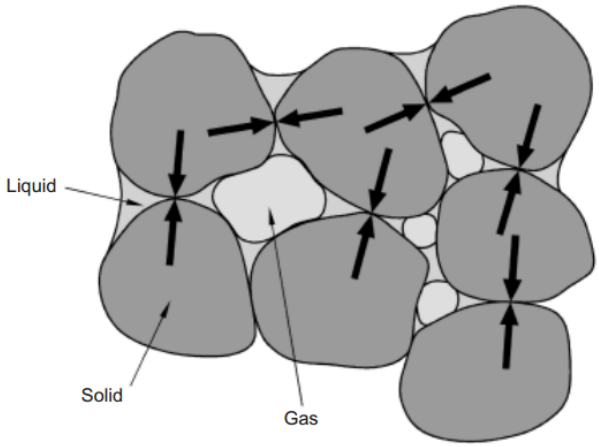

Figure 3-1 A simplified sketch of an unsaturated soil (Gens, 2010).

Generally, in the case of saturated soils located under the water table pore water pressure in the pores is positive. In unsaturated materials, water is present in three main ways: (i) bulk water, (ii) meniscus water and (iii) Adsorbed water (Wheeler and Karube, 1996). Adsorbed soil water is tightly bonded to soil particles and can be considered as a part of the soil skeleton. The pore water pressure acting in the bulk water in unsaturated soils is negative. The presence of the menisci at interparticle contacts in unsaturated soils provide

an additional component of interparticle force (approximately normal to the contact), it is these additional normal forces which have a stabilising effect on the soil skeleton.

3.2. Phase relationships

Phase relationship describe the relative volume or mass of one phase within a soil to the remaining phases. The volume of solid, water (liquid), and air (gas) phases can be expressed as V_s, V_w, and V_a respectively. Similarly, the combination of water and air phases are known as the volume of voids V_v. Volume relationships that are commonly used are void ratio e, porosity n, and degree of saturation S_r (Powrie, 2014, Das, 2010).

Void ratio e is defined as the ratio of the volume of voids V_v to the volume of solids V_s i.e.

$$e = \frac{V_v}{V_s} \tag{3.1}$$

Porosity n is defined as the ratio of the volume of voids V_v to the total soil volume V i.e.

$$n = \frac{V_v}{V} \tag{3.2}$$

The void ratio and the porosity are inter-related as follows:

$$n = \frac{e}{1+e} \tag{3.3}$$

The degree of saturation S_r is defined as the ratio of the volume of water V_w to the volume of voids V_v i.e.

$$S_r = \frac{V_w}{V_v} \tag{3.4}$$

Values for the degree of saturation must fall in the range between zero and one. A fully dry soil has a degree of saturation equal to zero; likewise, a fully saturated soil has a degree of saturation equal to one.

3.3. Suction in soils

Soil suction is a measure of the free energy of the pore-water in a soil. Soil suction in practical terms is a measure of the affinity of soil to retain water (ASTM, 2010). The term

soil suction was first defined by Scholfield (1935) to denote the pressure deficiency in the pore liquid of any soil saturated and unsaturated; driving water to enter during wetting or to flow out during the drying process. Croney and Coleman (1948) introduced the theory of soil suction into the context of civil engineering; by presenting the importance of soil suction in explaining the mechanical behaviour of unsaturated soils. Aitchison (1965) provided quantitative definitions of soil suction and suction components from a thermodynamic perspective.

For an unsaturated soil that has a continuous air phase, the pore air pressure is generally equal to the atmospheric pressure and the value of the pore water pressure is negative, relative to the air pressure. The negative water pressures are such that an affinity for water arises if the unsaturated soils are placed in contact with water that is under the atmospheric pressure (i.e. water is drawn towards the soil). The mechanisms contributing to soil suction include capillary action, surface energy, properties of soil particles (i.e. activity of clays), and ionic concentration of pore water (Bulut and Leong, 2009, Lu and Likos, 2004).

3.3.1. Total suction

Total suction, ψ has two primary components: matric suction, s and osmotic suction, π (Aitchison, 1965, Fredlund and Rahardjo, 1993, Fredlund et al., 2012).

$$\psi = s + \pi \tag{3.5}$$

Total suction can be quantified in terms of the relative humidity directly adjacent to the water surface of a specimen. Total suction, ψ is defined as the free energy state of soil water per unit volume. Described by Richards (1965) the free energy of soil water can be calculated in terms of the partial vapour pressure of the soil water. Total suction can be defined in terms of relative humidity using Kelvin's law:

$$\psi = -\frac{RT}{M_w} ln\left(\frac{p}{p_0}\right) \tag{3.6}$$

where: R, T, M_w, p, and p_o are respectively universal gas constant (8.314 J/mol.K), absolute temperature (K), molar mass of water vapour (kg/mol), partial pressure of water vapour in equilibrium with pure water in the soil (kPa), and saturation pressure of water vapour over a flat surface of pure water at the same temperature (kPa), (p/p_o) is the relative humidity of air in equilibrium with the pore water.

3.3.2. Osmotic suction

Osmotic suction is the result of dissolved solutes in the soil pore water. The development of an osmotic gradient occurs due to the concentration difference between cations present within clay interlayers compared to that within the bulk pore water (Tarantino, 2010). The effect of osmotic suction is generally considered to be negligible for non-active soils due to the lack of a semi-permeable membrane (Gens, 2010, Petry and Jiang, 2007).

3.3.3. Matric suction

Suction generated from mechanisms related to the solid phase contribute to the matric suction. This includes capillary effects, which are dominant in granular soils and the surface adsorption of water on to solid particles (which dominate in the high suction range) (Lu and Likos, 2004, Lu and Khorshidi, 2015).

Matric suction s is commonly defined as the pressure difference between pore-air u_a and pore-water pressures u_w. In this case, the value of matric suction is derived only from the capillary action of water. (Fredlund et al., 2012):

$$s = u_a - u_w \tag{3.7}$$

3.4. Soil fabric

The soil fabric refers specifically to the geometric arrangement of the soil (particle arrangements, assemblages/aggregates, and pore spaces) within a geomaterial (Holtz and Kovacs, 1981). Soil fabric has been shown to have an important influence on the hydraulic and mechanical behaviour of soils (Cerato et al., 2009). The term soil structure includes the combined effects of soil fabric and bonding (Mitchell, 1976).

3.5. Water retention behaviour

The water retention curve (WRC) (or soil water retention curve) defines the relationship for a porous material between the measurements of suction (matric suction or total suction) and water content retained within the soil (Williams, 1982). The water content can be expressed as gravimetric water content θ_g, volumetric water content θ, or degree of saturation S_r. At a particular suction the amount water retained within a soil depends on the pore shape, pore size distribution, mineralogy, surface activity of the solid particles, and the chemical composition of the pore water (Norambuena-Contreras, 2015).

The water retention behaviour is non-linear and can be directly measured in the laboratory or field. General aspects of the behaviour are that along a drying path, as water content decreases suction increases. Likewise, along a wetting path as water content increases, suction decreases. Specifically, the relationship between the amount of retained water and suction even for the same soil may be different depending on the hydraulic path due to hydraulic hysteresis and evolution of the soil structure during wetting and drying. Main features of water retention behaviour can be investigated in a main drying path (starting from a saturated conditions) or along a main wetting path (from a dry condition). Hydraulic paths that move from the main drying curve to the main wetting curve (or vice versa) occur inside this hysteresis domain and are defined as scanning curves (Ferrari et al., 2013).

The determination of water retention curves is becoming a well-established practice for the characterisation of unsaturated soils. A typical water retention curve for a soil is shown in Figure 3-2. At different points along a soil water retention curve, a soil will exhibit varying behaviour in terms of hydraulic conductivity, soil stiffness and shear strength as water content, soil suction and soil fabric changes (Leong and Rahardjo, 1997, Lu and Likos, 2004).

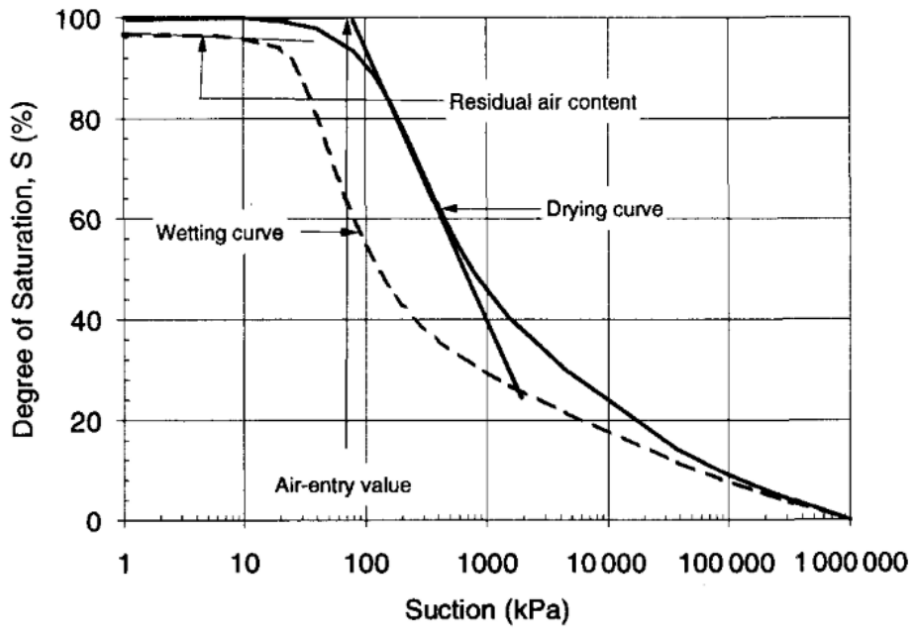

Figure 3-2 Typical water retention curve for a the drying and wetting of a soil (Vanapalli et al., 1996)

3.6. Material and methods

3.6.1. Colloidal silica grout

The colloidal silica material used in this research was MasterRoc MP320 supplied by BASF and manufactured in Sweden. MP320 has a 40% silica concentration by weight, particle size of 16 nm and a density of 1.3 kg/l. At 20^{o}C, the solution has a dynamic viscosity of 10 cP and a whitish/clear appearance (BASF, 2014). All specimens were prepared in a 5:1 ratio of colloidal silica to sodium chloride accelerator by volume respectively to provide a gel time of approximately 1-hour. Solutions of colloidal silica and NaCl accelerator were prepared separately and mixed together using a mechanical stirrer. The final colloidal silica grout molarity based on the prepared 5:1 ratio of colloidal silica to sodium chloride accelerator was 0.28M NaCl and pH was 8.5. This mixture delivered an equivalent gel time of 1-hour. The same colloidal silica grout mixture was used for all experiments in this chapter.

3.6.2. Soil preparation

The soils used in this study were silica sand and kaolin clay. Table 3-1 shows the properties of the silica sand acquired from Sibelco, UK and kaolin clay (Speswhite) respectively used in this study. Figure 3-3 shows the particle size distribution curve of sand, which is characterised as a very coarse sand.

Table 3-1 Sand (Sibelco, UK) and Kaolin Clay (Speswhite) properties

Property	Sand	Kaolin Clay
Specific Gravity, G_s [-]	2.6	-
Diameter, d_{50} [μm]	1242	-
Nominal Effective Size, [mm]	1.01	-
Coefficient of Uniformity, C_u [-]	1.26	-
Grain Shape Angularity	Sub Rounded	-
Grain Shape Sphericity	Medium	-
Specific Gravity, G_s [-]	-	2.6
Liquid Limit, w_L [%]	-	64
Plastic Limit, w_p [%]	-	32
Plasticity Index, I_p [%]	-	32

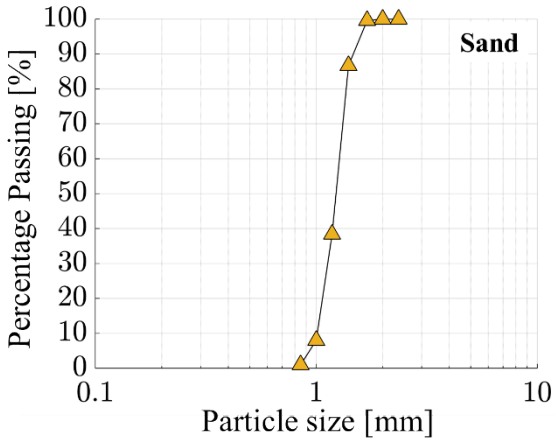

Figure 3-3 Sand particle size distribution curve (Sibelco, 2015)

3.6.3. Specimen preparation

To examine the unsaturated behaviour of colloidal silica (CS) grout five specimen types were investigated: (i) CS grout cured at 90% relative humidity, (ii) CS grout cured in distilled water, (iii) Sand & CS, (iv) Kaolin clay & CS, and (v) Sand and 10% Kaolin & CS, these specimens are outline in Table 3-2. A Sand and 10% Kaolin soil mixture was considered to reflect a predominately granular material with cohesive lenses. Initially, colloidal silica grout specimens were prepared to examine the influence of curing environment of 90% relative humidity (CMA) and curing in water (CMB). Subsequently, all specimens prepared with colloidal silica were cured in water (CMC-CME). Duplicate specimens were additionally prepared and tested under the same conditions.

Table 3-2 Test conditions for water retention behaviour specimens

Reference	Specimen Description	Curing Environment
CMA	Colloidal silica grout	90% RH
CMB	Colloidal silica grout	Water
CMC	Sand & Colloidal silica grout	Water
CMD	Kaolin Clay & Colloidal silica grout	Water
CME	Sand-10% Kaolin Clay & Colloidal silica grout	Water

Specimens were each prepared by firstly filling WP4-C sample cups (37.5 mm in diameter and 8.5 mm tall) with the soil mixture or colloidal silica grout only. Figure 3-4

shows the specimen preparation procedure; firstly, the masses of sample cups were recorded before and after the addition of the soil. For colloidal silica only and sand and colloidal silica specimens, a 10-ml syringe was used to saturated the specimens or fill the sample cup directly with CS. Test specimens of sand & kaolin clay mixtures were prepared by mixing sand together with 10% kaolin by dry mass. Kaolin clay & colloidal silica specimens were prepared by hand mixing 100 g of kaolin powder with 153 g of colloidal silica grout. The ratio between the mass of water in the CS and the mass of solids of kaolin was 0.96.

(a) Sample cup (b) Sand (c) Sand + CS

Figure 3-4 Preparation procedure for WP4-C specimens (a) sample cup, (b) specimen cup filled with soil, and (c) specimen cup filled with soil and colloidal silica

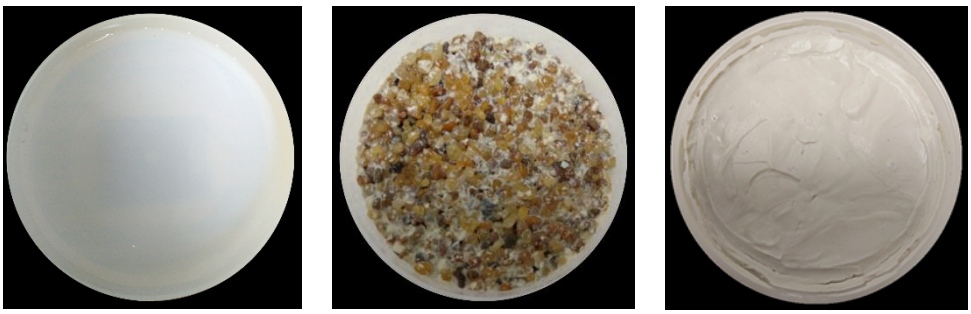

(a) CS only (b) Sand-10% Kaolin (c) Kaolin + CS

Figure 3-5 Example of WP4C specimen. (a) colloidal silica grout only specimen, (b) sand-10% kaolin specimen, (c) kaolin & CS specimen

3.6.4. Water retention measurements

In this study, total suction measurements for specimens were determined using a chilled-mirror psychrometer. The chilled-mirror dew-point technique has been used by many researchers to determine total suction under isothermal conditions in a sealed container

(e.g. Leong et al., 2003, Agus and Schanz, 2005). The principle of the dew point method is based on the equilibration of liquid phase water of a soil specimen and vapour phase water (relative humidity) in the air space above the specimen in a sealed chamber (Gee et al., 1992, Scanlon et al., 2002), Figure 3-6a. Measurements of soil water suction can be determined accurately and quickly using the established dew point technique (Gee et al., 1992). The working principle of the chilled-mirror dew-point technique is based on the thermodynamic relationship between relative humidity, temperature and total soil suction according to Kelvin's equation from equation (3.6) (Leong et al., 2003).

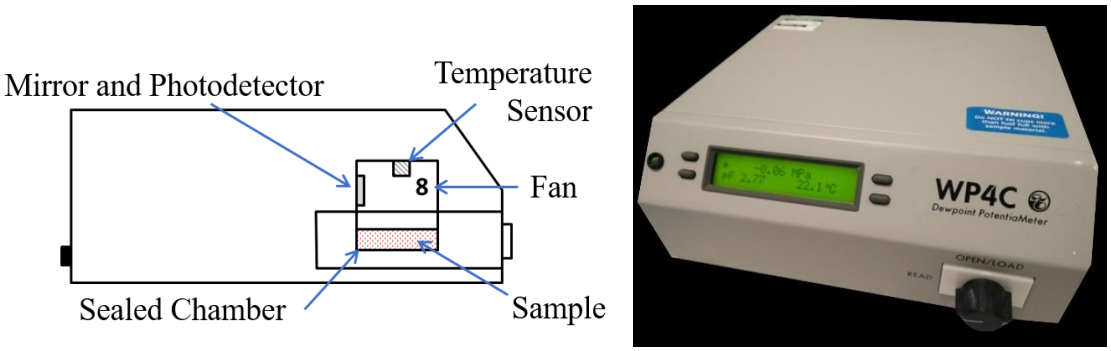

Figure 3-6 Chilled-mirror dew-point device: (a) schematic (Leong et al., 2003), (b) photograph.

A WP4-C dew-point potentiometer manufactured by Decagon Device Inc. was used in this study to measure total suction shown in Figure 3-6b. Accuracy of the dew point temperature measurements in the WP4-C for both the mirror and specimens are 0.001°C. This allows the WP4-C to provide water potential readings in the range of 1 x 10^2 kPa to 3 x 10^5 kPa (Decagon Devices Inc, 2010). The device has an internal sealed chamber in which specimens of ~12 cm^3 can be placed. Calibration standard salt solutions of potassium chloride (KCl) and sodium chloride (NaCl) were used according to the manufacturer's guidelines. After completing the calibration of the device, sample cups containing test specimens were placed in the instrument drawer to determine total suction.

At each water-content point the diameter, height, and mass of the test specimens were measured using a vernier caliper and mass balance (Figure 3-7). Specimens were progressively air dried under laboratory conditions at 20°C and subsequently rewetted to determine both drying and wetting curves of the specimens. After testing of drying and wetting the mass of dry solids and final water content of specimens were determined by oven drying. The degree of saturation at each water-content point was calculated by determining the volume of water present at each time-point and the measured values of

total volume at each time-point and the volume of the final dry solid mass to determine the volume of voids at each time-point.

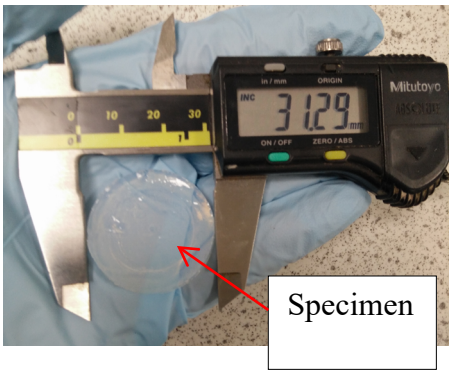

Figure 3-7 Water retention testing: specimen measurement

3.6.5. Specimen wetting

Two techniques were considered to wet test specimens: water droplet method and relative humidity hydration method. In both cases, the wetting procedures were initiated following drying tests and after suctions value of ~100,000 kPa had been measured.

In the water droplet method, droplets of deionised water were slowly added to the dried specimen with a plastic syringe (Figure 3-8a-b). During the wetting process, the propagation of fractures was observed because of volume expansion stresses. Furthermore, a distinct specimen transformation from an opaque white to a clear translucent appearance occurred at the same time shown in Figure 3-8c. After a 24-hour period in water the specimen appearance became a complete translucent colour with visible crack marks throughout the structure (Figure 3-8d). Subsequent testing of the wetted specimen recorded an increased mass confirming specimen hydration. During the subsequent testing, the specimen structure collapsed as shown in Figure 3-8e. Consequently, accurate measurements of specimen volume could not be taken. To reduce the impact of the wetting technique on the specimen structure an alternative hydration method via relative humidity control was considered.

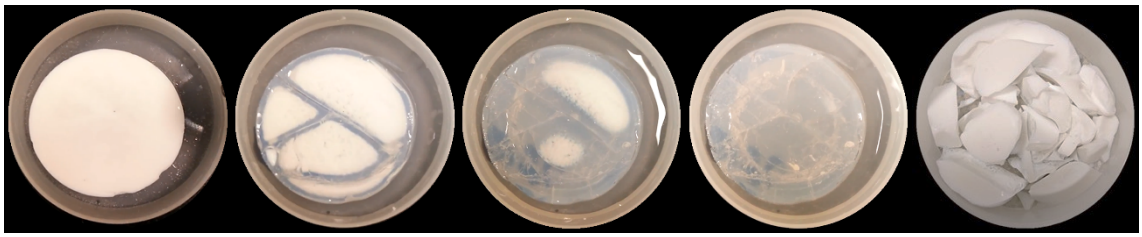

(a)	(b)	(c)	(d)	(e)
Dried Specimen	*Specimen + Water*	*Specimen + Water (30 min)*	*Specimen + Water (24 hrs)*	*Specimen after 2nd drying*

Figure 3-8 Water saturation wetting method specimen transition. a) dried specimen with suction > 1 x10^5 kPa, b) specimen saturated in water (fracture propagation < 1 mins after saturation, c) specimen saturated in water (after 30mins), d) water saturated specimen after 24 hrs, e) final drying state of wetted water saturated specimen

For the relative humidity hydration method, dried specimens were wetted by storing in controlled environmental conditions of 90% relative humidity at 20 ^{o}C. This method enabled a lower rate of wetting to occur preventing the development of fractures. Specimens were stored in controlled environmental conditions for a minimum of 72 hours as shown in Figure 3-9a. A similar observation of appearance change occurred using the relative humidity hydration method from opaque white (dried) to a translucent clear colour (wetted). Following the completion of the wetting process, the same water retention test procedure with the WP4C was implemented with measurement of specimen mass and volume (Figure 3-9b).

Both water droplet and relative humidity hydration techniques provided a successful method of specimen wetting. However, the wetting rate occurred significantly quicker via the water droplet method observable by the distinct transformation in appearance. Consequently, the combined effect of hydration rate coupled with the volume expansion stresses generated during the process caused specimens to fracture. On the other hand, a lower wetting rate occurred for the relative humidity hydration method reduced expansion stresses. Moving forward, wetting via relative humidity control was chosen for all water retention tests because of the reduced impact on specimen structure.

(a) Relative humidity wetted specimen

(b) Specimen after 2nd drying cycle

Figure 3-9 Relative humidity hydration method. a) dried specimen wetted using relative humidity method b) final state after 2nd drying cycle.

3.6.6. Modelling water retention behaviour

When two or more pore series exist in a soil, the corresponding WRC can be bimodal or multimodal. Measured experimental results were examined alongside the established unimodal WRC model from van Genuchten (1980) and a bimodal van Genuchten model developed by Smettem and Kirkby (1990), as described by Burger and Shackelford (2001). The two water retention models are presented below:

Unimodal van Genuchten (1980) model

$$\theta = \theta_r + (\theta_s - \theta_r)\ \frac{1}{\left[1 + \ (\alpha s)^n\right]^m} \qquad (3.8)$$

where θ is the water content ($cm^3\ cm^{-3}$), θ_r is the residual water content, and θ_s is the saturated water content, and where s is suction (kPa), and α (kPa^{-1}), n and m $(m = 1 - 1/n)$. α, n, and m are empirical parameters relating to the water retention curve where α, relates to the air entry value, n to the rate of change of the slope of the curve and m to the asymmetric shape of the curve.

$$S_e = \frac{\theta - \theta_r}{\theta_s - \theta_r} \qquad (3.9)$$

where S_e, is the effective degree of saturation.

A visual comparison and iterative refinement of the van Genuchten (1980) model and experimental results was conducted to determine the most suitable model fit.

Bimodal van Genuchten (Burger and Shackelford, 2001)

This method identifies and selects the suction value, s_j and corresponding volumetric water content, θ_j at the junction whereby the macroscopic porosity appears to have been completely desaturated, and the microscopic porosity begins to desaturate. Measured suction values greater or less than the s_j are fitted separately, using the unimodal forms of the van Genuchten functions for each set of data producing two sets of fitting parameters.

$$\theta = \begin{cases} \theta_r + (\theta_j - \theta_r)\ \dfrac{1}{\left[1 + \ (\alpha' s)^{n'}\right]^{m'}} \ ; s_j < s \\ \theta_j + (\theta_s - \theta_j)\ \dfrac{1}{\left[1 + \ (\alpha s)^{n}\right]^{m}} \quad ; s \leq s_j \end{cases} \tag{3.10}$$

where θ_j = junction volumetric water content; θ_r = residual volumetric content; θ_s = saturated volumetric content; s = suction; and s_j = junction suction.

3.6.7. Pore size distribution

The use of mercury intrusion porosimetry (MIP) to investigate the particle configuration (fabric) of colloidal silica test specimens within the matrix of the geomaterials was initially considered. MIP techniques has been used over the last 30 years for microstructural investigation in soil mechanics providing measurements of pore size distribution over a range of nanometres to several microns (Jung et al., Pedrotti, 2015). Pores within specimens must be free from water to accurately determine the pore size distribution, as the method relies upon the progressive intrusion of mercury into the soil pores. Conventional drying methods (oven and air) can cause significant soil structure alterations (Ahmed et al., 1974). Freeze drying has become the standard method of specimen preparation for MIP tests (Delage et al., 1982). From testing however, it was observed that freeze drying resulted in structural collapse of the CS specimen (Figure 3-10). The percentage of water within the CS specimens contributed to greater than 50% of the specimen volume and was considered to contribute towards the specimen fabric failure during the freeze-drying process. Consequently, MIP testing could not be successfully conducted on CS specimens due the collapse of the pore structure.

Figure 3-10 Colloidal silica specimen following freeze drying

3.6.8 Microstructural imaging

Microscope images were performed by means of a Field Emission Scanning Electron Microscope (Hitachi SU-66000). This apparatus is equipped with Energy dispersive spectroscopy, Oxford Inca 350 with 20mm X-Max detector and Wavelength Dispersive spectroscopy, Oxford Inca Wave 700 microanalysis system with. Energy to allow elemental analysis of metals and ceramic materials.

Microscope images were also obtained using a Tungsten Filament Scanning Electron Microscope (Hitachi S-3700). This apparatus has Energy Dispersive Spectroscopy capability, Oxford Inca 350 with 80mm X-Max detector to allow elemental analyses of materials. For SEM imaging specimens were oven dried at 150^{o}C for at least 24hrs.

X-ray micro computed tomography was performed by means of a Nikon XT H 320 X-ray CT scanner. No sample preparation is required for X-CT imaging, hence, samples remained entirely undisturbed. In this study, the voxel resolution was approximately 0.504mm and the scanner settings were energy 183kV and current 204μA. The reconstruction was carried out using CT Pro and CT Agent software (Nikon-Metrology). The visualisation and analysis of the CT data were performed with AVIZO software version. 9.0.

3.7. Results

3.7.1. Colloidal silica cured at 90% relative humidity [CMA]

Figure 3-11 show the water retention data in terms of degree of saturation for two colloidal silica only grout (CMA) specimens aged in 90% relative humidity. Fitting of the unimodal van Genuchten (1980) model was conducted based on the drying path data from both tests. Results from the water retention curve (WRC) show that as the CMA

specimens dries, the degree of saturation reduces and suction increases. From the WRC, both specimens show similar drying behaviour with an air entry value of ~20,000 kPa. In addition, the WRC shows degree of saturation $S = 0.2 – 0.3$ for the maximum test suction value approximately 100,000 kPa at the end of the testing.

Drying states of CMA specimens during water retention tests exhibited both shrinkage and colour changes as shown in Figure 3-12. Features of the drying behaviour explained by Vanapalli et al. (1999) and Tarantino (2010) by saturation state for soils were similarly observed for the CS specimen. Initially, the test specimen in the saturated state filled the container as shown in Figure 3-12a. Measurements during this phase corresponded to suction values less than 10,000 kPa and S = 0.95-1. Subsequently, arising from the drying process specimens enter a quasi-saturated state, shrinkage occurs throughout this state highlighted by the gap in the sample container (Figure 3-12b). At this phase, the suction value and degree of saturation are close to the beginning of the slope of the WRC. Figure 3-12c shows a partially saturated specimen after the shrinkage phase. During this stage, there is only a small amount of specimen shrinkage. However, a visible alteration to specimen appearance can be observed. The specimen appearances changes from translucent to a complete white colour over a period of less than 30 mins (Figure 3-12d). It is interesting to note, that the colour change of the specimen occurs firstly with the appearance of white dots. Suction values corresponding to the colour change phase are located on the main drying slope of the WRC. The specimen appearance remained the same as Figure 3-12d for increasing suction and decreasing degree of saturation until the residual saturation state is reached.

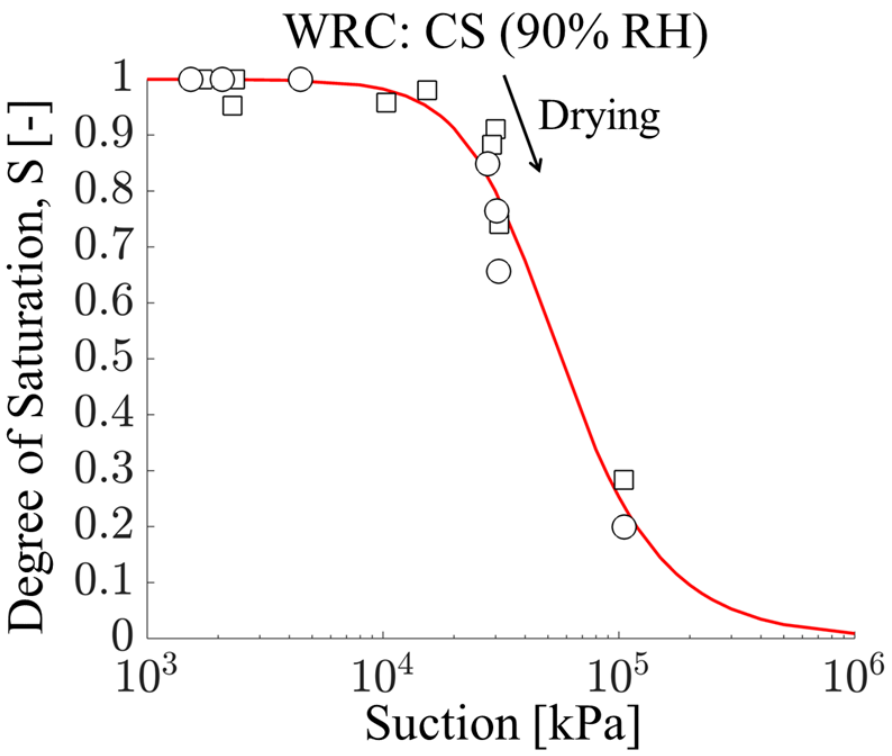

Figure 3-11 Variation of degree of saturation against suction for drying CMA specimens and van Genuchten (1980) model

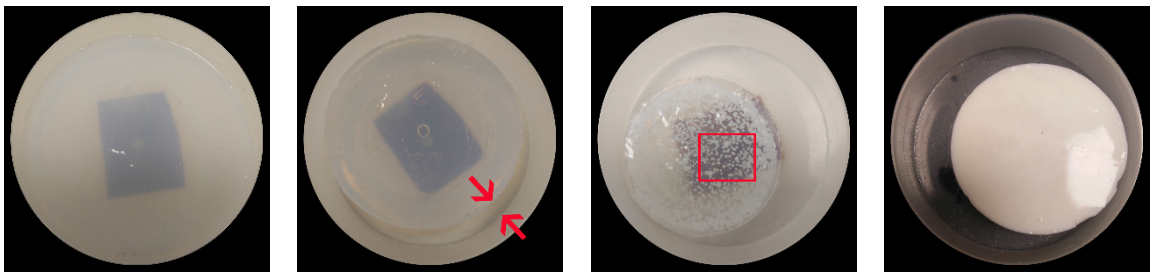

(a) *Initial specimen [saturated]*

(b) *Shrinkage [quasi-saturated]*

(c) *Colour change [partially saturated]*

(d) *White specimen [residual]*

Figure 3-12 Saturation states of CS specimen during testing

3.7.2. Colloidal silica cured under water [CMB]

The measured water retention data for three colloidal silica grout specimens cured in water (CMB) fitted with the unimodal van Genuchten (1980) function is shown in Figure 3-13. A similar drying behaviour was exhibited by all three CMB specimens represented as varying symbols. It can be observed from the WRC that results display an initial plateau at the start of the test. During this initial plateau phase the degree of saturation remains relatively constant across the three specimens for suction values between 2,000

kPa to 20,000 kPa. Following this saturation state the result of all three specimens show a similar trend with a progressive decrease in degree of saturation for increasing suction values. Air entry values ranging from 15,000 kPa to 20,000 kPa was estimated from the curves, corresponding to degrees of saturation of S = 0.9 to 1. Furthermore, the measured data indicates a 0.11 degree of saturation for suctions over 100,000 kPa. Similar to CMA, during drying the CMB specimens exhibited both volumetric shrinkage and colour alteration at higher suctions values beyond the air entry value.

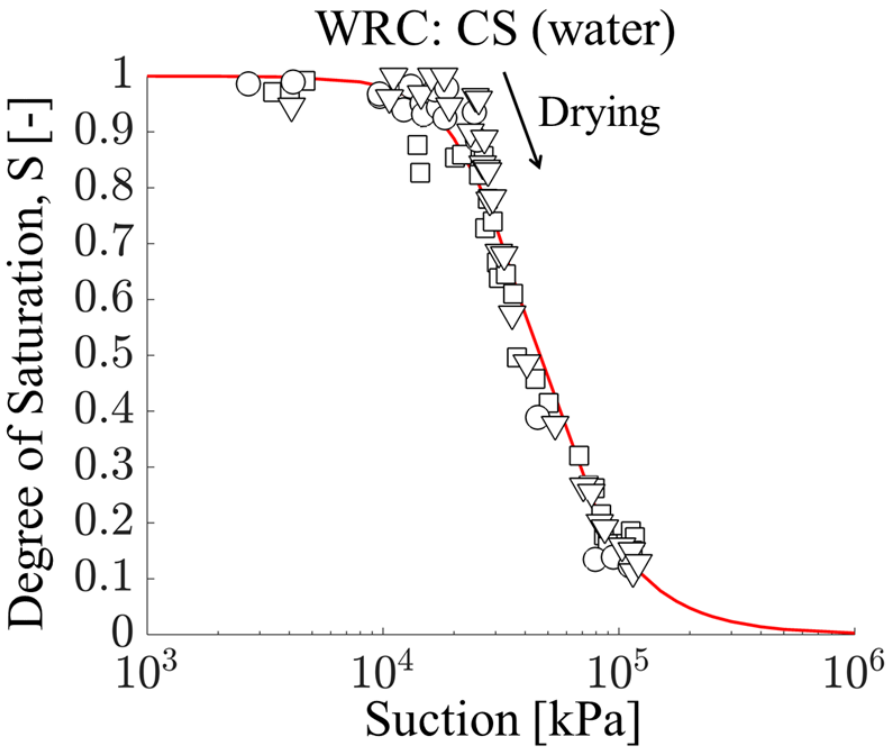

Figure 3-13 Drying water retention curves (WRC) for three repeat CMB specimens fitted with van Genuchten (1980) model

Figure 3-14 presents the wetting curves (solid symbols) for three CMB specimens in addition to the drying curves fitted with the van Genuchten (1980) model shown previously in Figure 3-13. Specimens were wetted in controlled environmental conditions of 90% relative humidity detailed in section 3.6.5. The relationship between the degree of saturation and suction is shown in Figure 3-14a. On this plot the wetting curves (solid symbols) for the CMB specimens all fall on the curves obtained during the drying path (open symbols) displaying a similar slope in all three of the tests. Results of the curves indicate that the specimens void were fully saturated during the wetting process. Figure 3-14b shows the main drying and wetting curves in terms of volumetric water content against suction fitted with the van Genuchten (1980) model. Differences between these

two curves occur due to the plastic specimen shrinkage that occurs during the drying process. Consequently, the total volume of the initial wetting specimen is significantly smaller than the initial specimen for drying tests. Structurally, the initial test specimen volume is formed primarily as water. In contrast, due to shrinkage, the subsequent saturated wetting test specimen can not hold the same volume of water. Illustrated in Figure 3-15 the initial drying test specimen is ~37.5 mm diameter; whilst the initial wetting test specimen is ~29 mm in diameter.

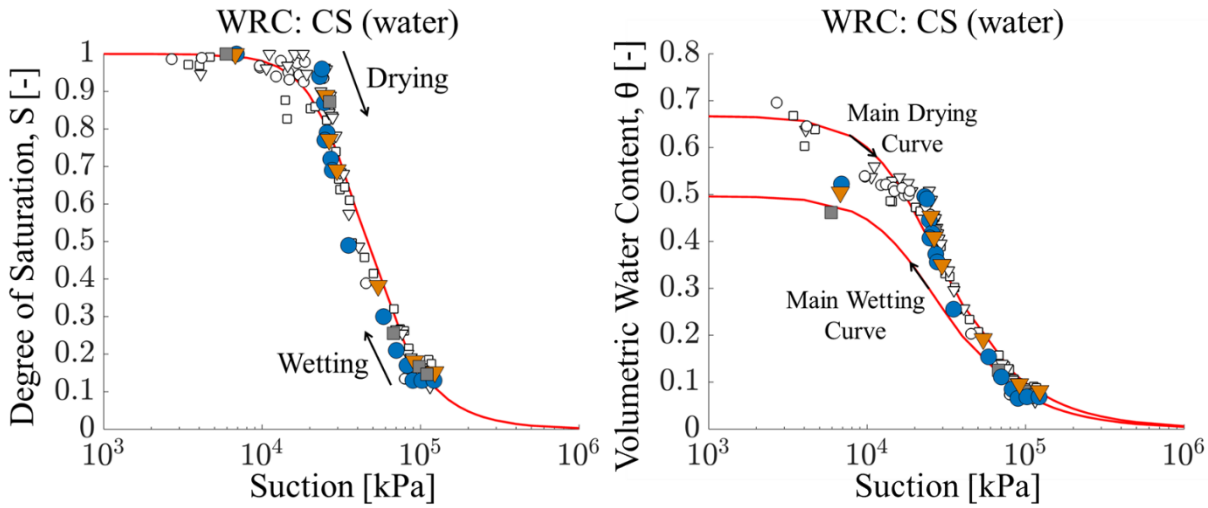

(a) (b)

Figure 3-14 Water retention curves for drying (open symbols) and wetting (solid symbols) cycles of CMB specimens with van Genuchten (1980) model. a) Degree of saturation vs. Suction, and b) Volumetric water content vs. Suction.

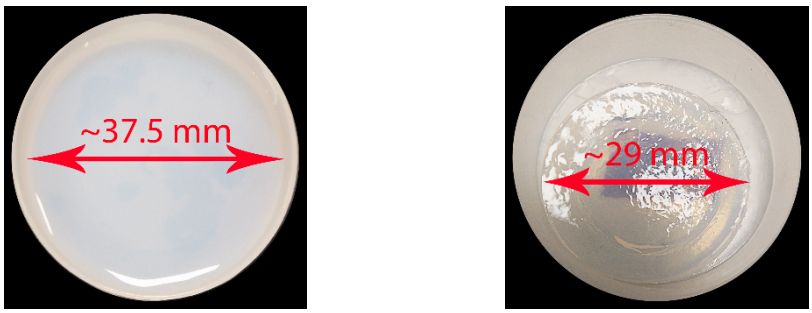

(a) Saturated drying test specimen (b) Saturated wetting test specimen

Figure 3-15 Saturated drying and wetting CMB test specimens

3.7.3. Water retention behaviour of CS in different curing conditions

Results of the van Genuchten (1980) model for colloidal silica specimens cured in 90% relative humidity (CMA) and water (CMB) is shown in Figure 3-16. From the two WRCs

the results indicate the influence of the environmental curing conditions had little effect on the water retention behaviour. Both WRC curves show a similar air entry value and drying slope with the specimen cured at 90% RH exhibiting a slightly higher air entry value. The reason is considered that the material fabric of the CS specimen aged in 90% relativity humidity experiences consolidation due to suction increasing the effective stress and thus resulting in altering the particle arrangement and reducing slightly the pore size.

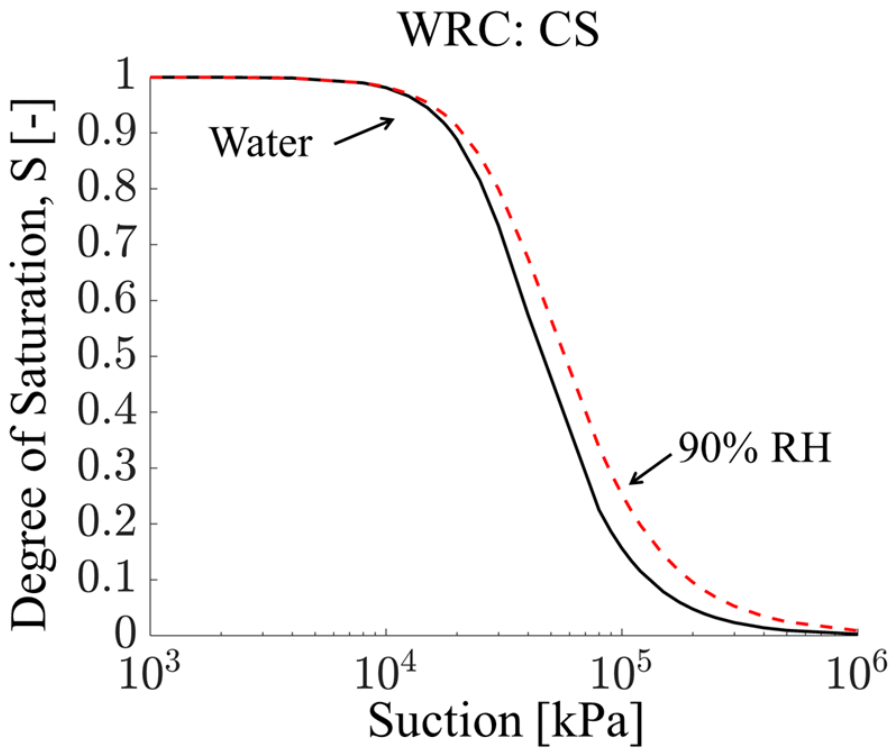

Figure 3-16 WRC of van Genuchten models for colloidal silica specimen cured in different environmental conditions

3.7.4. CS SEM imaging

Figure 3-17 shows the SEM images of colloidal silica grout. High image magnifications (300k and 450k) were required to capture individual silica particles. From the figure, clusters of silica particles formed from individual spherical silica particles bonded together can be seen at the nanometre scale. Within the matrix of colloidal silica, the material fabric is formed by several clustered groups of aggregated silica particles. It is likely that the continuous network of nano-cracks shown in Figure 3-17a was induced during oven drying in preparation for SEM imaging. From the SEM images and the unimodal water retention behaviour of CS specimens it can be concluded that the desaturation of the colloid silica grout is governed by the pore space which forms between clustered groups of silica particles (silica particles have a diameter ~15 nm) during drying.

As noted in section 3.6.7 direct measurements of pore size distribution were not possible with the CS test specimens.

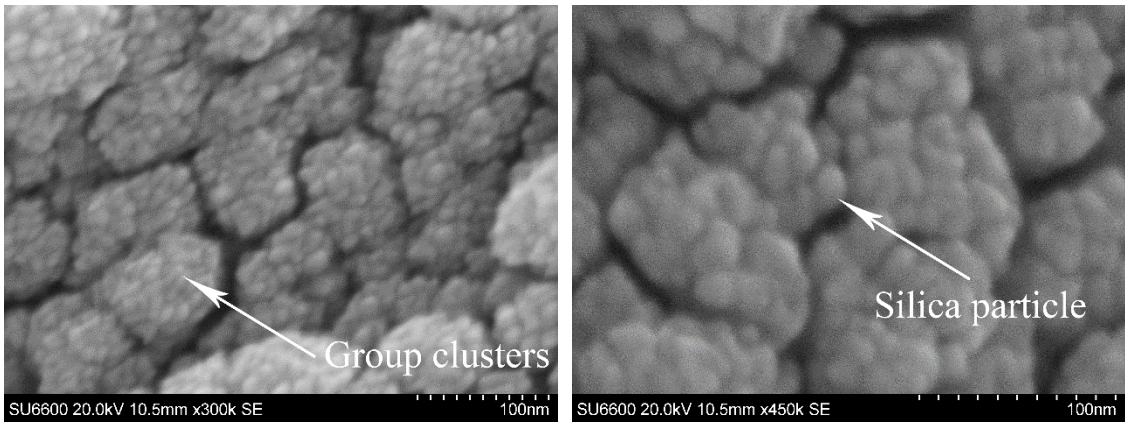

(a) magnification factor of 300k (b) magnification factor of 450k

Figure 3-17 SEM images of colloidal silica grout

3.7.5. Sand & colloidal silica grout [CMC]

The water retention curve data fitted with the bimodal van Genuchten function for sand & CS specimen (CMC) is shown in Figure 3-18. Just to note, the particle size of sand is ~2 mm and CS particles is ~15 nm. The data indicates that an asymptotic value for degree of saturation is approached as the specimen is dried from saturation to suction values ranging from 8,000 to 12,000 kPa. Furthermore, subsequent drying reduces the degree of saturation to 0.1 for suctions over 100,000 kPa. This behaviour arises from the dual porosity nature of the sand & CS specimen, and is attributed to the formation of two distinct pore-size distributions during drying (Burger and Shackelford, 2001). Firstly, macropores/cracks form on drying at the centre of CS filled pores between sand particles; these are associated with the first air-entry value at a suction value ~200 kPa. Secondly smaller pores spaces form between the colloidal silica clusters (shown in Figure 3-17a) during drying, and these desaturate at a suction value of ~25,000 kPa.

To investigate the effect of colloidal silica grouting on sand the water retention behaviour test results were examined against a comparable sand specimen. A comparable test data set for a similar sand material was identified in Burger and Shackelord (2001). Figure 3-19 shows the particle size distribution for the sand material used in the this study in the sand & CS specimen and the '10-20 sand' used by Burger and Shackelford (2001). Both sands are uniformly graded with a particle size between 1 to 2 mm.

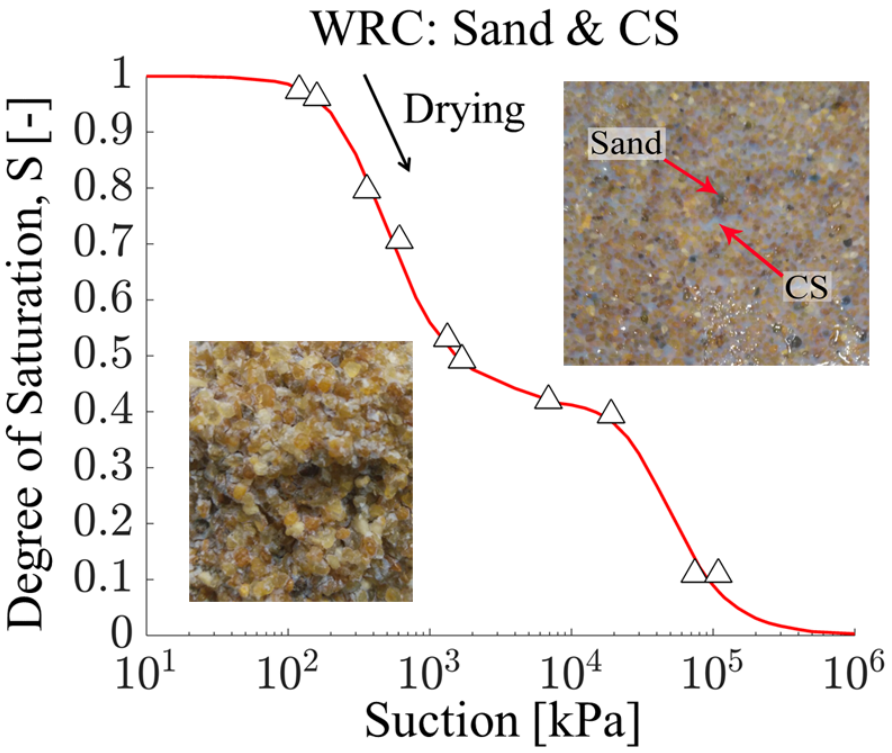

Figure 3-18 WRC for drying cycles of CMC specimens fitted with a bimodal van Genuchten (1980) model

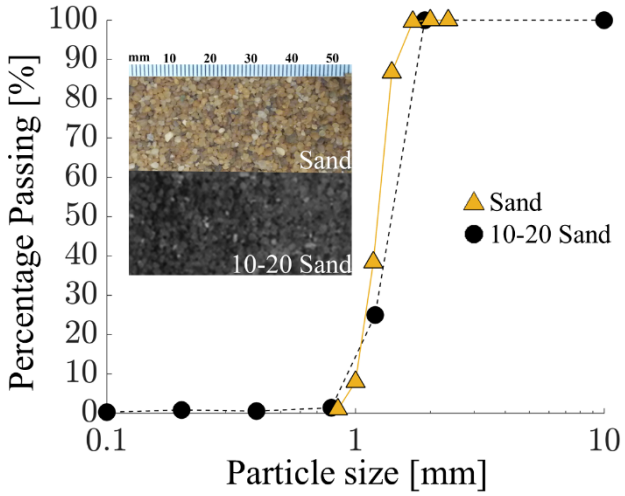

Figure 3-19 Particle size distribution for test sands and 10-20 sand (Burger and Shackelford, 2001)

In Figure 3-20, the water retention curve reported for '10-20 sand' by Burger and Shackelford (2001) alongside curves from the experimental tests for sand & CS (CMC) and CS only (CMB) specimens are presented. The '10-20 sand' only WRC illustrates typical behaviour for a coarse-grained material with an air entry value of ~1 kPa. Comparisons of the sand & CS (CMC) and '10-20 sand' specimen indicate that the addition of colloidal silica increases the initial air entry value by more than two orders of magnitude from ~1 kPa to ~200 kPa. Furthermore, the behaviour of the sand specimen alters from unimodal to bimodal due to the addition of colloidal silica grout. The effect arises due to the additional desaturation within the CS-CS pores; thus, the air entry value of the CS curve and the secondary air entry value of the sand & CS curve both occur at nearly identical suction values of ~20,000 kPa.

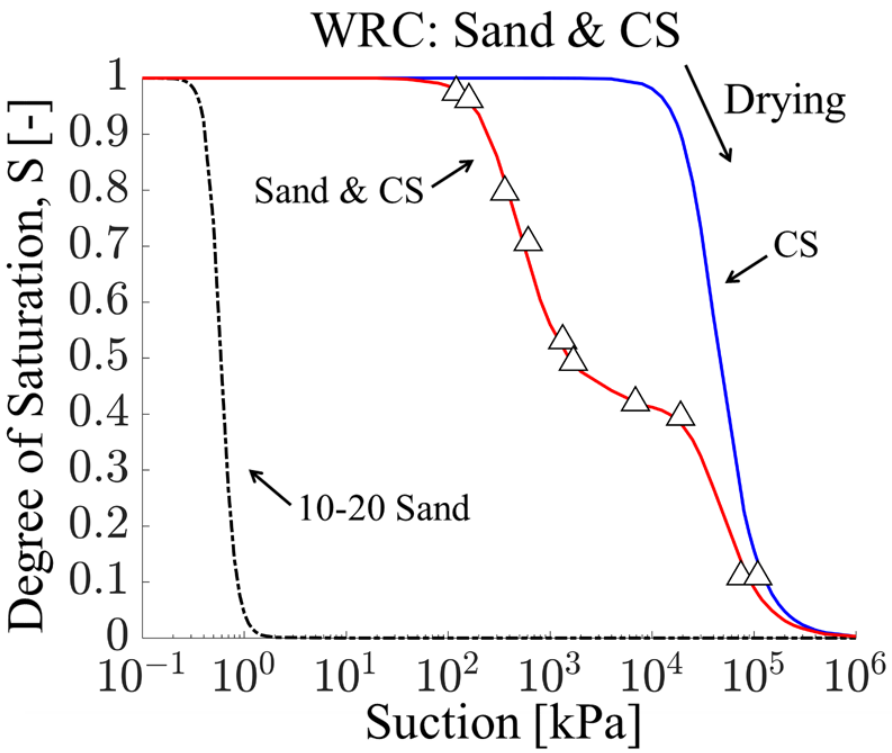

Figure 3-20 WRC of sand saturated in colloidal silica specimen (CMC) and a 10-20 sand specimen by (Burger and Shackelford, 2001)

3.7.6. Sand & CS imaging

A 3D reconstruction of a specimen of sand & CS scanned in the X-CT instrument is shown in Figure 3-21. The X-CT image shows that CS fills most of the voids with the sand matrix throughout the structure in a similar manner to the photographic image taken of the specimen surface. Figure 3-22 presents two SEM images of a specimen of sand & CS at the same location for two magnifications. The two SEM images appear to show

that the sand particles contain a continuous matrix of CS. At a higher magnification, the CS clusters are clearly visible on the surface (Figure 3-22b). Porosity of the sand specimen following mixture with CS is therefore governed by the bonding contact between sand-CS (macropore) and CS-CS (micropores) (excluding a few remaining bubbles of air) (Collins and McGown, 1974). This effect can be observed in the bimodal behaviour identified in the WRC in Figure 3-18.

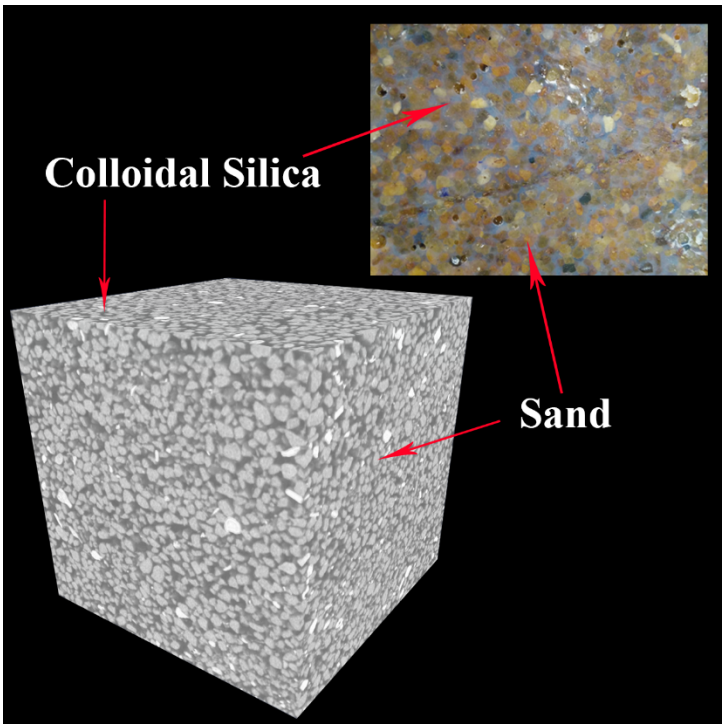

Figure 3-21 X-CT image of Sand & CS

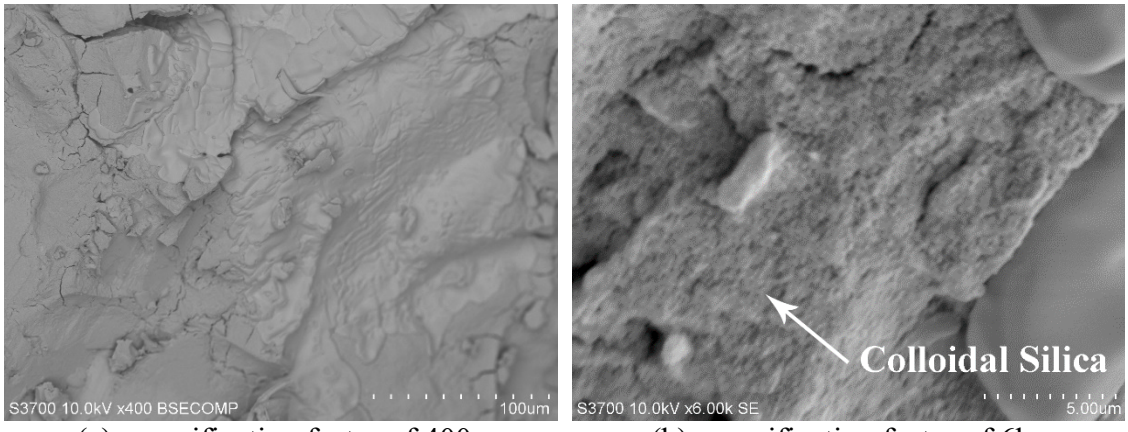

(a) magnification factor of 400 (b) magnification factor of 6k

Figure 3-22 SEM image of sand & CS

3.7.7. Kaolin clay & colloidal silica grout [CMD]

To investigate the influence of colloidal silica grout added to clay materials, mixtures of kaolin clay & CS were prepared following the procedure outlined in section 3.6.3. The particle size of kaolin clay is ~1 to 2 μm and CS is ~15 nm. Figure 3-23 shows the water retention data in terms of degree of saturation for three repeat kaolin clay & CS specimens (CMC) alongside the van Genuchten (1980) model. The drying paths for all three CMD specimens exhibited unimodal behaviour. From the WRC, an air entry value of ~2,000 kPa can be estimated from the curves, corresponding to a degree of saturation of S = 0.95. Furthermore, the measured data indicates a 0.1 degree of saturation for suctions over 100,000 kPa. Drying behaviour of the kaolin clay & CS specimen exhibited volumetric shrinkage with increasing suction and decreasing degree of saturation.

The drying and wetting curves in terms of volumetric water content against suction fitted with the van Genuchten (1980) model for kaolin clay & CS specimens are shown in Figure 3-24. Differences between these two curves occur due to the plastic specimen shrinkage during the drying process.

To investigate the influence of colloidal silica grouting on the drying behaviour of kaolin clay, experimental results were plotted alongside kaolin clay only test results by (Tarantino, 2009). The WRC data of kaolin clay only alongside the drying curves of the measured experimental data CMD is shown in figure 3-25. An air entry value for the kaolin only specimen is < 1,000 kPa. Similarly, the air entry value of kaolin clay & CS is slightly higher but around 2,000 kPa. The addition of colloidal silica to kaolin clay increases the suction values for the same degree of saturation. Such behaviour is a result of the smaller CS particles (~15 nm) filling the pores within the kaolin clay (~1 - 2 μm). Consequently, an increase in water retention behaviour and higher air entry value is observed in the specimens with CS added.

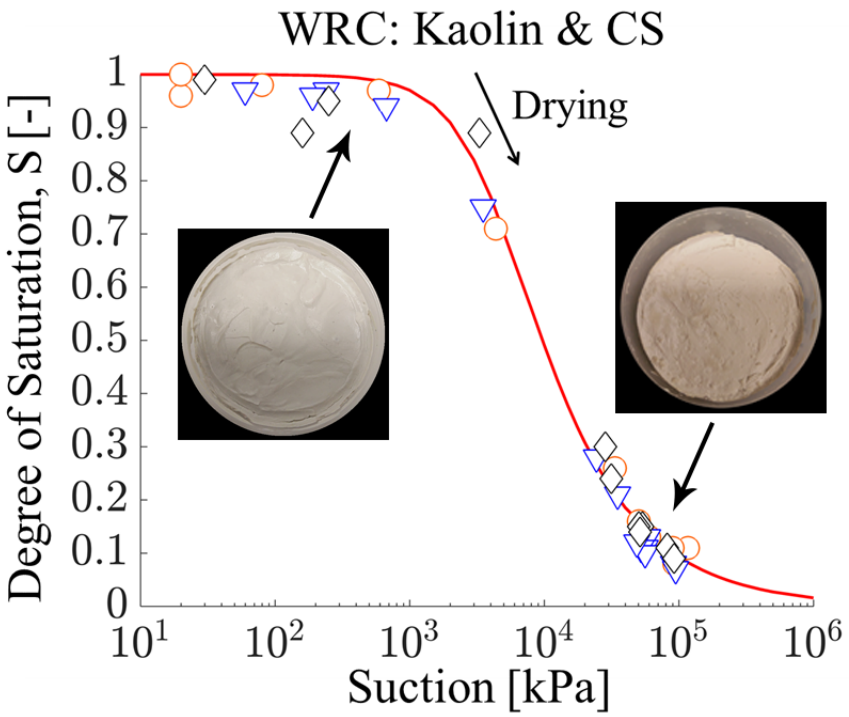

Figure 3-23 Drying water retention curves (WRC) for three repeat CMD specimens fitted with van Genuchten (1980) model

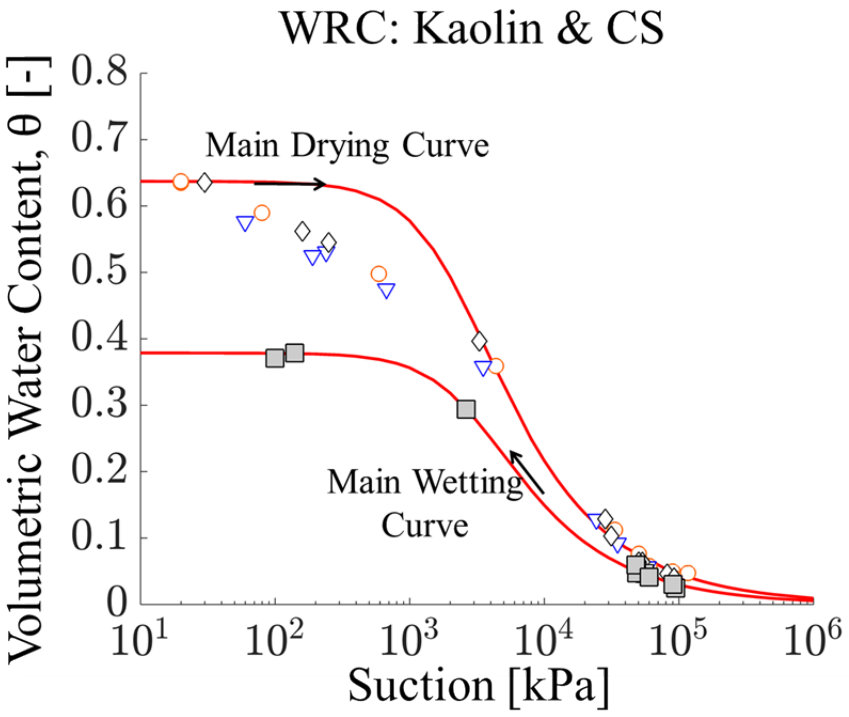

Figure 3-24 WRC for drying (open) and wetting (solid) cycles for CMD specimens and van Genuchten (1980) model

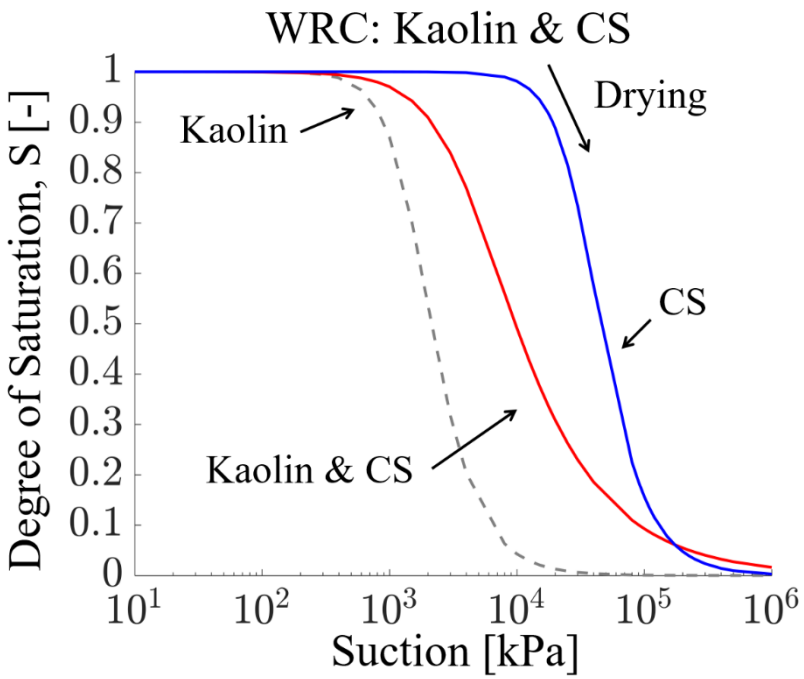

Figure 3-25 WRC for drying cycles of CMD specimens plotted alongside kaolin clay test data by Tarantino (2009)and CMB colloidal silica only specimens.

3.7.8. Kaolin clay & CS imaging

An SEM image of a specimen of kaolin clay & CS is shown in Figure 3-26. A highly heterogeneous matrix including particles of kaolin and CS can be seen in the images with two areas highlighted. In the centre (*circle*), it appears that only kaolin particles are present, characterised by their plate-like shape. Conversely, in the adjacent area (*square*) a mixture of kaolin particles submerged in a colloidal silica matrix can be seen. Throughout the whole specimen, regions comprised of kaolin particles with little CS were present; likewise, regions of CS in which kaolin particles seem to be isolated or not present at all could be identified. Further element analysis shows higher Si presence even in the areas where visibly only kaolin particles are identifiable, suggesting that, despite not being visible in the SEM images, CS particles must be present as a coating on all kaolin particles. Similar to results highlighted by (Coo et al., 2016) in their study on the effect of nano CuO on kaolin properties. A distinction between the two different matrices (kaolin vs colloidal silica) cannot be made by direct visual examination of the specimen (Figure 3-27).

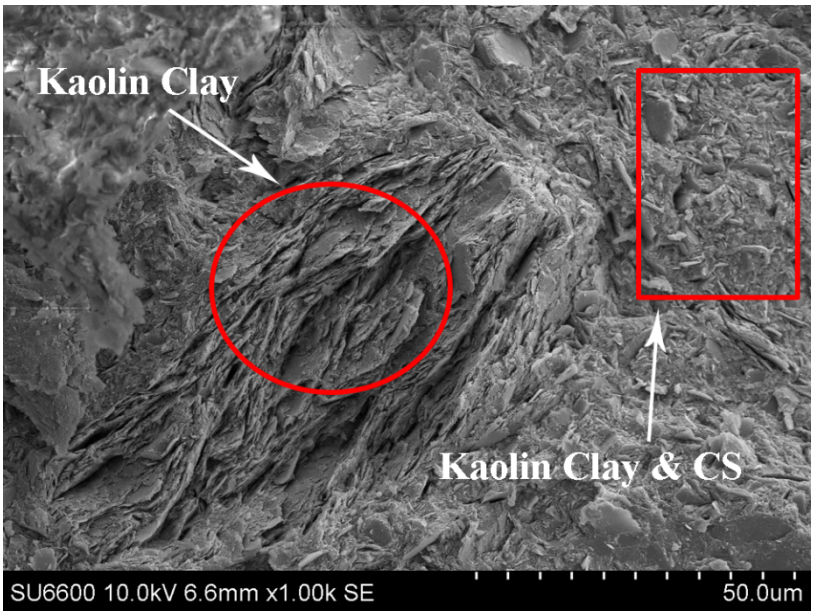

Figure 3-26 SEM image of kaolin clay & CS

Figure 3-27 Photographic image of kaolin clay & CS specimen

3.7.9. Sand-10% Kaolin clay & colloidal silica grout [CME]

A 'soil' mixture of sand and 10% kaolin clay (by dry mass) was prepared to investigate the effect of colloidal silica grouting in a mixed soil containing sand and clay fractions. Specimens were prepared following the procedure outlined in section 3.6.2. Figure 3-28 shows the measured water retention data for sand-10% kaolin clay and CS specimen (CME) alongside the bimodal van Genuchten (1980) function. An initial air entry value of ~60 kPa and secondary air entry value of ~10,000 kPa can be determined from the curve. Incorporated within the specimen matrix are three distinct particle sizes: sand (~2 mm), kaolin clay (~2 μm), and CS (~15 nm). The data indicates that an asymptotic value for the degree of saturation is approached as the specimen is dried from saturation to suction ranging from ~1,000 to 10,000 kPa, and that subsequent drying reduces the degree

of saturation to 0.1 for suctions over 100,000 kPa. This trend in the measured water retention curve data arises from the varied particles of the specimen. The bimodal behaviour of the WRC indicates that despite the presence of three materials of varying particle size the specimen drying behaviour is primarily dominated by the desaturation of two distinct pore sizes (Burger and Shackelford, 2001).

Water retention tests were carried out on a sand-10% kaolin clay (soil only) specimen mixtures to determine the drying behaviour without the presence of colloidal silica. Presented in Figure 3-29 is the WRC for experimental data of sand-10% kaolin clay specimens with and without colloidal silica. Results of the soil only curve exbibit unimodal behaviour with an air entry value ~50 kPa. As expected, the presence of kaolin clay (10%) in the specimen increases the air entry value compared to sand only Figure 3-20. However, 10% kaolin clay added to the sand was not sufficient to establish bimodal behaviour. On the other hand, with the addition of CS results show that the soil & CS specimen exhibit bimodal behaviour with a higher initial air entry suction value (~60kPa). Furthermore, the secondary air entry of the soil & CS specimen is located at a similar suction value to the CS only (CMB) specimens.

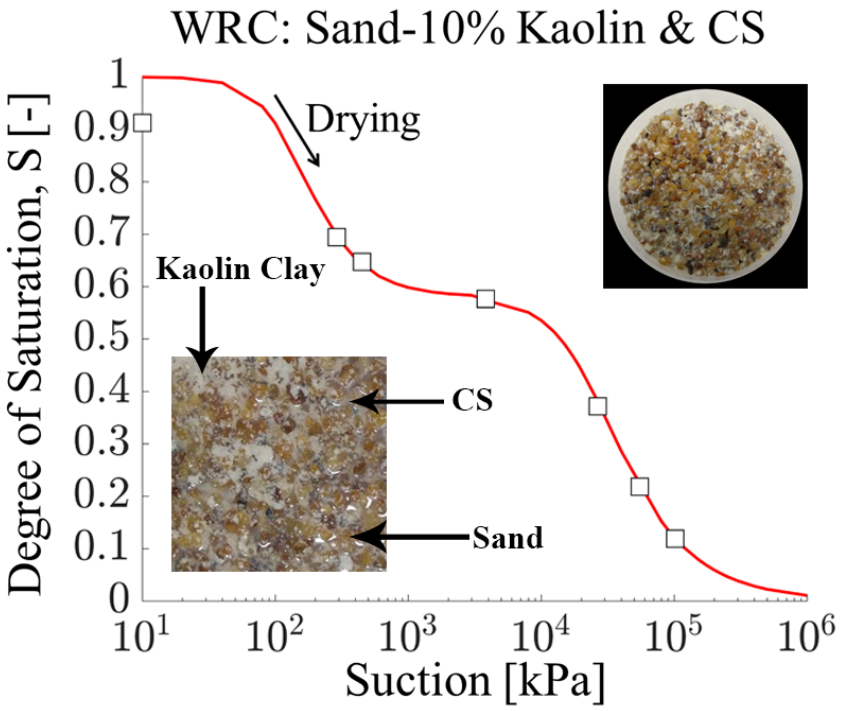

Figure 3-28 WRC for drying cycles of sand-10% kaolin clay (soil) & CS specimens plotted with the bimodal van Genuchten (1980) model

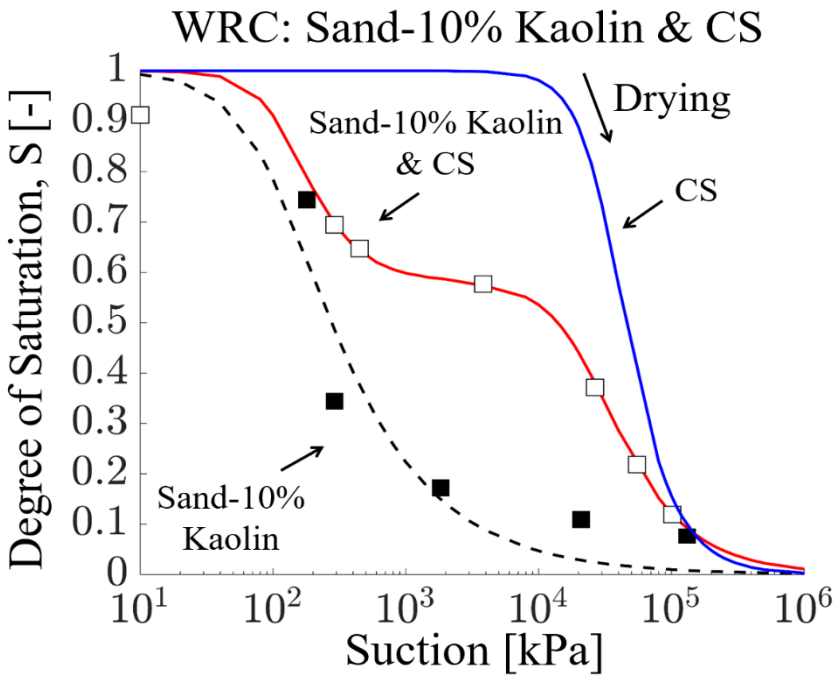

Figure 3-29 WRC for sand-10% kaolin clay only, sand-10% kaolin clay & CS (CME), and CS only (CMB) specimens with van Genuchten (1980) models

3.7.10. Sand-10% Kaolin Clay & CS imaging

Figure 3-30 shows a photographic image of a dried specimen of sand-10% kaolin clay & CS. It can be seen from the image that the sand particles are coated with a white coloured mixture of kaolin and CS throughout the material fabric. The porosity of the material is governed by two distinct pore sizes: pores between sand-kaolin-CS (macropores) and pores between CS clusters (micropores).

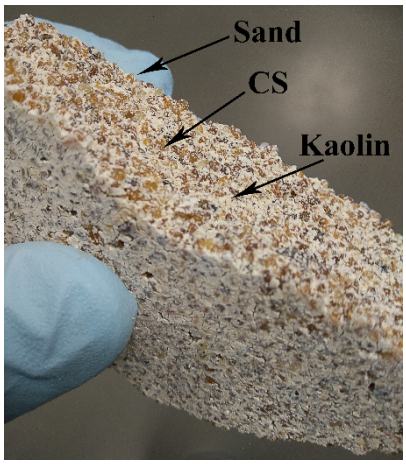

Figure 3-30 Photographic image of sand-10% kaolin clay & CS specimen

3.8. Influence of colloidal silica treatment on water retention behaviour

The water retention curves determined from the unimodal and bimodal van Genuchten (1980) models calculated fitted to the experimental data is shown in Figure 3-31. Comparable curves are presented for specimens of CS, sand, kaolin clay, and soil (*sand-10% kaolin clay*) with CS (*solid lines*) and without CS (*dashed lines*). The general observation is, as expected, that the air-entry value increases in specimen mixtures with smaller particle sizes and thus pore size distributions. An increasing water retention capacity can be seen with decreasing particle size comparing the untreated soils, i.e. the sand, soil (*sand-10% kaolin clay*), and kaolin clay specimens. Studies examining the effect of particle size on soil water retention behaviour identified a similar effect (Rezaee et al., 2011, Vanapalli, 1994). For all specimens treated with CS, it can be observed that for a given suction, the degree of saturation is higher for specimens with CS than its corresponding counterpart without CS. This suggests that the addition of colloidal silica

within the matrix of the materials contributes to increasing the water retention capacity of the mixture.

In the case of the sand and sand-10% kaolin clay specimens, the addition of CS results in a shift from unimodal (without CS) to bimodal (with CS) water retention behaviour. The addition of CS contributes to reducing the size of the macropores (i.e. inter-particle or inter-aggregate pores) which is responsible for the first air entry value and the secondary air entry value is due to the desaturation of pores between CS clusters. Test results showed a lower air entry value in the soil & CS specimen in comparison to the sand & CS specimen, which may be attributable to the CS saturation being more effective in the sand then the soil mixture. For the kaolin clay specimen addition of CS increase the water retention capacity of the material. However, the specimen maintains unimodal behaviour.

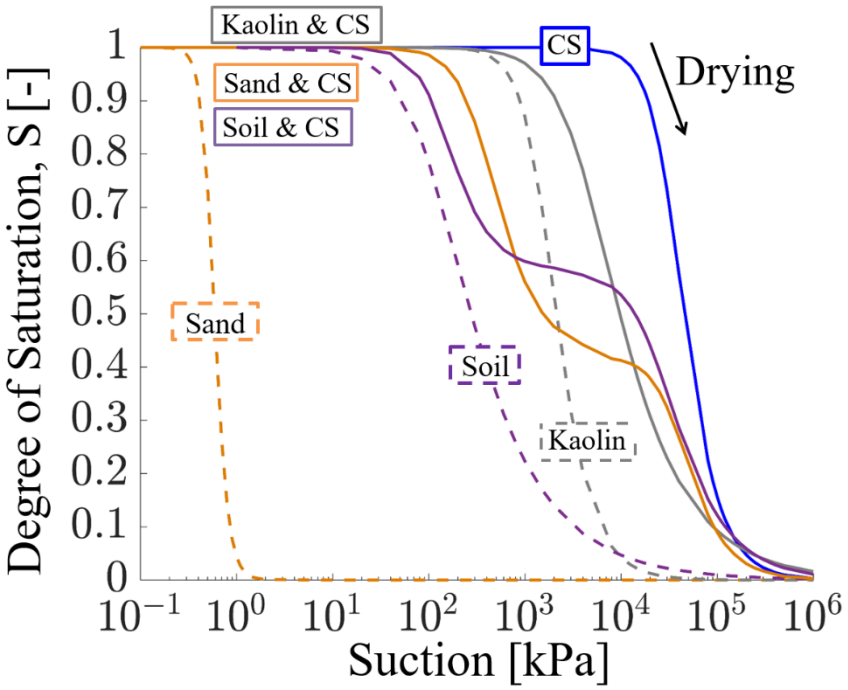

Figure 3-31 Water retention curves for test specimens with (*solid line*) and without (*dashed line*) colloidal silica

These results are important when considering the likely response of colloidal silica treated soils in situ. In the laboratory, rapid uneven drying (or restrained drying), or wetting of extremely dry specimens can result in cracking. This behaviour would be undesirable in field applications where colloidal silica is to be used to create a hydraulic barrier to prevent contaminant migration in an initially permeable soil layer. The water retention behaviour presented here, indicates that very high suctions (10,000-20,000kPa) are

required to desaturate the colloidal silica micropores. Considering also the air entry value of the macropores within the sand-colloidal silica specimens is ~200kPa; this corresponds to a potential capillary rise of ~20m. In temperate climates, i.e. where the water table is generally <20m below the ground surface, as long as the engineered barrier intersects with the water table, then the colloidal silica will remain saturated and colloidal silica treated sands would not crack and the barrier would retain its function to act as a low hydraulic conductivity barrier.

3.7 Conclusion

This chapter presents an investigation into the unsaturated behaviour of soil specimens mixed with colloidal silica grout. A detailed investigation of the water retention behaviour of colloidal silica grout and soil mixtures treated with CS grout is presented here for the first time. The main findings are listed below:

- CS only grout has a high air entry value ~20,000kPa which is attributed to the pores induced on drying between clusters of silica particles (i.e. groups of tens of particles).
- Colloidal silica only specimens cured in water were compared to those cured in a controlled 90% relative humidity environment. These exhibited similar water retention behaviour. Although the specimen cured at 90% RH exhibited a slightly higher air entry value likely due to the influence of suction (during curing) on effective stress resulting in a reduced pore size. Full saturation was achieved via rewetting at 90% relativity humidity.
- The addition of colloidal silica to sand, kaolin clay, and to a sand-10% kaolin mixture resulted in an increase in the first air entry value. The increase in water retention behaviour can be attributed to the reduction of macropore sizes. Images analysis of soil specimens with colloidal silica showed that macropores were filled with colloidal silica.
- Treatment of sand and sand-10% kaolin specimens with colloidal silica resulted in a shift from unimodal to bimodal water retention behaviour. This change can be attributed to the initial desaturation of macropores between soils coated with colloidal silica and/ formation of cracks within macropores filled with CS and the formation of nanocracks between colloidal silica clusters.

Chapter 4. Hydro-mechanical behaviour of colloidal silica grout

In this chapter, the mechanical and hydraulic behaviour of colloidal silica grout (CS) will be presented. To study the behaviour of colloidal silica from a geotechnical perspective, a series of one-dimensional consolidation and direct shear tests were conducted and are presented as two sections in this chapter. In these tests, CS specimens were prepared and cured for varying lengths of time: 1, 2, 4, and 8 weeks under different environmental conditions: water, 2.5% NaCl saline solution, and 90% relative humidity. Furthermore, three CS grouted soil mixtures were investigated: sand, kaolin clay, and sand-10%kaolin.

To date, the reported mechanical behaviour of colloidal silica has mainly considered the undrained behaviour of grouted sand for applications of liquefaction mitigation. Unconfined compressive strength (UCS) tests of grouted soils have reported UCS values up to several hundreds of kPa. Also, increasing concentrations of silica in the colloidal suspension increases the UCS, and the UCS increases with curing time (Persoff et al., 1994, Spencer et al., 2007, Gallagher and Mitchell, 2002, Changizi and Haddad, 2017, Mollamahmutoglu and Yilmaz, 2010). For the context of liquefaction mitigation, grouted sand specimens have also been reported to demonstrate reduced deformation when subjected to cyclic loading (to simulate earthquake loading) in undrained triaxial tests (Gallagher and Mitchell, 2002).

Assessment of the mechanical behaviour of CS grout is critical for the evaluation of its potential for ground stabilisation and hydraulic barrier formation. At many large sites, such as nuclear legacy sites, decommissioning is highly complex, requires the construction of containment structures to prevent both airborne emissions and restrict contaminant migration in the groundwater. Decommissioning works can take many decades, e.g. at the Sellafield site decommissioning works are expected to take ~100 years. Over such long periods, soil grouted using CS to form barriers to inhibit contaminant migration may be subjected to a variety of loading conditions. At present, the long-term behaviour and stability of CS and CS & soil systems remain unknown. Such

barriers could take the form of vertical or horizontal barriers below existing containment buildings, or for example treatment of unlined trenches containing legacy waste.

4.1. 1D compression testing

To examine the hydro-mechanical behaviour of colloidal silica grout and mixtures of soil & CS, typical laboratory testing methods used for geotechnical ground investigations were adopted. In this research one-dimensional oedometer tests were used.

4.1.1. Oedometer test

The basic conventional oedometer cell comprises a rigid ring containing the specimen, which is in contact with two porous stones at the top and bottom surfaces to allow double drainage. Figure 4-1 and Figure 4-2 shows the components and the experimental setup of the test. Oedometer consolidation tests were performed using oedometer rings of 20 mm in height and 75 mm in diameter under saturated conditions according to BSI (2017). Loads were applied in five stages from 25 kPa to 1000 kPa with each load left for 24 hours to consolidate. Unloading was carried out in a single stage to 1 kPa and left for 24 hours. On completion of the test, the specimens were removed weighed and placed in a drying oven for determination of the final moisture content. Vertical displacements were monitored during consolidation at each load step. Initial compliance movements at each loading step due to the system were subtracted from the measured displacements. The coefficient of consolidation and consolidation time (t_{90}) was determined at each loading stage using the conventional Taylor root-time method (Craig, 2004).

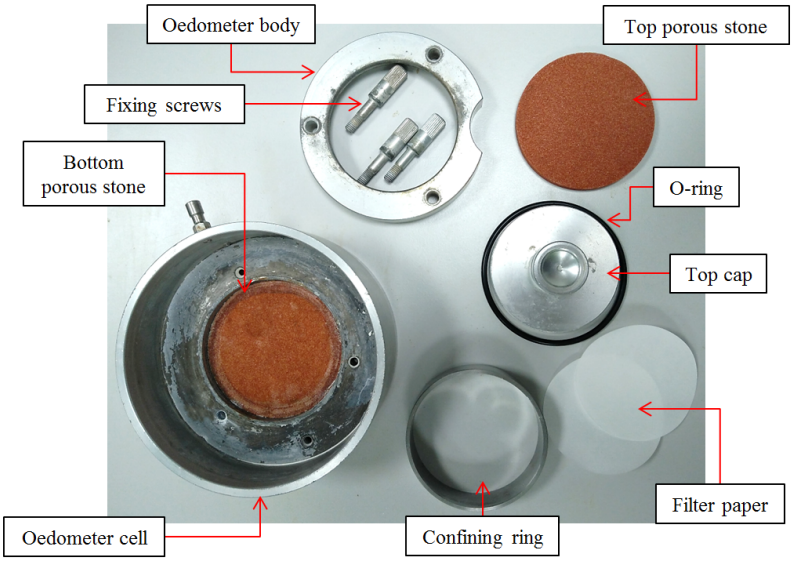

Figure 4-1 A photograph of oedometer test apparatus

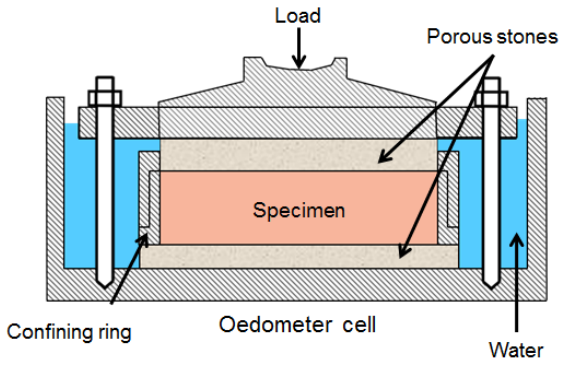

Figure 4-2 Schematic drawing of the experimental setup

4.1.2. Specimen preparation

For oedometer testing, all specimens of CS only and CS & soil were directly gelled and cured in oedometer ring moulds to minimise any specimen disturbance. The moulds were made up of a steel ring (75 mm in diameter and 20 mm in height) attached to a removable plastic base as shown in Figure 4-3. Silicon grease was applied around the contact between the ring and base to preventing grout leakage before gelling.

Colloidal silica specimens

Grout mixtures of colloidal silica and electrolyte accelerators were prepared according to test conditions following the same procedure outlined in the previous chapter. The 'typical' grout mixture used in this study was colloidal silica and 0.28M sodium chloride (NaCl) at a 5 to 1 ratio delivering a 1-hour gel time. Additional, grout mixtures were prepared for comparison purposes using potassium chloride accelerator (KCl) at concentrations of 0.22M and 0.28M. After mixing, a plastic syringe was used to transfer

87 ml of grout mixture into the mould. The mixing and placement procedure lasted approximately 5 minutes for all specimens.

Sand specimens grouted with CS

Specimens were gelled under controlled environment condition of 90% relative humidity at 20 ^{o}C reaching a solid state based at the 1hr gel times. Upon reaching the 1 hr gel time specimens were placed in environmental conditions (water, 2.5% saline water, and 90% relativity humidity) for curing between 1-week to 4-weeks. After curing, the plastic base was removed from the mould, the steel ring moulds (containing the specimens) were directly mounted into the oedometer test cell with filter papers and porous stones at either end.

Kaolin clay specimens

Speswhite kaolin clay with a plastic limit, $W_P = 0.32$ and a liquid limit, $W_L = 0.64$ was used for the experimental study. The grain size distribution showed it to have 0.20 silt fraction and 0.80 clay fraction. Kaolin clay specimens were prepared reconstituted from slurry with a water content of 1.5 times the liquid limit (w = 0.96).

Specimens of kaolin clay mixed with CS were, instead, prepared by hand mixing 100 g of kaolin powder with 153 g of CS. In this way, the ratio between the mass of water (present in the CS) and the mass of solids of kaolin was the same as that for the specimen of kaolin alone ($M_w/M_{s\_kaolin} = 0.96$). The 'typical' CS grout mixture as previously explained was prepared using a NaCl solution to produce a gel time of about 1 hour. Pre-prepared mixtures of kaolin clay and CS were transferred into the oedometer ring moulds. These moulds containing kaolin clay and CS were subsequently left to set, cure, and age using the process described for the CS specimens.

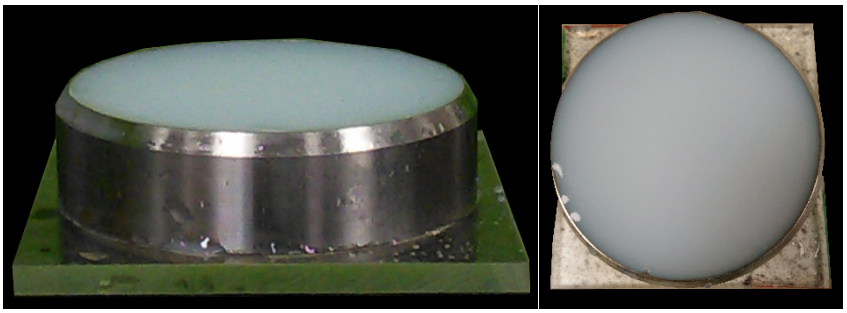

Figure 4-3 Oedometer colloidal silica grout specimen curing in oedometer ring

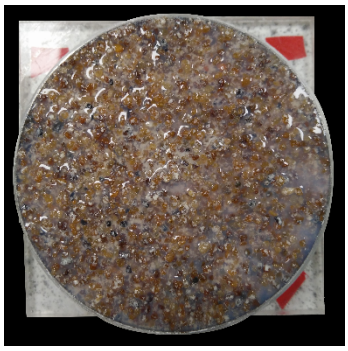

Figure 4-4 Oedometer colloidal silica-sand specimen

4.1.3. Curing conditions and grout gel time

In this study, the 1D compression and hydraulic behaviour of colloidal silica (CS) grout specimens prepared under a range of different conditions were investigated: environmental conditions (water, 90% RH, and 2.5% NaCl solution), curing times (1 week, 2 weeks, 4 weeks, and 8 weeks), grout gel time (1 hour and 5 hours), and grout accelerator type (NaCl and KCl).

Furthermore, CS grouted soil specimens comprising sand and kaolin clay were also investigated. Table 4-1 outlines all oedometer tests performed in this study and their test conditions.

Table 4-1 List of all one-dimensional compression tests performed in the study and their test conditions.

Series	Specimen	Curing time (days)	Curing environment	Gel time [1]
CS-water-1week	0.28M NaCl CS	7	Water	1-hour
CS-water-2week	0.28M NaCl CS	14	Water	1-hour
CS-water-4week	0.28M NaCl CS	28	Water	1-hour
CS-water-8week	0.28M NaCl CS	56	Water	1-hour
CS-2.5%NaCl-1week	0.28M NaCl CS	7	2.5% NaCl	1-hour
CS-2.5%NaCl-2week	0.28M NaCl CS	14	2.5% NaCl	1-hour
CS-2.5%NaCl-4week	0.28M NaCl CS	28	2.5% NaCl	1-hour
CS-90%RH-1week	0.28M NaCl CS	7	90% RH	1-hour
CS-water-LG [2]	0.22M NaCl CS	7	Water	5-hours
CS-water-0.22M KCl	0.22M KCl CS	14	Water	1-hour
CS-water-0.28M KCl	0.28M KCl CS	14	Water	20 mins
Sand & CS	0.28M NaCl CS & Sand	7	Water	1-hour
Kaolin & CS	0.28M NaCl CS & Kaolin	7	Water	1-hour
Sand	Sand only	-	-	-
Kaolin Clay	Kaolin clay only	-	-	-

[1] Standard = grout mixture ~1-hour gel time

[2] LG = Long gel time

4.2. Results: 1D compression tests on CS specimens

4.2.1. Effect of environmental conditions

To investigate the influence of environmental conditions three CS specimens cured in different environmental conditions of water (CS-water), relativity humidity (CS-90%RH), and saline solution (CS-2.5%NaCl) were prepared and tested. All three specimens were cured for 1 week prior to testing prepared with the 'typical' grout mixture i.e. gel time =1hr (see section 4.1.2). Figure 4-5 presents the oedometer compression curves for the three specimens plotted in terms of void ratio against effective vertical stress. For comparison, the plots have been separated into two figures showing the same CS-water specimen result alongside CS-90% RH and CS-2.5% NaCl specimens in Figure 4-5(i) and Figure 4-5(ii) respectively.

The initial void ratio for the CS-90% RH specimen is shown to be lower than the specimen cured in water. The result indicates the occurrence of water loss and shrinkage due to evaporation at environmental conditions of 90% RH. This shrinkage is not fully recovered after saturation in the oedometer cell during testing. Therefore, the initial void ratio at the start of the compression test is smaller than the water cured specimen. The compression behaviour of the CS-water and CS-90% RH specimen in Figure 4-5i shows that the two curves diverge with a stiffer response observed in the specimen cured at 90% RH. An initial average suction of 1620 kPa was measured in a similar CS-90% RH specimen after 1 week of ageing. As such it is reasonable to assume that the "equivalent" vertical pre-consolidation stress is higher than the maximum applied vertical stress applied from testing of 1000 kPa. Thus, the different compression behaviour between the CS-water and CS-90% RH specimen can be explained due to the pre-consolidation stress developed due to the suction stresses developed at 90% RH. The stiffer compressive behaviour in the CS-90% RH specimen can be explained regarding the physical effect of over-consolidation (Skempton and Jones, 1944, Sridharan and Nagaraj, 2000). During testing, pre-consolidation stress was not overwhelmed, consequently, it could not be determined of the normal compressibility could be recovered.

It can be seen in Figure 4-5(ii) that the void ratio against stress behaviour of the CS-water and CS-2.5% NaCl exhibits a similar compression slope. During curing both specimens remained under saturated conditions and after curing the initial void ratio was the same (this was observed for repeat specimens). Despite this the 2.5% NaCl cured specimens

exhibited slightly stiffer behaviour and higher final void ratio. This is likely due to the interaction between the colloidal silica grout and saline solution. It is likely, that the additional electrolytes within the saline solution facilities the formation of additional siloxane bonds within the specimen.

For all colloidal silica specimens tested the expansion index (i.e. the slope of the unloading line) is small with specimens exhibiting very little elastic recovery upon unloading.

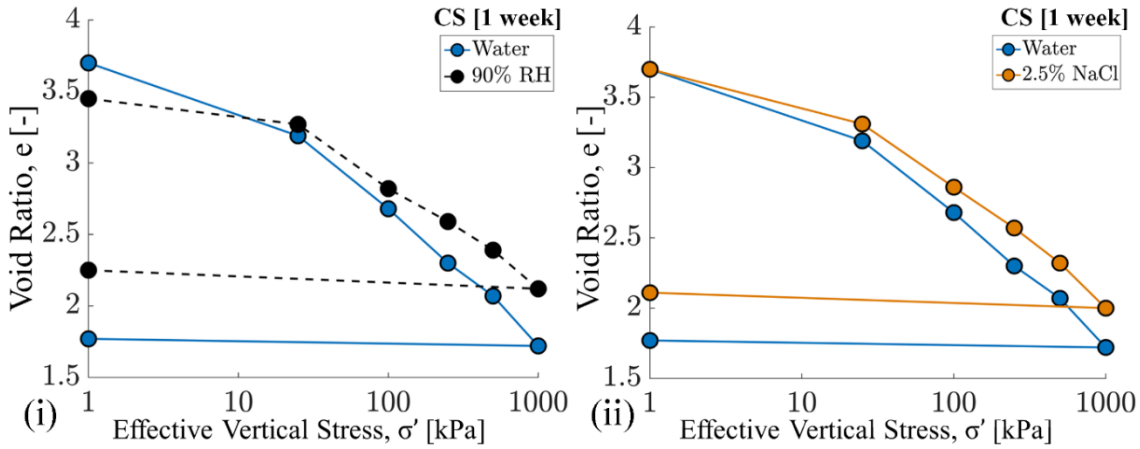

Figure 4-5 Void ratio against stress obtained by the oedometer tests for 0.28M NaCl colloidal silica grout specimens cured in different conditions: (i) water and 90% relative humidity (ii) water and 2.5% saline solution.

4.2.2. Effect of curing time

Several CS specimens were prepared in the same manner and cured under similar environmental conditions (water and 2.5% NaCl) to investigate the influence of curing time. Consolidation tests were carried out on specimens after curing for 1, 2, 4, and 8 weeks. All specimens were prepared with a 'typical' grout mixture stated in section 4.1.2 delivering a 1-hour gel time. An additional load step of 50 kPa was applied for 24 hours in the 'CS-water 8-week' and 'CS-2.5% NaCl 2-week' tests.

Figure 4-6 shows the mechanical behaviour in terms of void ratio against stress for four CS-water specimens cured for 1, 2, 4, and 8 weeks respectively. Since no deformation occurred during curing, the initial void ratio and specimen height are the same for all these specimens. Two comparable compression curves can be observed in the four curves. While all specimens exhibit the similar compressibility post-yield, specimens cured for 4 and 8 weeks appear to have a higher yield stress than those cured for 1-week and 2-week where the yield stress and compression curves are very similar. The curves demonstrate that material stiffness increases with curing time, most likely because of additional particle bonding in CS. This behaviour suggests that additional siloxane bonds continue to be formed after two weeks of curing. As the compression stress increases the compressibility of the 4-week and 8-week specimens become like that of the 1-week and 2-week, although the two pairs of curves never merge. Lastly, all four specimens exhibit the same rebound behaviour from unloading, with all exhibiting little elastic expansion on unloading.

Figure 4-7 shows the compression behaviour of three specimens of CS cured in a saline solution (2.5% NaCl) after 1, 2, and 4 weeks loaded under saturated conditions. Similar to the specimens cured under water, the specimens cured for a longer duration (CS 2.5% NaCl 2-week and 4-week) specimens exhibit a higher yield stress than the CS 2.5% NaCl 1-week specimen). At the maximum vertical stress (1000 kPa), the three curves converge and show similar void ratio. Furthermore, the unloading behaviour of the three specimens appears to be very similar. In the case of the three CS 2.5% NaCl specimens the mechanical behaviour is influenced by the additional curing duration and corresponding chemical interaction from Na^+ and Cl^- ions within the curing solution.

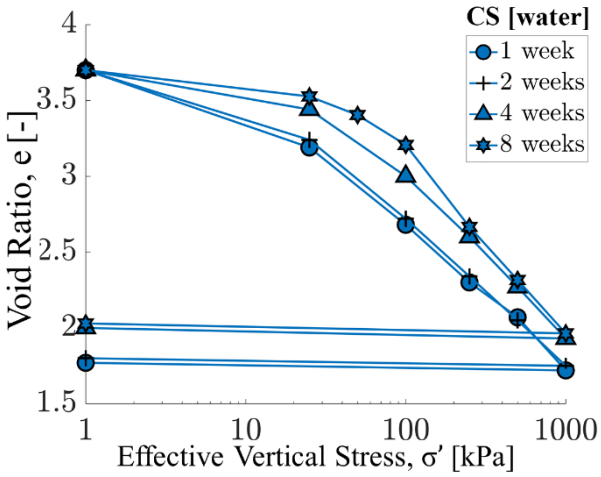

Figure 4-6 Void ratio-stress curves obtained by the oedometer tests for 0.28M NaCl colloidal silica grout specimens cured in water

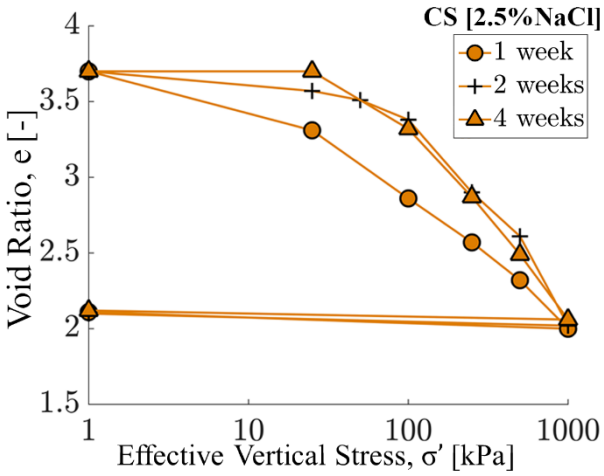

Figure 4-7 Void ratio-stress curves obtained by the oedometer tests for 0.28M NaCl colloidal silica grout specimens cured in saline solution (2.5% NaCl)

4.2.3. Effect of gel time

In Figure 4-8 the effect of the gel time on the one-dimensional compression behaviour of CS was investigated. Two specimens were prepared by mixing CS grout mixture with different NaCl electrolyte solution of 0.28M NaCl and 0.22M NaCl at the same pH value of 7.5, such that specimen gel times were 1 hour (closed symbol) and 5 hours (open symbol) respectively. In both specimens, the same grout accelerator concentration is used. Furthermore, both specimens were cured under the same environmental conditions of water each for 1-week. The two compression curves behave in a very similar manner, with a slightly higher void ratio at 25 kPa in the 1-hour gel time specimen. However, at higher stresses both specimens show the same compression behaviour, demonstrating little mechanical difference arises from the difference in initial gel time of 1 hour and 5 hours.

4.2.4. Effect of electrolyte type used as an accelerator

To investigate the influence of electrolyte species on the mechanical behaviour of colloidal silica grout, three specimens were prepared and cured underwater with different grout accelerators. For comparable results, NaCl and KCl accelerators were used, both comprised of monovalent cations. It is important to note that the cation size of potassium K^+ is larger than sodium Na^+. A 0.28M NaCl specimen and two KCl specimens at concentrations of 0.22M (same gel time of 1hr) and 0.28M (same electrolyte concentration, gel time of 20mins) were tested. The results of the tests are presented in Figure 4-9. The electrolyte solution concentrations at 0.28M NaCl and 0.22M KCl were designed such that both specimens gelled after 1 hour. No change in volume was observed during gelling or curing, and the void ratio at the beginning of the compression test was the same for all specimens. At lower vertical stress, the KCl specimens exhibited a slightly stiffer behaviour than the NaCl specimen. At higher vertical stress, the KCl specimens exhibit a slightly higher compressibility.

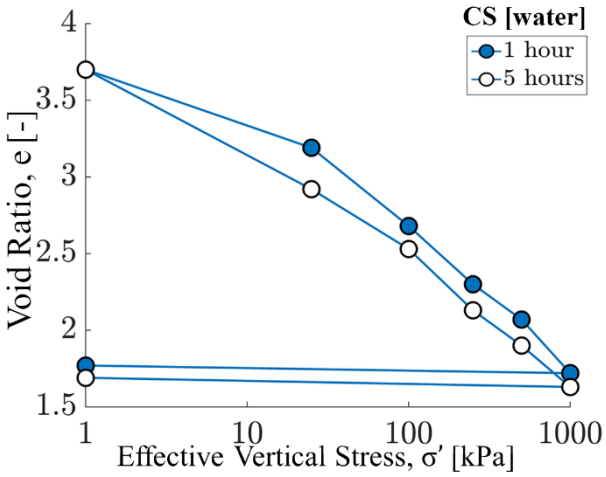

Figure 4-8 Influence of gel time to the relationship of void ratio-stress

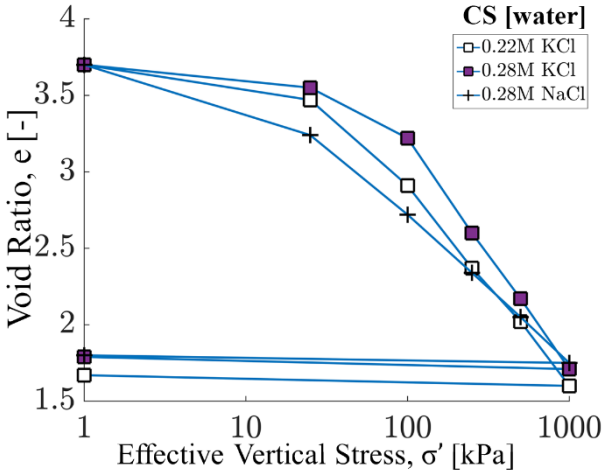

Figure 4-9 Void ratio-stress curves obtained by the oedometer tests for CS grout specimens prepared with different electrolytes cured in water for 2 weeks

4.3. Results: 1D compression tests on soil & CS

The influence of colloidal silica grout treatment on the compression behaviour of soil mixtures was investigated on specimens of sand & CS and kaolin clay & CS. Specimens were prepared following the procedure outlined in section 4.1.2.

Figure 4-10 presents the compression curves for sand only and sand & CS. Both the sand only and sand & CS specimens were prepared with the same mass of sand. The curves of the specimen with CS is initially offset from the sand only curve due to the lower initial void ratio as CS is occupying the available void space. It is understood that the one-dimensional consolidation in sands occurs through three principal mechanism of particle rolling, particle sliding, and particle crushing (due to deformation of grains) at high vertical stresses (Bowles, 1968, Uygar and Doven, 2006). At the microstructural scale, upon vertical loading, particles in the sand only specimen are free to achieve a denser configuration by rearranging into the available pore space through particle rolling and sliding. However, for the sand & CS specimen, the rearrangement of sand particles is inhibited by the presence of the CS particles, which occupies accessible pore space around the sand particles. The overall compression exhibited by the colloidal silica grouted sand is considerably smaller than that observed in the sand only specimen.

Figure 4-11 shows the compression behaviour for CS & kaolin clay specimen and a corresponding kaolin clay specimen reconstituted from slurry. A lower initial void ratio can be seen in the curve of CS & kaolin (again due to voids now being filled with CS) with an initial 'apparent' pre-consolidation stress of around 30 kPa. At higher loads above 30 kPa, the compressibility of the two specimens becomes very similar although the void ratio of the kaolin specimen mixed with CS remains lower (i.e. the specimen is denser) than the specimen reconstituted from the slurry.

Figure 4-12 shows the corresponding effective vertical stress against strain for the same soil & CS specimens presented in Figure 4-10 and Figure 4-11. For sand, the specimen of sand & CS showed less vertical strain in contrast to the sand only specimen. Thus, CS in the pore space of the sand & CS specimen shows that it not only generates a denser specimen, but also a stiffer one. For kaolin clay, the specimen with CS is less compressible than the specimen with kaolin only. The reduced compressibility appears to be related to stiffer behaviour at the lowest load steps, caused by the presence of the CS. While, at higher vertical load, the two specimens have the same compressibility. Upon

unloading, the rebound of the CS & kaolin curve is smaller than the kaolin only curve. Hence, it appears that the presence of CS inhibits the recovery of elastic deformation.

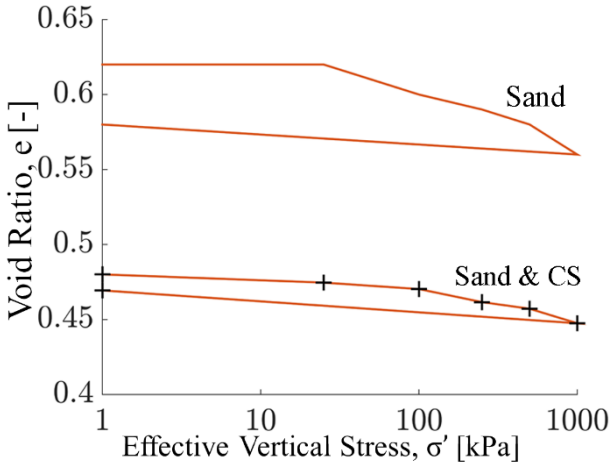

Figure 4-10 Void ratio-stress curves obtained by the oedometer tests for Sand only and Sand & CS

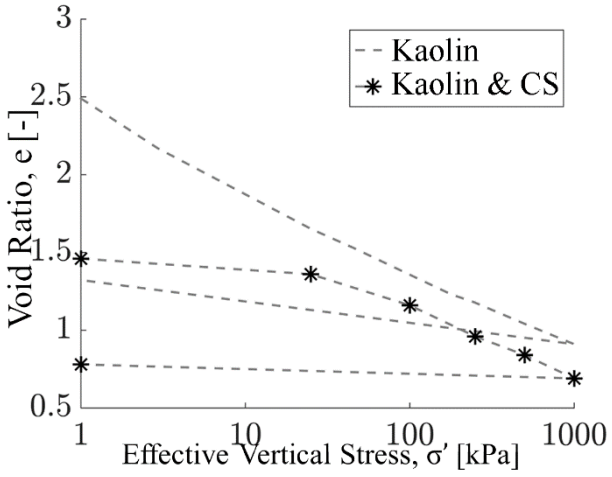

Figure 4-11 Void ratio-stress curves obtained by the oedometer tests for Kaolin clay only and Kaolin clay & CS specimens

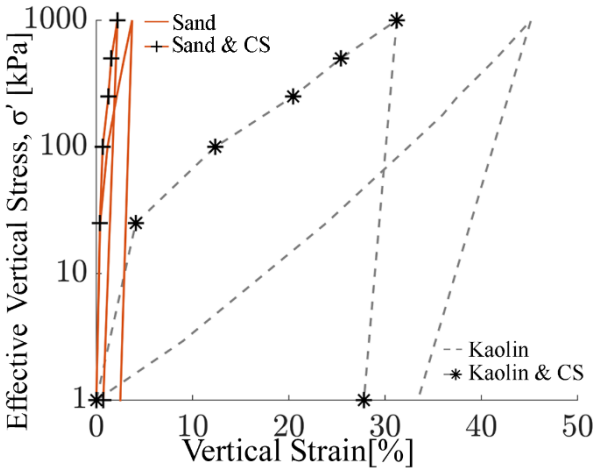

Figure 4-12 Effective stress against vertical strain curves for CS & soil specimens

4.4. Hydraulic behaviour of CS and soil-CS mixtures

Figure 4-13 shows a plot of hydraulic conductivity against void ratio obtained from the 15 oedometer tests on specimens of CS only, sand only, sand & CS, kaolin only and kaolin-CS as in presented section 4.2 and section 4.3. Hydraulic conductivity values, k is presented in terms of m/s. The two soils only results showed the highest hydraulic conductivity values from the oedometer data. For sand, constant hydraulic conductivity was determined in the range of 1.0 x 10^{-6} m/s similar to findings by Sobti and Singh (2017). Kaolin clay only results showed hydraulic conductivity values ranging from ~1.0 x 10^{-8} to 5.0 x 10^{-9} m/s decreasing with decreasing void ratio. In the case of sand addition of CS reduces the hydraulic conductivity value to 5.0 x 10^{-9} m/s, i.e. by more than 2 orders of magnitude. In the case of kaolin & CS, the addition of CS reduces the hydraulic conductivity to 1.0 x 10^{-9} to 5.0 x 10^{-11} m/s (up to 2 orders of magnitude).

Moreover, from the plot, results of CS only specimens prepared under different environmental conditions and curing times display hydraulic conductivity values ranging from 10^{-9} to 10^{-12} m/s for void ratios from 3.7 to 1.9. With the exception of the sand only specimen the hydraulic conductivity was observed to decrease as the void ratio decreased.

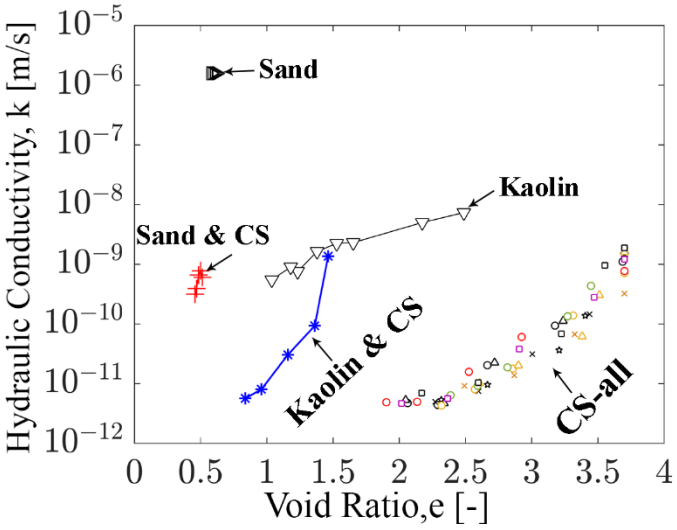

Figure 4-13 Hydraulic conductivity against void ratio for all oedometer test specimens: colloidal silica only, soil & colloidal silica, and soil only.

4.5. Shear testing of colloidal silica grouted soil

A series of direct shear tests were carried out on sand and kaolin soil mixtures grouted with MP320 colloidal silica (CS). The objective of these tests was to determine the influence of curing conditions and time after gelling on the stress-strain behaviour of the MP320 grouted specimens.

Shear strength of soils provides essential knowledge required for any form of stability analysis. The process of shear failure occurs by the slippage of soil particles, one on another, which may lead to the sliding of one body of soil relative to the surrounding mass. Failure occurs when the shear stresses set up in the soil mass exceed the maximum shear resistance which the soil can offer, i.e. its shear strength.

Presented by Mohr in 1900, failure along a plane in a material occurs by a critical combination of normal and shear stress. The functional relation of this theory between normal and shear stress on the failure plane can be expressed as follows (Das, 2009).

$$\tau_f = f(\sigma_f) \tag{4.1}$$

where τ_f is shear stress at failure and σ_f is normal stress on the failure plane.

The Mohr-Coulomb failure criteria in accordance with the principle that shear stress in a soil can be resisted only by the skeleton of solid particles, shear stress expressed as a function of effective normal stress on the failure plane (σ_f') is shown.

$$\tau_f = c' + \sigma_f' . tan\phi' \quad (4.2)$$

where τ_f is the shear strength, c' is cohesion and ϕ' is the angle of internal friction determined based on effective normal stresses.

Direct shear tests determine the shear strength of soils along a predetermined failure surface typically located at the mid-height of the specimen. A schematic of the shear box instrument used for shear tests is shown in Figure 4-14. During testing one half of the test specimen is made to slide relative to the other by the action of a steadily increasing horizontal shear force, while a constant load is applied normal to the plane of relative movement (Head, 1992). The failure plane of the test specimen may not necessarily be along the weakest plane. As a result, the planes of principal stress may rotate during the test with the distribution of stresses along the plane of shear being non-uniform. Despite its limitation, the direct shear test is useful because of its simplicity for practical application and is used widely in geotechnical engineering (Caruso and Tarantino, 2004). For a comparative study of specimens treated with and without CS, the technique is deemed suitable as these limitations can be reasonably assumed to affect all samples in the same way and differences in response can still be detected.

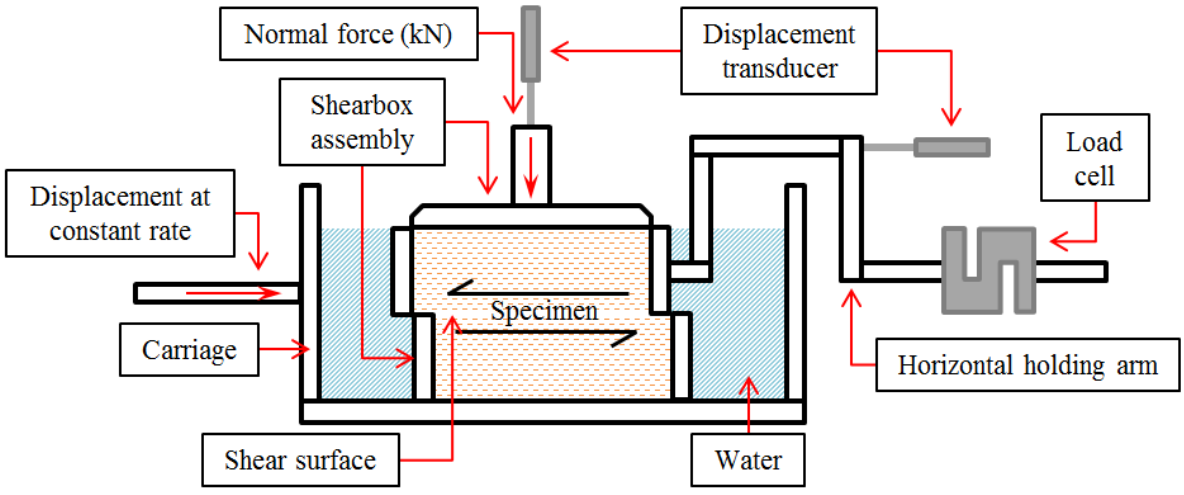

Figure 4-14 Schematic of the shear box layout

4.5.1. Shear box test

Drained direct shear box tests were conducted using a digital direct shear apparatus (ELE International, Sheffield, UK) according to BS1377-7 standard (BSI, 1990). The instrument consists of a shear box assembly for holding test specimens, a shear box carriage running on roller bearings, and step motor drive unit to apply constant rate

horizontal displacements. Figure 4-15 shows the various components of a shear box assembly. For measuring the horizontal shear force and both horizontal and vertical displacement, the apparatus is equipped with a 5 kN capacity load cell and two displacement transducers for measuring the specimen movement. Vertical load are applied with a lever-arm loading system with 10 : 1 beam ratio (Caruso and Tarantino, 2004).

To ensure excess pore water pressure generated in the soil is completely dissipated by drainage, the shearing rate was kept as low as reasonably possible. From consolidation data of the CS specimens, it was determined that a very low shearing rate of 0.001 mm/min was required to prevent pore water pressure build-up. All CS specimens were sheared at this rate, with each test, therefore, taking place over a period of approximately 6 days. Drained conditions were maintained throughout the test duration. Normal effective stresses of 100, 200, and 300 kPa were applied to reflect stress at the near subsurface. The internal dimensions of the shear box body were 60 x 60 mm and 20 mm height.

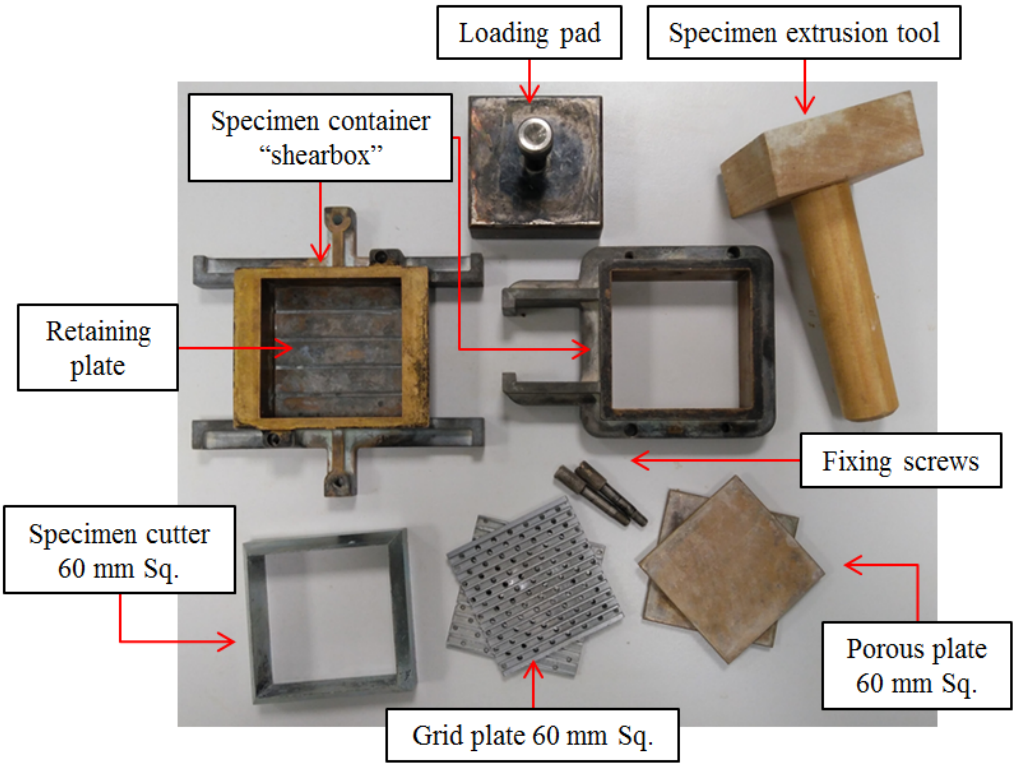

Figure 4-15 Components of a shear box assembly

4.5.2. Specimen preparation

Three soil compositions (sand only, kaolin clay only, and sand & kaolin mixture) were investigated in this research as is and grouted with colloidal silica (CS). Table 4-2 shows the properties of the sand and kaolin (Speswhite) clay used in this study. Sand & kaolin clay mixtures were prepared by mixing sand with 10% by dry mass of kaolin clay.

All specimens were prepared in moulds made up of a steel square (60 mm x 60 mm x 20 mm height) attached to a plastic base with silicon grease as shown in figure 4-16. The plastic base attached by silicon grease prevented leakage of CS grout during the gelling process. After curing and subsequent ageing, the plastic mould bases were simply detached. Using an extraction tool, grouted soil specimens were removed without damage and placed into the shear box.

Table 4-2 Soil properties

Property	Sand	Kaolin Clay
Diameter, d_{50} [µm]	1242	-
Nominal Effective Size, [mm]	1.01	-
Coefficient of Uniformity, C_u [-]	1.26	-
Specific Gravity, G_s [-]	2.65	2.6
Liquid Limit, w_L [%]	-	64
Plastic Limit, w_p [%]	-	32

(a) (b) (c)

Figure 4-16 Shear box specimen preparation soil & colloidal silica (CS) (a) specimen mould, (b) specimen in the mould, and (c) cured test specimen removed from the mould.

4.5.2.1. Sand & CS

Sand & CS specimens were prepared by placing 124 g of dry sand into a shear mould as shown in Figure 4-16b. Each mould of sand was then saturated with 28 ml of colloidal

silica grout Figure 4-16c. A 0.28M NaCl colloidal silica grout mixture prepared in a 5:1 ratio of colloidal silica to accelerator was used for all shear box specimens. This mixture delivered an equivalent gel time of 1-hour. After gelling of the colloidal silica, specimens were kept inside the moulds to cure in water. Cured specimens were then tested in the shear box after 7 days (1-week) and after 28 days (4-weeks).

4.5.2.2. Kaolin & CS

Kaolin & CS specimens were prepared following the same procedure described for oedometer specimens (see section 4.1.2). Shear results of kaolin clay reconstituted from slurry and consolidated to 50, 100, 150 and 300 kPa were taken from Glamheden (2010) and Galvani (2003).

4.5.2.3. Sand-10%Kaolin Clay & CS

Mixtures of sand and kaolin clay were prepared at weight proportions of 10% by dry weight of kaolin clay to sand denoted as Sand-10%Kaolin clay. Sand-10%Kaolin Clay & CS specimens were prepared following the same procedure described for Sand & CS shown in Figure 4-16.

4.5.2.4. CS specimen

Figure 4-17 shows damaged specimens of colloidal silica only that were prepared for shear box testing. Following the same procedure outlined for Soil & CS, CS only specimens were prepared and gelled in shear moulds (Figure 4-16). However, after curing, the removal and subsequent placement of CS specimens into the shear box regardless of curing period resulted in specimen damage as shown in Figure 4-17. Consequently, specimens of CS only were unable to be tested in the shear box.

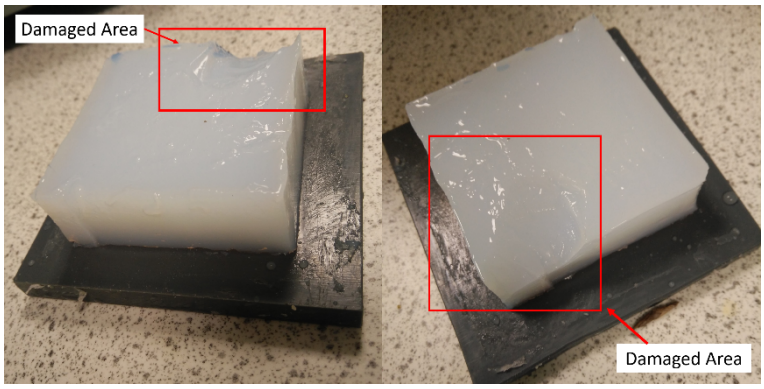

Figure 4-17 Shear box colloidal silica only specimens

4.5.3. Drained direct shear tests: testing campaign

In this study, 27 drained direct shear tests conditions were performed to examine the shear behaviour of soil & CS mixtures. Table 4-3 presents a description of soil and colloidal silica grout specimens investigated in drained direct shear test alongside details of each test conducted. Three soil mixtures were considered as part of this study (sand, kaolin clay, and sand-10% kaolin clay). CS grouted mixtures of each soil condition were test under normal stresses of 100 kPa, 200 kPa, and 300 kPa. The same CS mixture of 0.28M NaCl delivering a 1-hour gel time was used for all shear testing after aging of 1 week and 4 weeks.

Variations in symbols and colours were used to denote specimen type and normal effective stress respectively for each test condition investigated. Shear test result plots were generated with symbols used at every 50th measured data point to maintain a clear distinction between each test plot

Table 4-3 List of soil and colloidal silica grout specimens used in drained direct shear test and details of each test carried out

Series	Specimen	Curing time	Curing environment	Shear rate [mm/min]	Normal stress, σ [kPa]
SB_S	Sand only	-	-	0.1	100, 200, 300, 400, 600
SB_K	Kaolin clay[1] ([1]data from literature)	-	-	0.02 - 0.005	50, 100, 150, 300
SB_SK	Sand-10% kaolin clay	-	-	0.001	100, 200, 300
SB_SCS-1W	Sand & CS	1 week	Water	0.001	100, 200, 300
SB_SCS-4W	Sand & CS	4 weeks	Water	0.001	100, 200, 300
SB_KCS-1W	Kaolin clay & CS	1 week	Water	0.001	100, 200, 300
SB_SKCS-1W	Sand-10% kaolin clay & CS	1 week	Water	0.001	100, 200, 300
SB_SKCS-4W	Sand-10% kaolin clay & CS	4 weeks	Water	0.001	100, 200, 300

SB = shear box test, S = Sand, K = Kaolin clay, SK = Sand & kaolin, CS = Colloidal silica, and W = week

4.6. Results: Shearing behaviour of sand

Test results presented in Figure 4-18(i) show the shear stress normalized by the effective vertical stress vs horizontal strain and in Figure 4-18(ii) the volumetric change in terms of vertical strain against horizontal strain for three sand specimens (SB_S) at different effective normal stresses. Shearing was carried out under saturated conditions. All specimens were sheared to at least 10 % horizontal strain. Different coloured symbols are used to designate specimens tested at different normal stresses.

From Figure 4-18(i), it can be observed that at higher vertical stress the peak ratio of shear stress ratios/effective vertical stress ($\frac{\tau}{\sigma'_v}$) was lower; at 300 kPa corresponding to a ratio of 0.87. Likewise, at a lower vertical stress 100 kPa, the peak normalized shear stress ratio was higher at 0.99. As expected all specimens tend towards the same value of ultimate shear strength.

Figure 4-18(ii) presents the corresponding volumetric behaviour of these specimens. Positive vertical strain values indicate the occurrence of dilation (an increase in the volume of the sheared specimen), whereas negative volumetric strain represents contraction (a decrease in volume of the sheared specimen) (Head, 1992). At the higher vertical stress of 300 kPa, the sand exhibits a compressive behaviour, as the vertical stress decreases to 200 and 100 kPa the volumetric behaviour becomes dilative.

The shear strength and effective normal stress relationship of results from drained direct shear tests of sand only specimens are shown in figure 4-19. In addition to the test results shown in Figure 4-18 peak and ultimate shear strength results were determined from 15 further tests at the effective normal stresses of 100, 200, 300, 400, and 600 kPa. Determined from the shear envelope a peak angle of shearing resistance, ϕ'_{peak} of 42^o and ultimate angle of shearing resistance, ϕ_{ult} of 37^o was determined. In both cases, the envelopes were forced to pass through the origin, i.e. no cohesion was allowed.

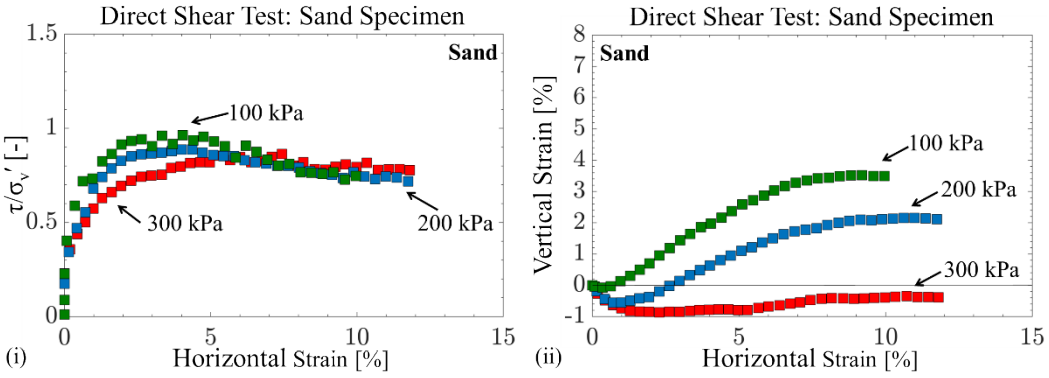

Figure 4-18 Direct shear test data for sand specimens i) normalized shear stress ratio vs horizontal strain, ii) vertical strain vs horizontal strain

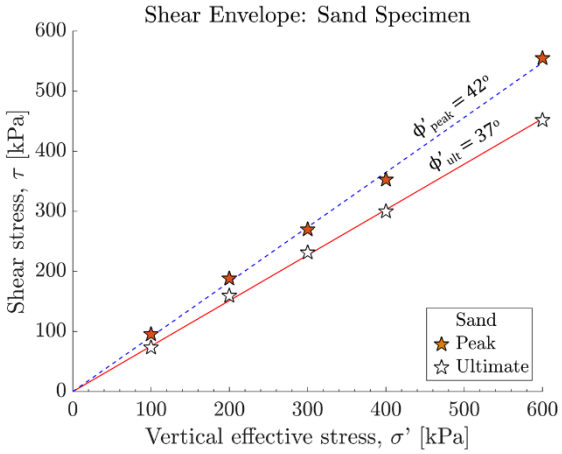

Figure 4-19 Shear envelope for sand specimens (SB_S) passing through the origin

4.7. Results: Shearing behaviour of sand & CS

Figure 4-20 shows the relationship of normalized shear stress ratio vs horizontal strain, and Figure 4-21 shows the vertical strain vs horizontal strain. Results from specimens of sand only (SB_S), sand & CS cured for 1-week (SB_SCS-1W) and sand & CS cured for 4-weeks (SB_SCS-4W) have been plotted. Test specimens of sand & CS are plotted with open symbols representing specimens cured for 1-week prior to testing; closed symbols denote specimens cured for 4-weeks. All shear tests were conducted under saturated conditions following test details outlined in Table 4-3.

Influence of colloidal silica grouting of sand specimens across all test specimens demonstrated increased peak shear strength. This effect can be observed by comparisons between sand only specimens and the six sand & colloidal silica specimen curves shown in Figure 4-20. The peak shear strength values of 1-week and 4-weeks sand & CS specimens were similar at 100 kPa and 300kPa, indicating no influence of ageing period on the peak shear strength. However, the results of testing at 200 kPa Figure 4-20(ii) indicate higher peak shear strength in the 4-week sand & CS specimen than the 1-week specimen. In all cases, specimens with CS exhibited peak shear strength much higher than the corresponding sand only. After the peak, the ultimate shear strength of the sand & colloidal silica specimens generally approximates to the ultimate shear strength of the sand material itself.

As illustrated in Figure 4-20(i) both 1-week and 4-week cured sand & CS specimens exhibited greater dilatancy behaviour than the sand only specimen and that dilatancy increases for longer ageing periods. A similar effect can be seen at in Figure 4-20(ii), and Figure 4-20(iii) sand & CS specimens all exhibit more dilative behaviour than the corresponding sand only specimen. However, the volumetric behaviour of sand & CS at higher vertical stress (200 and 300 kPa) exhibits a greater difference in comparison to the corresponding sand only specimen.

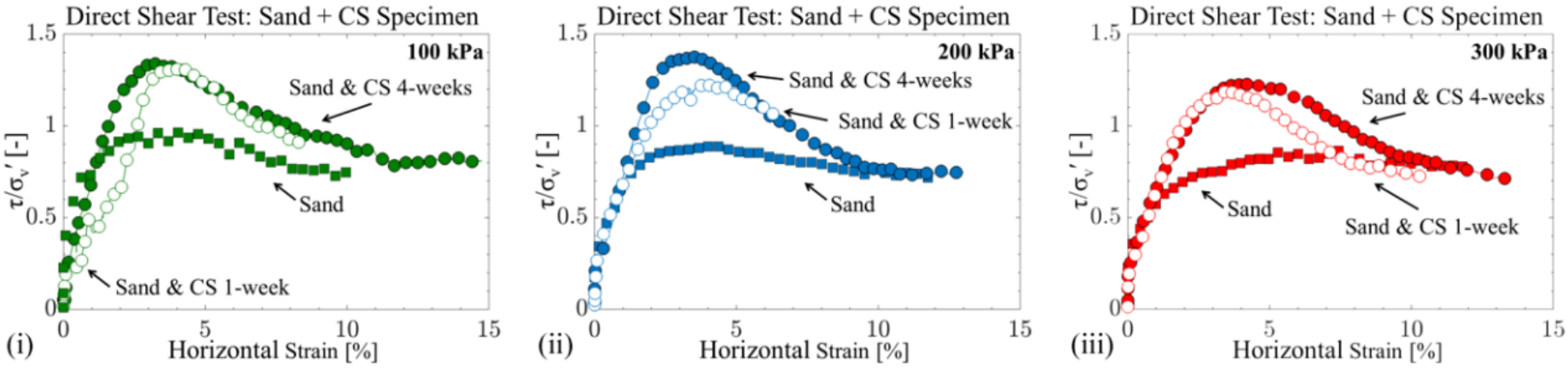

Figure 4-20 Direct shear results for sand & 0.28M NaCl CS specimens shear stress vs. horizontal strain i) 100 kPa, ii) 200 kPa, and iii) 300 kPa

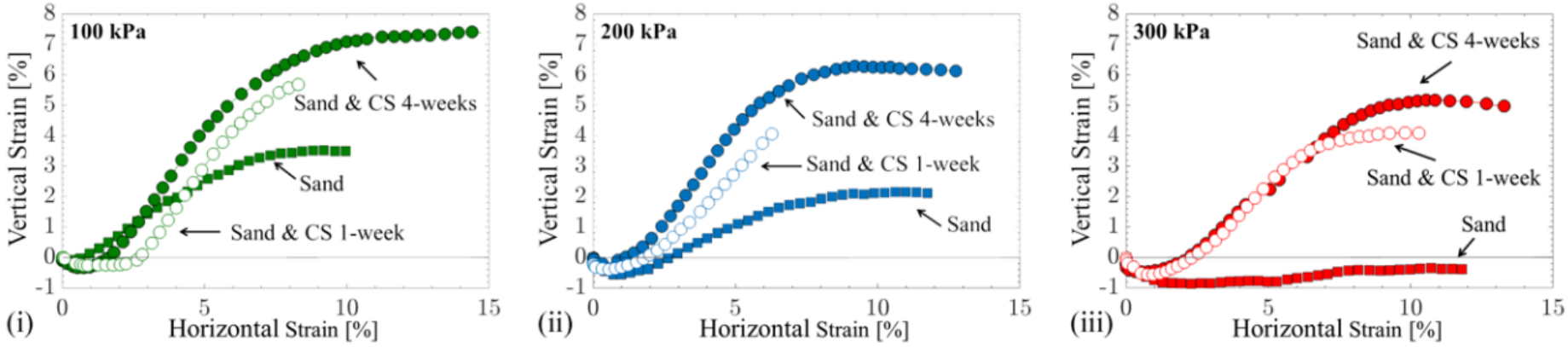

Figure 4-21 Direct shear results for sand & 0.28M NaCl CS specimens vertical strain vs. horizontal strain. i) 100 kPa, ii) 200 kPa, and iii) 300 kPa

4.7.1. Shear envelope

Figure 4-22i shows the peak shear envelope for all the sand & CS tests shown in Figures 4-20 and 4-21. An average peak angle of shearing resistance, ϕ'_{peak} of 49° for sand & CS specimens was determined, compared to the sand only specimens ϕ'_{peak} was 42°. In addition, the sand & CS specimens exhibited a drained cohesion of 21 kPa, which is attributed to the bonding provided by the CS before failure. The ultimate angle of shearing for both sand only and sand & CS specimens were the same at ϕ'_{ult} = 37° as shown in Figure 4-22ii. A slight difference was 0.26 kPa cohesion to the ultimate shearing resistance behaviour in the sand & CS.

This behaviour occurs because the continuous matrix of CS that surrounds the sand particles provides a weak bonding between particles, which macroscopically generates some cohesion until the CS matrix is broken along the shearing plane. After failure, the presence of the CS prevents compression upon shearing; forcing a dilative behaviour (Figure 4-21), which in turn increases the peak resistance. However, once the strength of the CS matrix is overwhelmed the sand particle-to-particle friction controls the ultimate conditions.

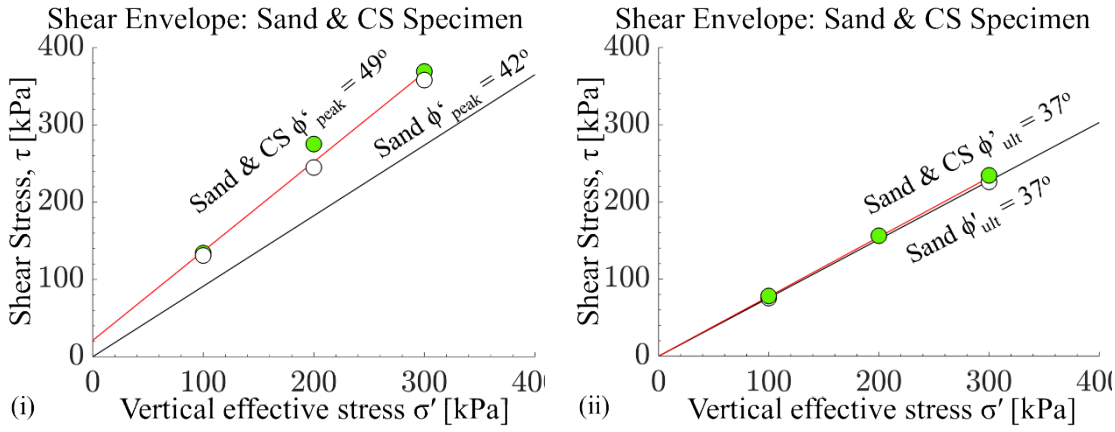

Figure 4-22 Shear envelope for sand & CS specimens 1-week (open), 4-week (closed). i) Peak, ii) Ultimate

4.8. Results: Shearing behaviour of kaolin clay

Figure 4-23 shows the results of shear tests performed on kaolin clay reconstituted from slurry and consolidated to 50, 100, 150, and 300 kPa data from (Glamheden, 2010) and Galvani (2003). A pronounced peak shear stress is not observed in any of the tests. All specimens exhibit compressive behaviour. The ultimate angle of shearing resistance, ϕ'_{ult} for the kaolin clay specimens was determined as 16° with a 1.7 kPa drained cohesion (Figure 4-24). No peak conditions were considered.

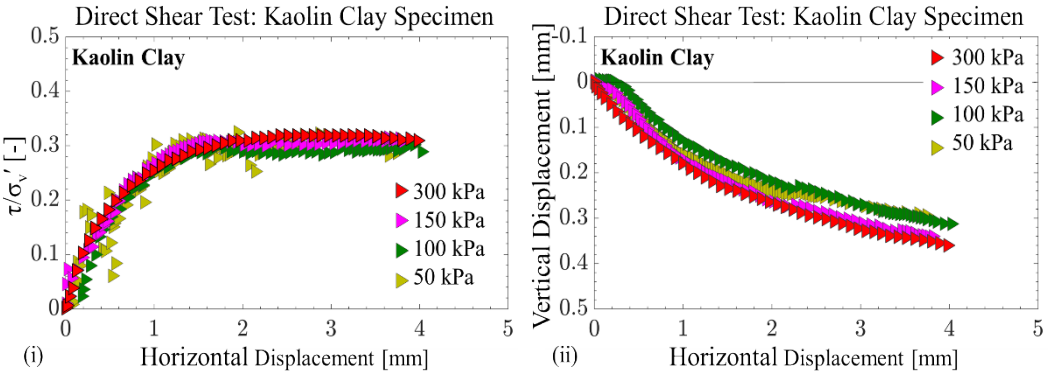

Figure 4-23 Direct shear test data for kaolin clay specimens i) normalized shear stress ratio vs horizontal strain, ii) vertical strain vs horizontal strain

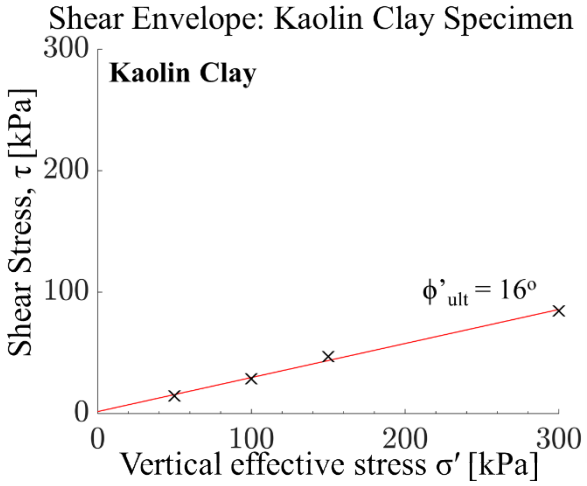

Figure 4-24 Shear envelope for kaolin clay specimens

4.9. Results: Shearing behaviour of kaolin clay & CS

The behaviour of kaolin clay & CS specimens at vertical effective stresses of 100, 200 and 300 kPa is shown in Figure 4-25. For comparison, the data for kaolin clay only specimens are also plotted. A more pronounced ultimate shear stress/effective vertical stress ratio peak is shown than in the tests performed with kaolin only. Based on the curves a similar behaviour is exhibited between the two specimens of kaolin clay & CS tested at 200kPa and 300kPa with a shear stress/vertical stress ratio peak value of about 0.45 and an ultimate value of about 0.37. The 100 kPa kaolin clay & CS specimen exhibited a slightly higher ultimate shear stress/ effective vertical stress ratio than the corresponding specimens tested at 200kPa and 300 kPa.

Compressive behaviour is exhibited in all kaolin clay & CS specimens (Figure 4-25(ii)). The degree of compression decreases with increasing vertical stress with the 300 kPa specimen being the least compressive. Moreover, specimens with CS were shown to be more compressible than samples prepared with kaolin clay only, with the exception of the 300 kPa specimens which demonstrated similar behaviour.

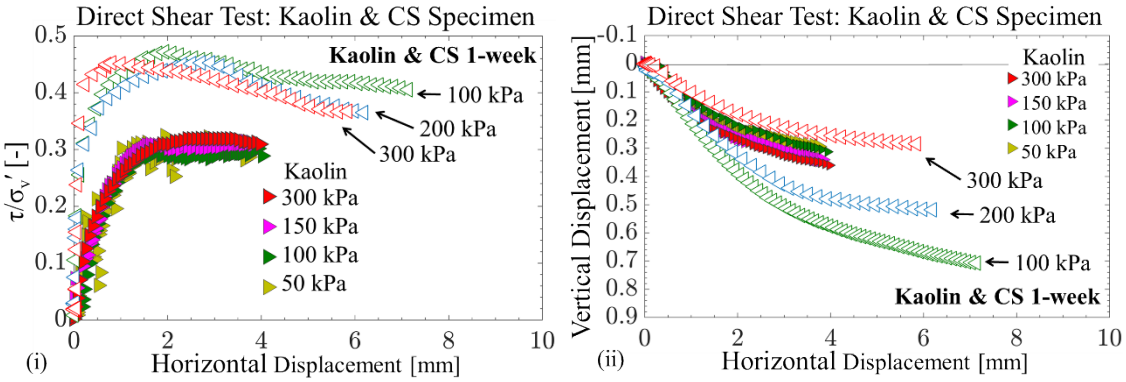

Figure 4-25 Direct shear test data for kaolin clay & CS specimens i) shear stress vs horizontal displacement, ii) vertical displacement vs horizontal displacement

4.9.1. Shear envelope

The shear envelope for both the peak and ultimate shear strength is plotted in Figure 4-26. Using a linear fit, an angle of shearing resistance ϕ'_{peak} =24° and ϕ'_{ult} =19 ° was determined for peak and ultimate conditions for kaolin clay & CS specimens. Likewise, drained cohesions of 3 kPa for peak and 5 kPa for ultimate shear strength conditions were calculated. Comparatively, grouting of kaolin clay with CS showed an increase in the angle of shearing resistance in terms of both peak and ultimate shear strength compared to kaolin only specimens. A similar drained cohesion for both kaolin only and kaolin specimens mixed with CS was determined, suggesting that no relevant particle bonding due to the CS grouting is formed.

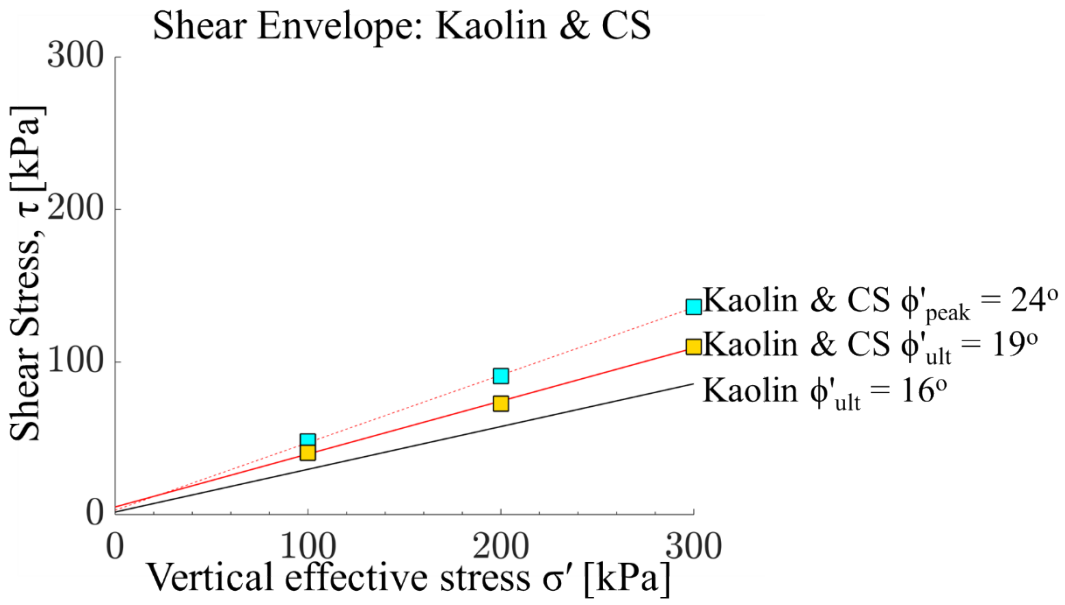

Figure 4-26 Shear envelope for kaolin clay & CS specimens

4.10. Results: Shearing behaviour of sand-10% kaolin clay

From Figure 4-27, the direct shear test results of sand-10% kaolin clay specimens was carried out at effective vertical stresses of 100, 200, and 300 kPa. The behaviour of the three specimens varies slight dependent upon the applied vertical load; although none of the specimens exhibit a distinct peak shear strength value. Computed from the figure the ultimate angle of shear resistance, $\phi'_{ult} = 36^o$ and drained cohesion, c' = 14.5 kPa (Figure 4-28).

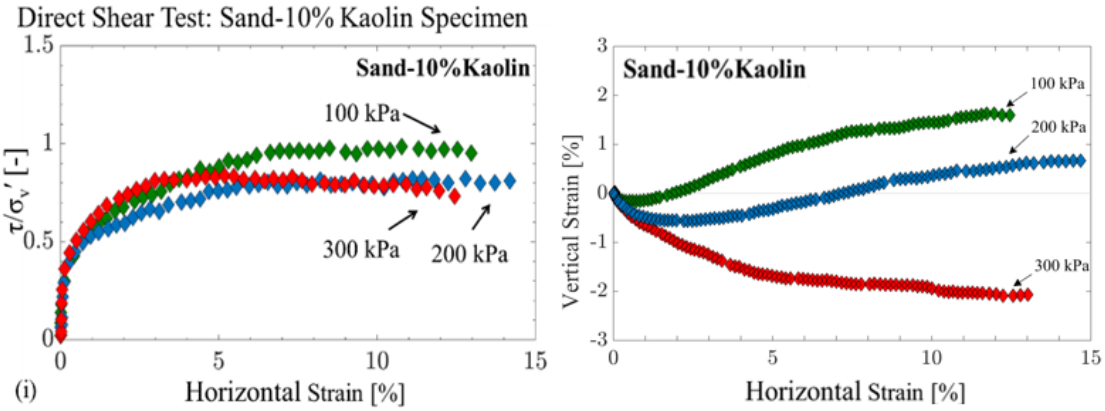

Figure 4-27 Direct shear test data for sand-10% kaolin clay specimens

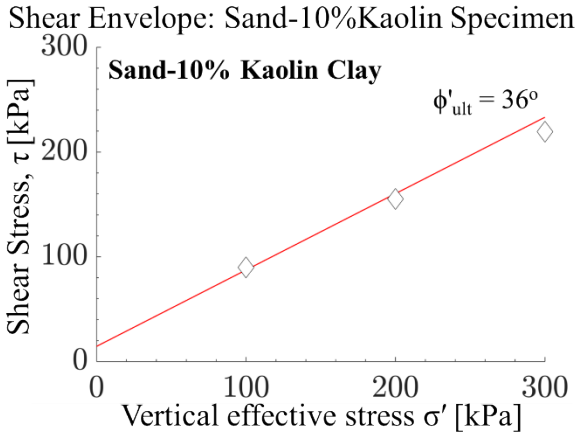

Figure 4-28 Shear envelope for sand-10% kaolin clay specimens

4.11. Results: Shearing behaviour of sand-10% kaolin clay & CS

The relationship of shear stress/effective vertical stress against the horizontal strain and vertical strain against horizontal strain for sand-10% kaolin clay & colloidal silica specimens is shown in Figure 4-20. Tests specimens with colloidal silica (CS) are plotted with open and closed triangle symbols representing specimens cured for 1-week and 4-weeks respectively. Likewise, effective normal stresses of tests are presented as green, blue, and red to represent 100, 200, and 300 kPa respectively.

The peak value of shear stress/effective vertical stress is higher for specimens treated with colloidal silica at each of the effective normal stresses. In the 100 kPa and 200 kPa tests with CS, the specimens exhibited a more pronounced peak behaviour than in the corresponding specimens without CS. For the 300 kPa test, the behaviour of the sand-10% kaolin clay & colloidal silica specimens performs similarly to the ungrouted soil only specimen (Figure 4-20iii). Test results of all the Sand-10%kaolin & CS specimens converge towards the ultimate shear strength of the ungrouted soil.

Furthermore, the influence of additional curing between 1-week and 4-weeks did not affect the behaviour of the 100 kPa and 300 kPa CS with tests both resulting in similar values of peak and ultimate shear strength. At 200 kPa test the 4-week specimen exhibiting a higher shear stress/effective vertical stress peak ratio than the corresponding specimen that was cured for 1-week.

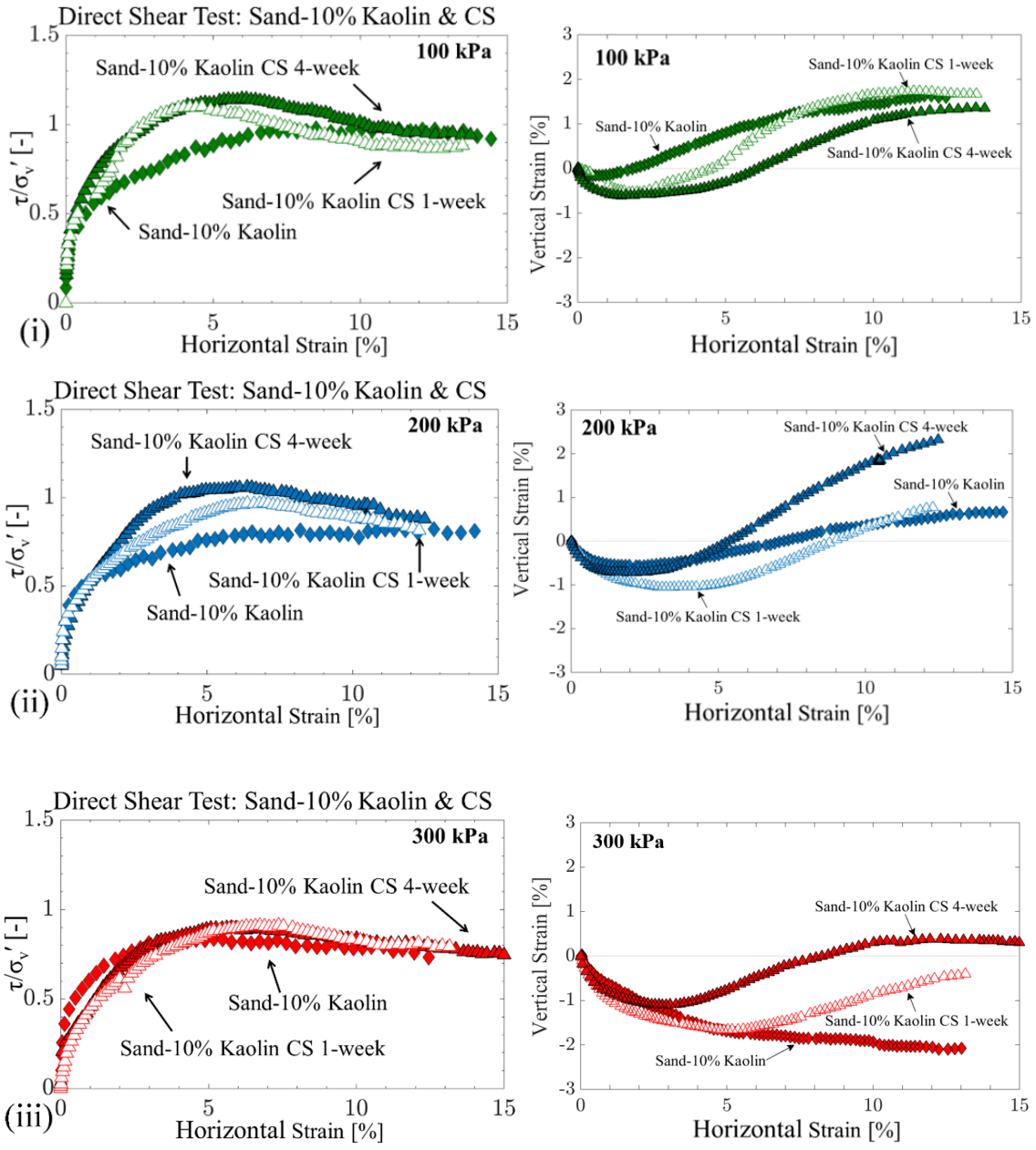

Figure 4-20 Sand-10% Kaolin clay & 0.28M NaCl colloidal silica specimens shear stress vs. horizontal strain and vertical displacement vs horizontal displacement i) 100 kPa, ii) 200 kPa, and iii) 300 kPa

4.11.1. Shear envelope

The shear envelope for sand-10% kaolin clay & CS specimens is shown in Figure 4-21. Results from tests indicate the influence of CS grouting leading to a peak friction angle ϕ'_{peak} = 39º and c' = 36 kPa. Notably, the peak friction angle has increased only slightly from the untreated ultimate friction angle of the ungrouted specimens (ϕ'_{ult} = 36º). Whereas the drained cohesion has increased considerably from 14.5kPa in the ungrouted specimen to 36kPa for the CS grouted specimens. The ultimate friction angle is shown to be the same for the grouted and ungrouted sand and kaolin clay specimens, ϕ'_{ult} = 36º.

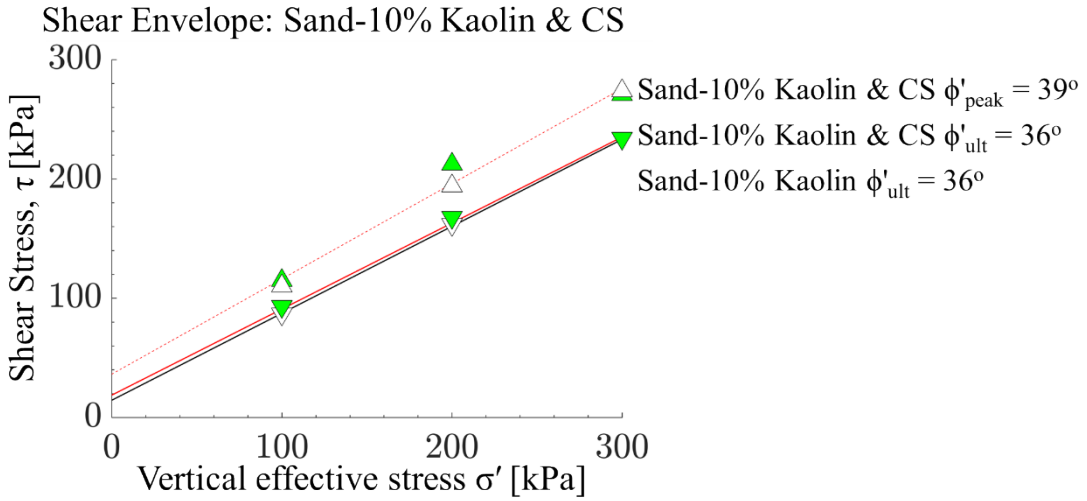

Figure 4-21 Drained shear strength failure envelope

4.12. Discussion: Interaction of colloidal silica grout and soil

A conceptual model for particle configuration in the sand only and sand & CS is shown in Figure 4-22. In the oedometer tests shown in Figure 4-10 and Figure 4-12, upon compression, the presence of CS reduced the overall volumetric deformation exhibited by grouted sand samples with increased stiffness over the range of stresses investigated. Within the conceptual model for the sand only specimen, upon vertical compression, sand particles are free to achieve a denser configuration by rearranging into the pore space. Conversely, the rearrangement of sand particles in the sand & CS specimen is inhibited by the presence of the colloidal silica particles already present within any accessible pore space around the sand particles as shown in Figure 4-23. Therefore, the presence of CS in the pore space, not only generates a denser sample but also a stiffer one. Likewise, hydraulic conductivity is significantly decreased due to the presence of CS filling the pore spaces between sand particles.

Similarly, considering the shear behaviour of sand & CS, because of the continuous matrix of CS that surrounds the sand particles a weak bond between particles exists, generating cohesion until the CS matrix is broken along the shearing plane (Figure 4-22). After failure, the presence of the CS prevents compression upon shearing, forcing a dilative behaviour (Figure 4-21), that in turn increases the peak resistance. However, once the strength of the CS matrix is overwhelmed the sand particle-to-particle friction controls the ultimate conditions.

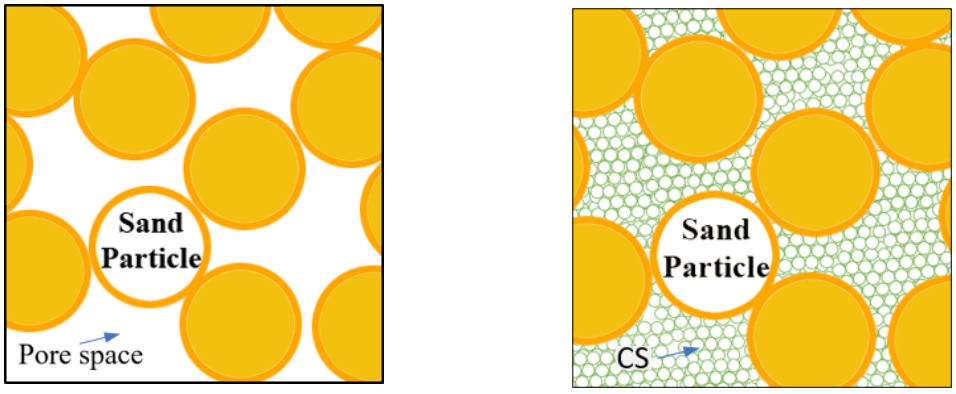

Figure 4-22 Conceptual model for particle configurations i) sand ii) Sand & CS

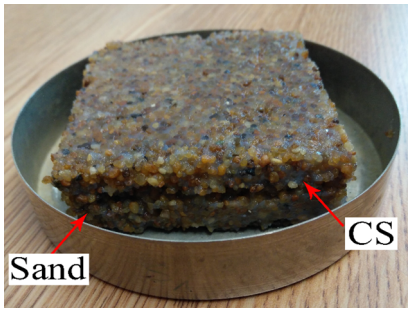

Figure 4-23 Sand & CS shear specimen

A simplified conceptual model of particle configurations for kaolin clay only and kaolin clay & CS is shown in Figure 4-24. Firstly, a kaolin clay only particle configuration is shown highlighting the characteristic hexagonal platy appearance (Mitchell and Soga, 2005). Secondly, two regions of kaolin clay & CS particle configurations are shown as identified via SEM, regions where (i) kaolin particles dominate with isolated CS particles (Figure 4-24ii) and (ii) regions where CS particles dominated with isolated kaolin particles (Figure 4-24iii) respectively. Upon vertical compression, the kaolin clay & CS specimens showed a reduced volumetric deformation and increased stiffness at low stresses, above 100kPa the compressibility of the kaolin clay & CS was found to be like that of the kaolin clay only.

In the sub-regions where kaolin particles dominate (Figure 4-24ii) the kaolin clay & CS particle configuration is comparable to the arrangement of kaolin clay only. However, since CS is present within the pore water space, the kaolin clay & CS particle structure is denser and therefore stiffer. Likewise, in the CS dominate sub-regions of kaolin clay & CS (Figure 4-24iii) the density is higher than a specimen with CS particles only, due to the reduced amount of water present, as water is shared with the kaolin clay particles. Both sub-regions are therefore expected to be at higher density and consequently exhibit a stiffer behaviour. During vertical compression, as the vertical stress increases (exceeding 100 kPa) the difference in density (and water content) between the kaolin clay & CS and the kaolin clay only specimen decreases. Consequently, similar compressibility behaviour is exhibited by both specimens at higher stress (Figure 4-11). This behaviour suggests that the macroscopic compression is governed by the kaolin clay particles for both specimens.

The micro-mechanisms controlling the shear strength of clays are not well understood and are therefore difficult to discuss here (Morgenstern and Tchalenko, 1967, Sridharan and Rao, 1973, Tarantino and Tombolato, 2005). At a macroscopic scale the peak shear strength and ultimate shear strength of kaolin clay both increased due to mixing with CS, whereas the drained cohesion increased only slightly as shown in Figure 4-25. It may be expected that the frictional resistance between silica to silica contact compared to kaolin-kaolin contact is higher increasing the peak shear stress, which explains why the ultimate condition of the kaolin clay & CS specimen remains higher than the clay only specimen. Additionally, the distance between kaolin clay particles is reduced, increasing the number of kaolin clay particle contact. As a result, the presence of CS to kaolin clay improved both the interfacial bond strength and the ultimate frictional resistance. Similar, findings were reported by Changizi and Haddad (2017) and Landman et al. (2014)

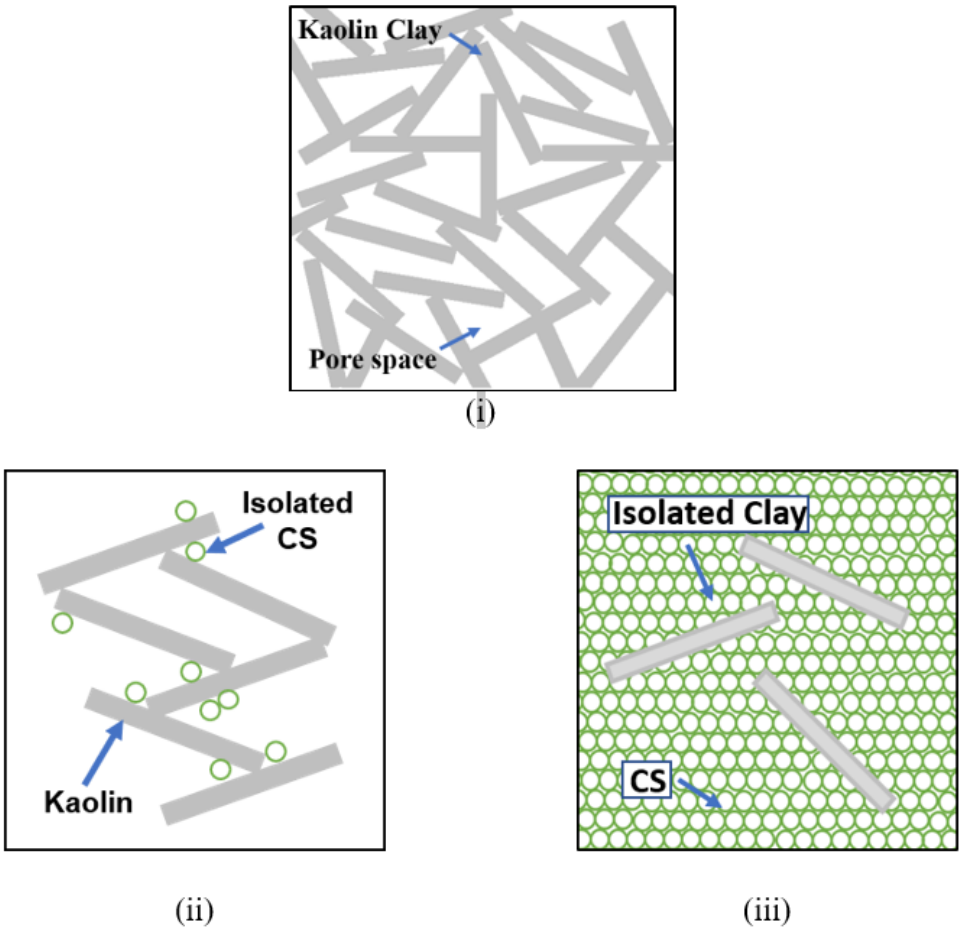

Figure 4-24 Conceptual model for particle configurations i) kaolin clay, ii) kaolin & isolated CS, and iii) isolated kaolin & CS,

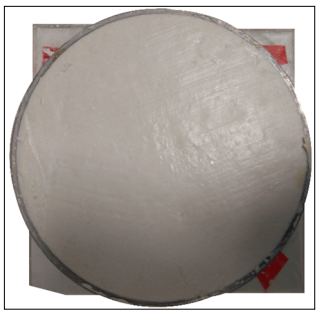

Figure 4-25 Kaolin & CS oedometer specimen

In the case of the sand and kaolin mixture, the soil skeleton is formed of grain to grain contacts, with the finer particles partially filling the large interparticle pores (Figure 4-26). A conceptual model of the particle configurations for the sand and 10% kaolin clay mixture is shown in Figure 4-27. The large sand particles form the soil skeleton and leave large interparticle pores between the coarse particles, which are partially filled with kaolin particles in the sand and 10%kaolin clay specimen. In the corresponding specimen mixed with CS, the interparticle pores present between sand grains are filled with both kaolin and CS (Zhao et al. 2013). It can be seen from the shear test results that the addition of kaolin clay within the sand mixtures reduces the peak shear resistance compared to sand only. In a similar manner to sand only the addition of CS to sand-10% kaolin specimens generates a more pronounced peak shearing resistance. However, once overcome the ultimate shearing resistance is governed by the soil mixture of sand-10%kaolin clay, which is similar to that of the sand only specimen (i.e. it is the sand-sand contacts governing ultimate shear strength).

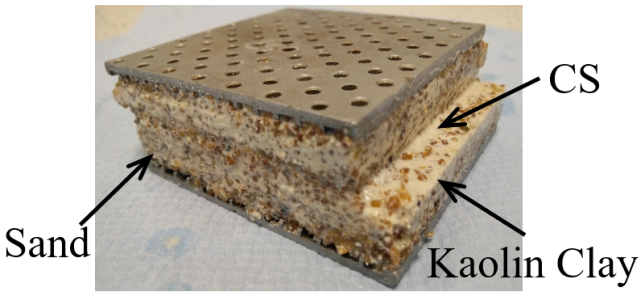

Figure 4-26 Sand-10% Kaolin Clay & CS shear specimen

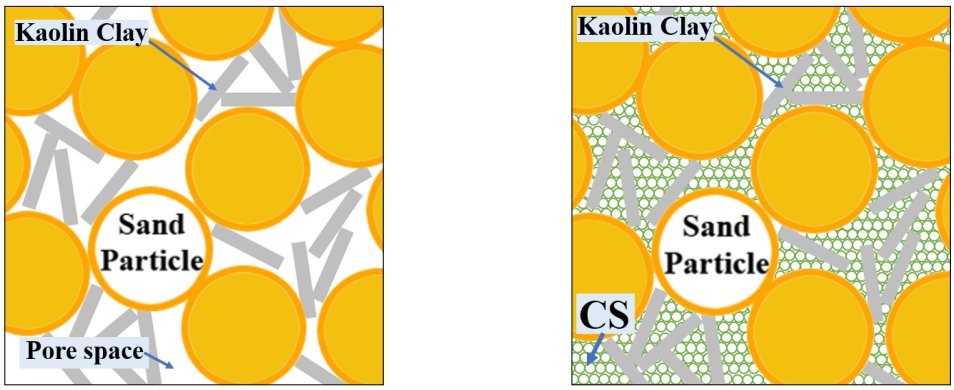

Figure 4-27 Conceptual model for particle configurations i) sand-10%kaolin clay ii) sand-10%kaolin clay & CS

4.13. Conclusion

This chapter presents the drained mechanical behaviour, in terms of compression and shearing behaviour of colloidal grout (CS) only and soil mixtures of sand, kaolin clay, and sand-10%kaolin clay grouted with CS. Additionally, the hydraulic behaviour of CS and soil & CS specimens are examined. It is well understood that the CS has a low hydraulic conductivity and can be adopted for application for controlling fluid flow in porous media. In addition to its hydraulic behaviour, this work has illustrated for the first time that under drained conditions CS can provide mechanical improvement. In the case of sand, CS grout is capable of increasing material stiffness beyond that of sands and enhancing the peak friction angle. In addition, this can be achieved while maintaining a very low hydraulic conductivity (~10^{-10} m/s), typical of intact clay. Likewise, this work also presents results on kaolin clay mixed with CS which have the potential to be novel materials. Their application could be deployed in environments where not only hydraulic containment is critical but where reduced deformation and resistance to shearing would be beneficial, for example in landfill capping or in the outer fill layers of embankments designed to minimise internal seepage and infiltration.

Chapter 5. Gelation behaviour of colloidal silica grout

Colloidal silica has significant potential for hydraulic barrier formation in a range of applications including to (i) control radionuclide migration at nuclear sites, (ii) to seal rock fractures in tunnelling and underground construction operations and (iii) to control fluid-flow during hydrocarbon extraction. Despite the demonstrated potential of colloidal silica in the literature, research has not yet translated into widespread industrial use. A key factor in this limited commercial uptake is the lack of understanding regarding the influence of grout composition and environmental conditions on gel time and viscosity evolution (Trompette and Clifton, 2004). In the past, the difficulty of predicting the gel time for in-situ conditions has prevented the exploitation of colliodal silica in grouting campaigns in particular in coastal or marine environments with elevated salinity (e.g. Dounreay shaft isolation project, Donalsons Associates Ltd, 2006 and Jurinak and Summers, 1991). Two issues have inhibited grout use in saline environments: first, if local untreated water is employed for grout preparation, there is an inability to control the grout gel time, second, even where grout is prepared with fresh water, interactions with local groundwater may cause premature gelling of the grout front and compromise barrier emplacement and performance.

Furthermore the lack of understanding regarding grout gelling is also restricting the manner in which colloidal silica is currently being deployed in practice. At present, colloidal silica for grouting purposes is sold as two components, which are mixed together on site to give a gel time set by the manufacturer. An ability to predict gel time would enable grouting contractors to design their own mix of the components to achieve their desired gel time, for example reducing the colloidal silica content in order to increase the gel time and hence achieve greater penetration. This would greatly extend the engineering applications in which colloidal silica could be deployed.

This chapter presents an extensive experimental study to establish the gelling behaviour of colloidal silica grouts for a broad range of grout compositions and environmental conditions. To investigate the gelation characteristics of colloidal silica based grouts a series of preliminary gel state assessment tests were conducted based on a gel state qualitative assessment developed by Sydansk (1990). Further to this, a detailed study investigating the effect of varying pH, accelerator electrolyte, accelerator cation valency, accelerator molar mass, silica particle size, silica concentration, and temperature on the grout viscosity evolution and gel times was conducted. These experimental results underpinned the development of an analytical model of colloidal silica grout gelling as presented in Pedrotti et al., (2017). At the end of the chapter, this analytical model is applied to a case study to demonstrate how in situ conditions could be taken into account during grout mix design.

5.1. Colloidal silica grout

Colloidal silica is formed from a stable aqueous suspension of microscopic silica particles SiO_2. Silica nanoparticles are approximately uniform in size and are generally range in size from several to hundreds of nanometres. Colloidal silica solutions can be destabilised through the addition of an accelerator electrolyte compound, inducing a rapid viscosity increase. This mechanism of viscosity increase is known as gelation. Upon destabilisation, siloxane bonds are formed and the colloids form a connected gel network. The gelation rate and gel time is controlled by varying several factors that influence solution stability including particle size, particle concentration, pH, electrolyte concentration, valency, and temperature (Iler, 1979, Bergna and Roberts, 2005).

The viscosity behaviour of colloidal silica grout is that of an evolutive Newtonian fluid where viscosity remains low and initially constant and then rapidly increases over time, rather than a pure Newtonian fluid (where viscosity remains constant until setting) as found with other chemical grouts or a Bingham fluid (where viscosity rises continually) such as cementitious particulate grouts. Photographic images of colloidal silica grout gelation behaviour are shown in Figure 5-1. The images highlight the various phases of viscosity development from an initial low viscosity mixture similar to water (see Figure 5-1(i)) to a rigid gel (see Figure 5-1(iii)). Figure 5-2 shows a typical viscosity

development profile of colloidal silica over time. The gel time (t_{gel}) is defined by the intersection of the linear regression of all the points at viscosity higher than 2000 mPas and the x-axis (Bergna and Roberts, 2005, Jurinak and Summers, 1991).

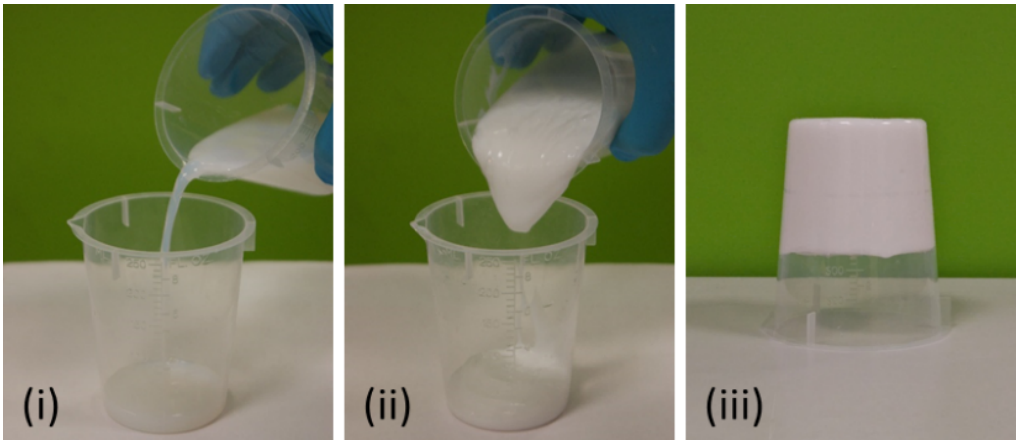

Figure 5-1 Gelling behaviour of colloidal silica grout over time (i) initial highly flowing low viscosity, (ii) barely flowing, & (iii) rigid gel.

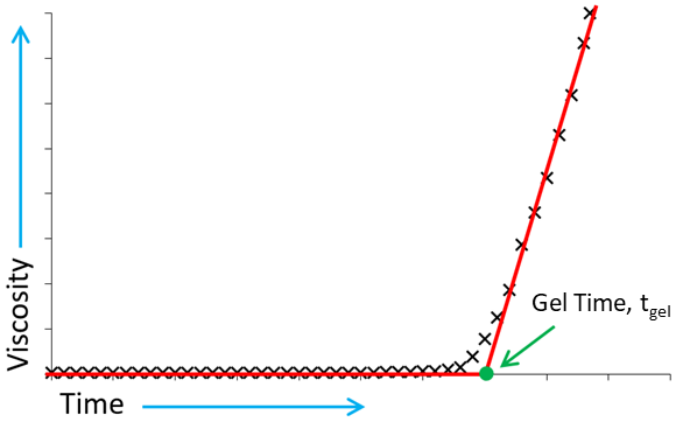

Figure 5-2 Viscosity development of colloidal silica grout over time

5.2. Gel-state experimental study

5.2.1. Material & method

5.2.1.1. Specimen preparation

In this study, the same type of colloidal silica solution was used as in the previous chapters; MasterRoc MP320. MP320 is a colloidal silica suspension which is destabilised by the additions of an electrolyte accelerator, with no solvent or toxic components. According to the manufacturer specifications MP320 has a dynamic viscosity of around 10 cP (water at 20°C has a viscosity of ~1cP), a density of 1.3 g/cm^3, a pH of 9.5 to 9.8, and a 40 ± 1 % silica concentration (by weight) (BASF, 2014). All specimens were prepared in a 5:1 ratio of colloidal silica to electrolyte accelerator by volume respectively.

For gel state tests, all specimens were prepared using a NaCl electrolyte accelerator at concentrations ranging from 0.017 M to 0.333 M (Table 5-1). To investigate changes in pH conditions, HCl and NaOH were used to adjust the grout solution pH. The pH varied from 3 to 8 in 0.5 increments (Table 5-1). Values of pH above and below this range resulted in a stable colloidal silica solution with significant longer gel times beyond reasonable use for practical application and therefore were not considered. Colloidal silica grout mixtures were prepared with 200 ml of colloidal silica solution and 40 ml electrolyte accelerators together to achieve a 5 to 1 solution ratio. Final measurements of solution pH were measured using an Oakton PC700 pH meter. Individual specimens were prepared by transferring 24 ml of the colloidal silica grout mixture at the test pH value into a 50 ml centrifugal test tubes. Specimens were prepared within 5 minutes of initial mixture of colloidal silica solution and electrolyte accelerator.

To test if the presence of sand influences the gelling behaviour, gel state tests were also conducted on a series of sand specimens saturated with colloidal silica grout. Specimens were each prepared by firstly filling the test tubes with washed and dried Leighton Buzzard sand and then subsequently saturated with colloidal silica grout prepared using a 0.333 M NaCl accelerator.

Table 5-1: Colloidal silica specimens for gel state tests

Type of CS	Silica concentration (weight %)	Accelerator	Final accelerator concentration (M)	pH
MasterRoc MP320	40	NaCl	0.017 to 0.333	3 to 8

5.2.1.2. Determining the gel state time

The gel state assessment scale (see Table 5-2) and testing method outlined by Persoff et al. (1999) and Sydansk (1990) were used in this study. The gel state can be examined by observing the movement of the colloidal silica grout mixture and a glass marble within a test tube as illustrated in Figure 5-3 and Figure 5-4. The gel state assessment scale provides a semi-quantitative measurement of gelation rate and gel strength. The specimen gel state can be determined by considering the speed at which marble movement occurs. Initially, at gel state 1 the movement of the marble from one end of the tube to the other would take less than one second. As the gelling proceeds, an increase in gel state can be observed by the increased time taken for the marble movement within the grout solution upon inversion as the grout becomes more viscous. Gallagher (2000) considered gel states 4 & 5 to occur if the movement of the marble upon inversion took longer than 15 seconds. Specimens are considered to have achieved gel state 9 if no movement of the gel is observed upon tiling the centrifuge tube 90° to the horizontal.

In this study, the time taken to achieve gel state 9 (rigid gel) was examined for each colloidal silica grout mixture. Once the colloidal silica grout mixes were prepared (see section 5.2.1.1), the following steps were undertaken for testing:

1. 24 ml of the colloidal silica grout mixture was poured into a 50 ml plastic centrifugal test tube with a glass marble using a plastic syringe.
2. A cap was placed on the test tube to seal the mixture and time recorded.
3. The tube was inverted at time intervals ranging from minutes to hours dependant on grout mixture specimen.

4. The movement and flow of the grout mixture in the tube was observed using the marble within the tube as guidance.
5. Periodically the movement and flow of the grout mixture was examined by gently tilting the tube.
6. The time at which no movement of the grout mixture nor the marble was observed upon tiling the test tube 90° to the horizontal was recorded, corresponding to gel state 9.

The same procedure was followed for the gel state 9 assessment of sand + CS specimens with movement of the gel surface used to assess gel state (i.e. no marble was used in these specimens).

Table 5-2: Gel test state assessment descriptions (Persoff et al., 1999)

State	Gel state descriptions
1	No detectable gel formed. Gel appears to have the same viscosity as the original solution.
2	Highly flowing gel. Gel appears only slightly more viscous than original polymer.
3	Flowing gel.
4	Moderately flowing gel.
5	Barely flowing gel.
6	Highly deformable non-flowing gel.
7	Moderately deformable non-flowing gel.
8	Slightly deformable non-flowing gel.
9	Rigid gel. There is no gel-surface deformation.
10	Rigid ringing gel. Tuning-fork-like mechanical vibration can be felt.

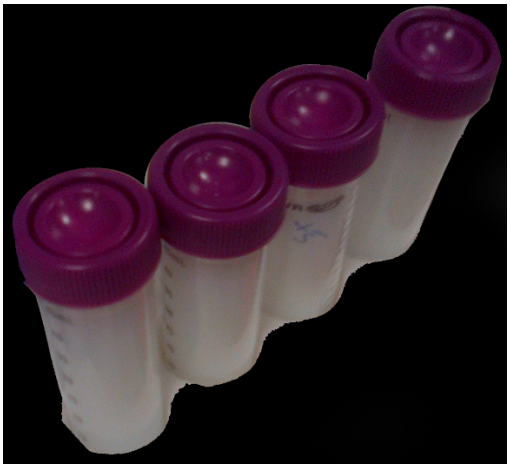

Figure 5-3 Gel state test specimens

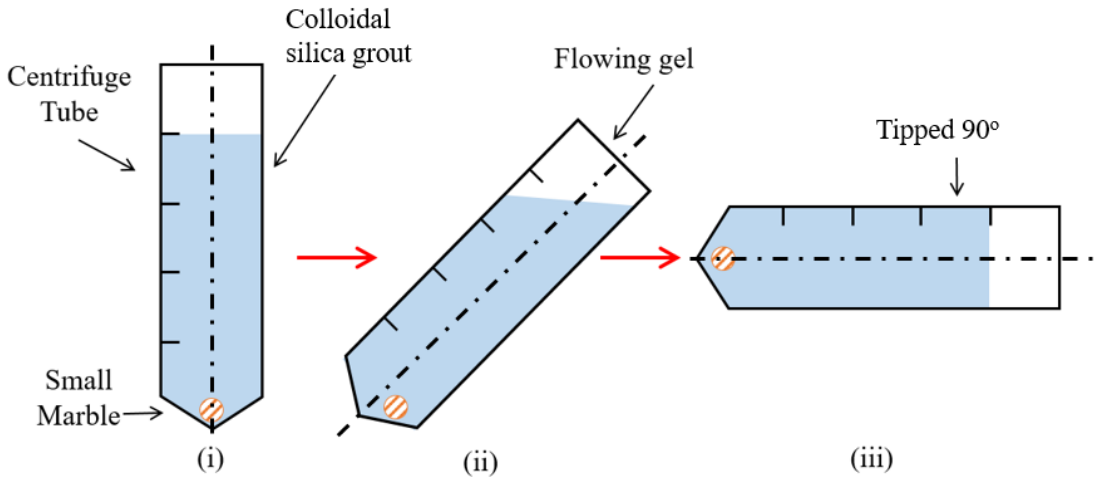

Figure 5-4 Gel state test (i) Initial position (ii) Flowing gel (iii) Rigid gel with no deformation of grout at grout/air interface at 90° horizontal.

5.2.2. Results

Figure 5-5 presents the time taken to reach gel state 9 for specimens of colloidal silica grout with final concentrations of NaCl of 0.017 M and 0.333 M NaCl. For both grout mixtures, a range of specimen pH solutions was tested from 3 to 8. It is clearly shown that increasing the NaCl concentration acts to reduce the time to reach gel state 9. This effect was more significant at higher pH values (>5.5). For example, at pH=7, increasing the NaCl concentration from 0.017M to 0.333M reduced the gel time from 16,000 to 40 mins, whereas at pH = 3 the same increase in NaCl concentration resulted in only a very slight reduction in the time taken to achieve gel state 9. It can also be observed that increasing the NaCl concentration acted to also shift the pH at which the minimum time to reach gel state 9 occurred. For the colloidal silica specimens prepared using 0.017 M NaCl, the minimum time was observed to be between pH 3.5 to 4.5. On the other hand, in the gel state curve of colloidal silica specimens prepared with 0.333 M NaCl a minimum time was recorded, at pH 7.

Figure 5-6 presents gel state curves for all the colloidal silica specimens prepared with different concentrations of NaCl accelerator ranging from 0.017 to 0.333 M at pH values between 3 to 8. Similar trends are observed across all the specimens. At pH values >4 the curves show that increased accelerator concentrations reduce the time taken to reach gel state 9. The influence of electrolyte accelerator concentration was reduced at lower pH values. A trend observed across all the gel state curves showed that at higher NaCl concentrations the minimum time region occurred at a higher pH value.

Figure 5-7 shows the gel state curve for a control CS only specimens against sand specimens saturated with the same CS mixture. It can be seen by the overlapping circles and crosses that the presence of sand at varying pH conditions did not affect the time taken to reach a rigid gel.

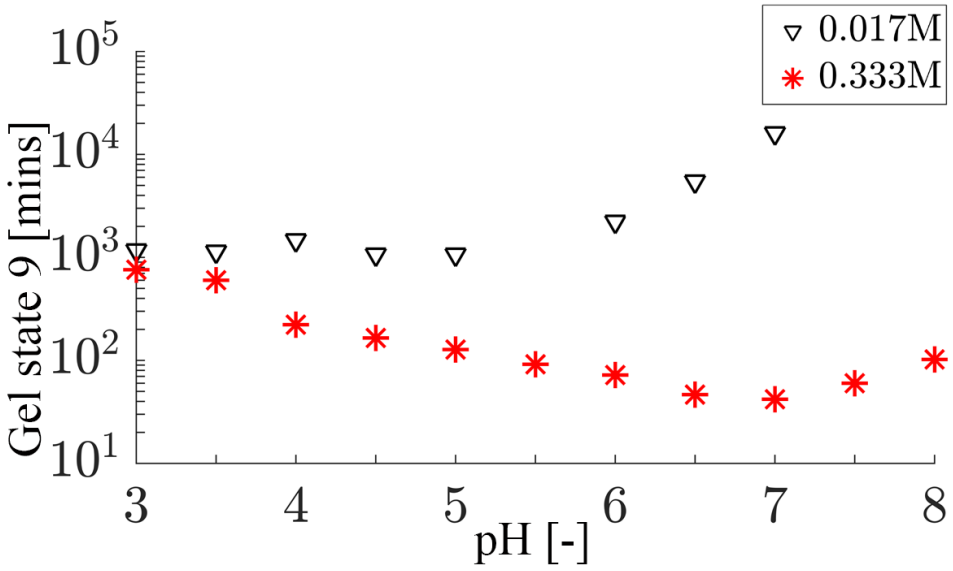

Figure 5-5 Time taken to gel state 9 for CS mixtures with 0.017M NaCl & 0.33M NaCl

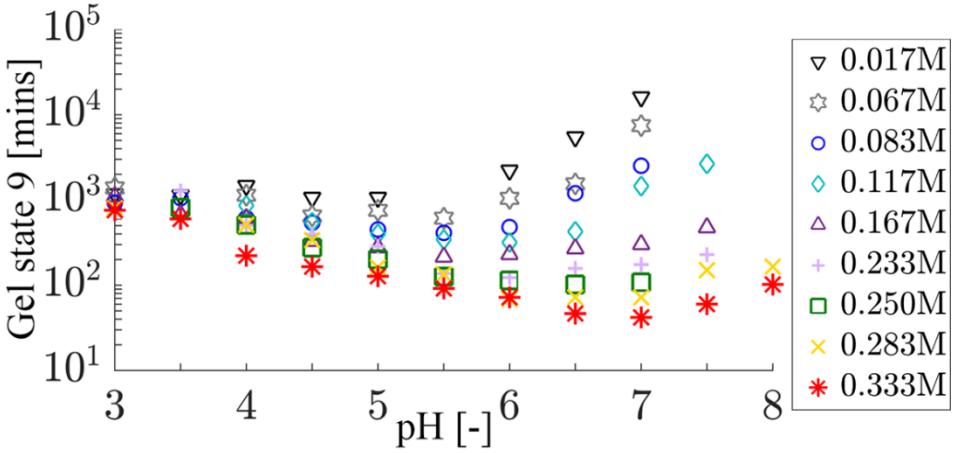

Figure 5-6 Time taken to gel state 9 for CS mixtures of varying NaCl concentration

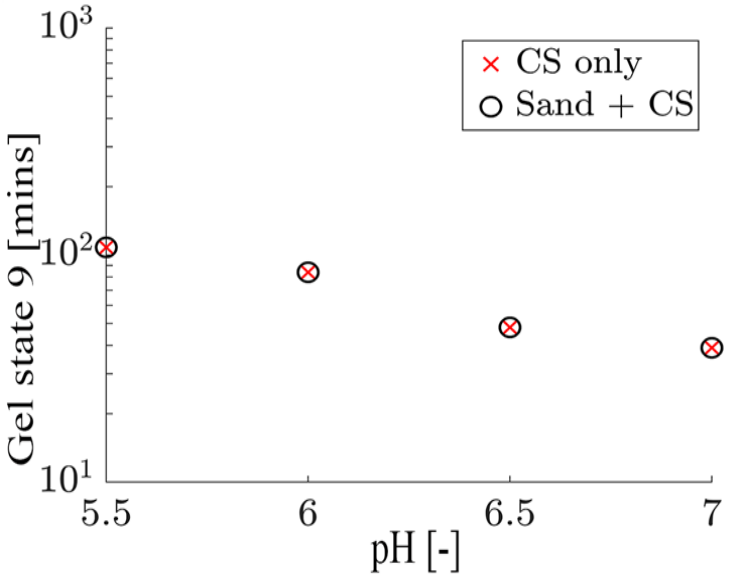

Figure 5-7 Time taken to gel state 9 for CS only and Sand + CS

5.3. Viscosity evolution study

5.3.1. Materials & methods

This section contains the test procedure for the viscosity evolution tests of different colloidal silica mixtures. The tests aimed to determine the viscosity evolution of colloidal silica grouts during the gelling process and determine the grout gel time. Figure 5-8 shows a typical viscosity test set up.

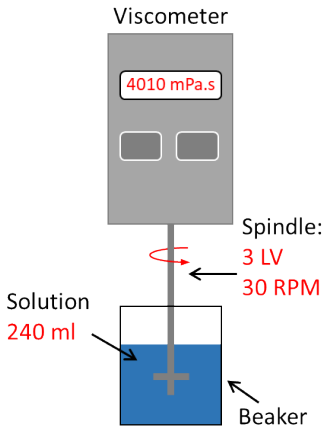

Figure 5-8 Typical viscosity test configuration.

5.3.1.1. Specimen preparation

For viscosity testing, the colloidal silica solution MasterRoc MP320 was used. The product specification of MasterRoc MP320 is located in section 5.2.1.1. Grout solutions were all prepared in a 5:1 ratio of colloidal silica to electrolyte accelerator by volume respectively.

In the viscosity tests, 200 ml of colloidal silica were mixed with 40 ml of electrolyte accelerator corresponding to a 5:1 ratio of colloidal silica solution to electrolyte accelerator by volume respectively. Different accelerators were investigated in this test study, (i) sodium chloride (NaCl), (ii) calcium chloride ($CaCl_2$), and (iii) potassium chloride (KCl) to achieve final accelerator concentrations in the grout mix ranging from 0.083 M to 0.333 M. Colloidal silica grouts prepared using $CaCl_2$ accelerator at concentrations above 0.083 M were unsuitable for viscosity testing, due to the immediate gelation upon mixing. To investigate changes in pH conditions, HCl and NaOH were used to adjust the grout solution pH to values between 3 and 8. A series of specimens were also prepared at 37% of silica concentration by diluting the 'as-delivered' silica with distilled water before being mixed with the NaCl accelerator. To investigate the influence of temperature, the colloidal silica solution and accelerator solution were both stored separately for 24 hours at the test temperature environment (ranging from 10-30°C) before mixing the solutions immediately prior to testing.

The composition of all colloidal silica grout mixtures prepared for viscosity testing is shown in Table 5-3.

5.3.1.2. Viscosity evolution testing

The viscosity evolution of colloidal silica specimens were recorded using a Brookfield digital viscometer model LVT DV-II attached with LV spindle 3 providing a maximum readable viscosity of 4010 mPas. Tests were conducted following ASTM (2014) with two reference standards ASTM N1000 and ASTM S200. Viscosity data was recorded every second for the duration of testing to provide the grout viscosity evolution. To calculate gel time as shown earlier in Figure 5-2, viscosity is plotted against time, with the gel time given by the intersection between the linear regression of all the points at viscosity higher than 2000 mPas and the x-axis (Bergna and Roberts, 2005, Funehag and Axelsson, 2003).

For standard conditions, tests were conducted in a temperature-controlled laboratory environment at 20°C. Standard viscosity tests with the prepared colloidal silica grout mixture (see section 5.3.1.1). Further viscosity temperature test conditions were investigated ranging from 10°C to 30°C. For colder temperature conditions, the viscosity measurement tests were carried out in a controlled refrigerated environment at 10°C. For warmer temperature conditions, specimens were kept in a temperature-controlled water bath at 25°C and 30°C for the duration of viscosity testing. All tests were terminated when the viscosity reached 4010 mPas.

Table 5-3: Composition of colloidal silica grout mixtures tested

				Accelerator concentration c_acc (M)		
Series	**Temp (°C)**	**SiO_2 conc. (%)**	**Accelerator**	**Initial**	**Final**	**pH**
0.083M_NaCl_CS	20	0.40	NaCl	0.5	0.083	3 - 7
0.167M_NaCl_CS	20	0.40	NaCl	1.0	0.167	3 - 8
0.233M_NaCl_CS	20	0.40	NaCl	1.4	0.233	3 - 7
0.250M_NaCl_CS	20	0.40	NaCl	1.5	0.250	3 - 8
0.283M_NaCl_CS	20	0.40	NaCl	1.7	0.283	3 - 8
0.333M_NaCl_CS	20	0.40	NaCl	2.0	0.333	3 - 8
0.083M_CaCl2_CS	20	0.40	$CaCl_2$	0.5	0.083	3 - 7
0.167M_KCl_CS	20	0.40	KCl	1.0	0.167	5 - 8
0.333M_NaCl_CS_0.37	20	0.37	NaCl	2.0	0.333	3 - 8
0.333M_NaCl_CS_T10	10	0.40	NaCl	2.0	0.333	5 - 7
0.333M_NaCl_CS_T25	25	0.40	NaCl	2.0	0.333	4 - 8
0.333M_NaCl_CS_T30	30	0.40	NaCl	2.0	0.333	4 - 8
0.167M_NaCl_CS_T10	10	0.40	NaCl	1.0	0.167	5 - 7
0.167M_NaCl_CS_T30	30	0.40	NaCl	1.0	0.167	4 - 7

5.3.2. Results: Influence of pH and electrolyte concentration

Viscosity profiles for the colloidal silica grout specimens prepared using 0.333 M NaCl accelerator (0.333M_NaCl_CS) at pH conditions from 5 to 8 are presented in Figure 5-9. The gel time ranges from approximately 33 min to 135 min with the shortest gel time at pH 7.0. Conversely, the longest gel time occurred in the specimen prepared at pH 5.0. Across the pH range, the viscosity profiles display a non-monotonic trend. It can be seen that the pH 8.0 specimen (black crossed dash line) exhibited a longer gel time than both the pH 7 and 6.5 specimens. With decreasing pH, the gel time reduces between pH 8.0 to 7.0, whereas further decreases from pH 7.0 to 5.0 result in increasing the gel times.

The effect of pH on grout gel times can be understood by considering the influence of the electrical charge of the surface of the silica particles arising from changing pH conditions and formation of siloxane bonds (Si-O-Si). When siloxane bonds start to form, gelation begins. Silanol (SiOH) bonds condense to form siloxanes (Si-O-Si). The formation of silanol bonds is promoted by the presence of OH^- anions in solution. However, at higher pH the more negative the electrical charge is, resulting in increased repulsion between particles and as such decreasing the rate of silanol bond formation, consequently increasing gel times. This explains why a minimum gel time is reached at an intermediate pH value.

Figure 5-10 shows the viscosity profiles for colloidal silica grouts prepared using different NaCl accelerator concentrations all prepared at pH 6.0. As the concentration of NaCl accelerator increases from 0.083 M to 0.333 M, the gel time reduces from 324 min to 45 min.

The effect of electrolyte concentration on gelation behaviour can be explained by the repulsion between silica particles. When an electrolyte is added to colloidal silica, the presence of the cations act to reduce the thickness of the diffuse double layer and thus the repulsion between particles is reduced, leading to an increased collision rate of the silica particles and hence reduced gel times.

In both Figure 5-9 and Figure 5-10 the viscosity curves show that for grout mixes with a longer gel time, the rate of viscosity increase (i.e. gradient of the viscosity curve) after the gel time is lower than for grout mixes with a shorter gel time. Thus, the rate of viscosity development post-gel time in Figure 5-9 from 1000 mPas to over 4000 mPas is

faster at pH 7.0 and 6.5. Likewise, the viscosity development is faster for grouts prepared using a higher NaCl concentration.

Figure 5-11 presents the gel times of the grout mixes from Figure 5-9 and Figure 5-10. A range of gel times was identified from 30 min to 1140 min. For each set of grout mixtures prepared at a given NaCl accelerator concentration, the gel time showed a non-monotonic trend when plotted against pH. In the alkaline pH range, increasing the NaCl concentration reduces the gel time (i.e. faster gelation). In contrast, in the acidic pH range, the gel time was not affected by any variation in the NaCl concentration. At pH = 3.0 similarly, gel times were identified for all grout mixes prepared. A minimum region of colloidal silica occurs between pH 5 to 7, consequently the fastest gel times occur in this region across the different grout mixtures.

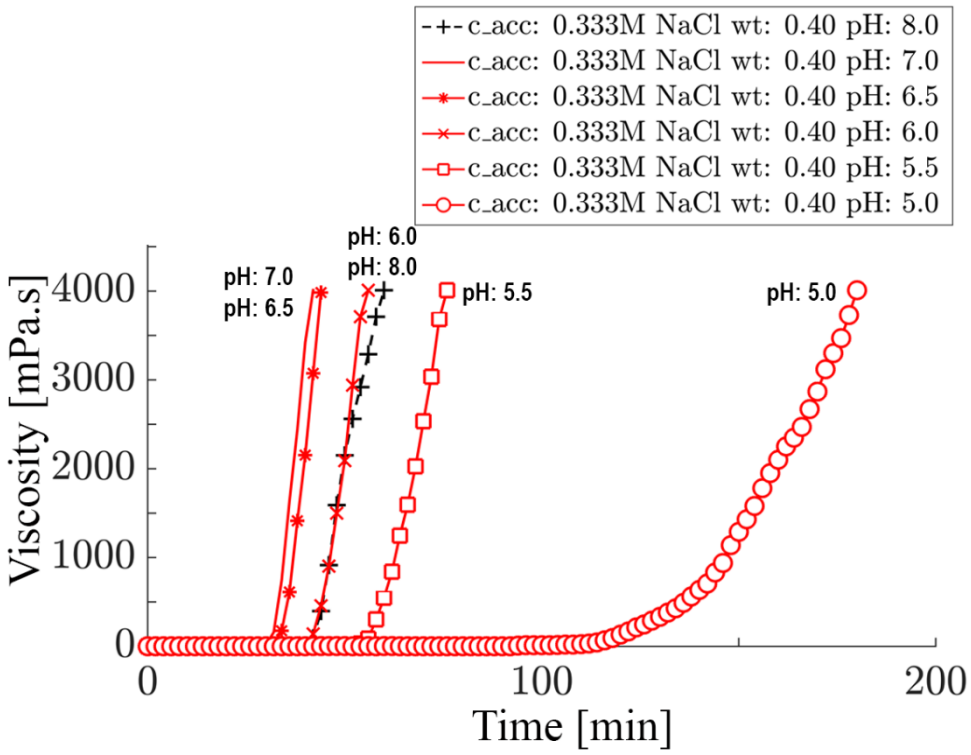

Figure 5-9 Viscosity profile for 0.333M NaCl & CS colloidal silica grout at different pH conditions.

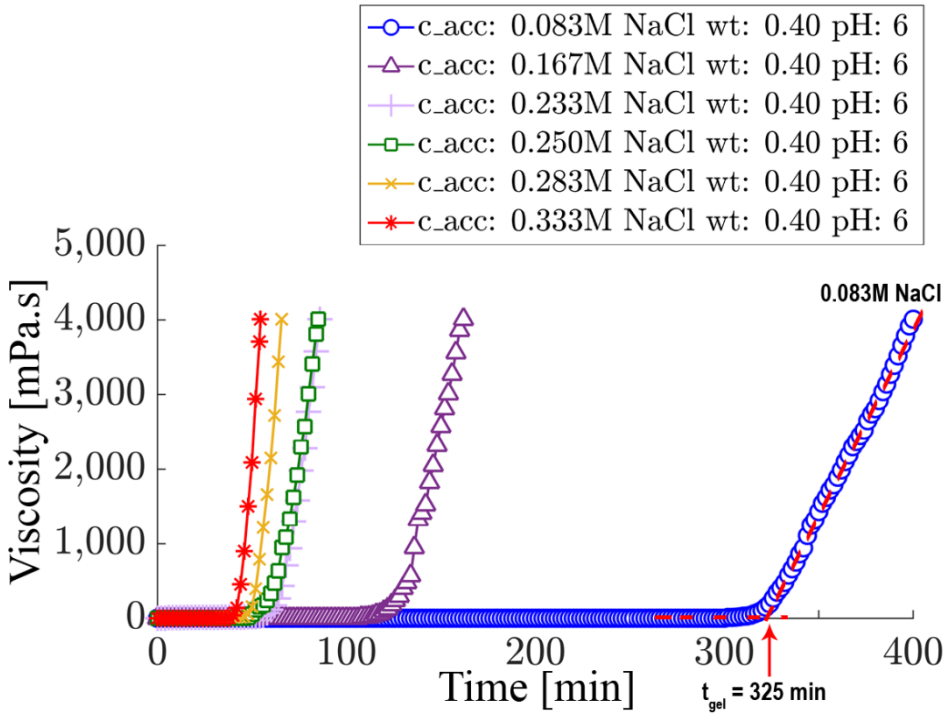

Figure 5-10 Viscosity profile for colloidal silica grouts prepared using different NaCl concentration at pH 6.

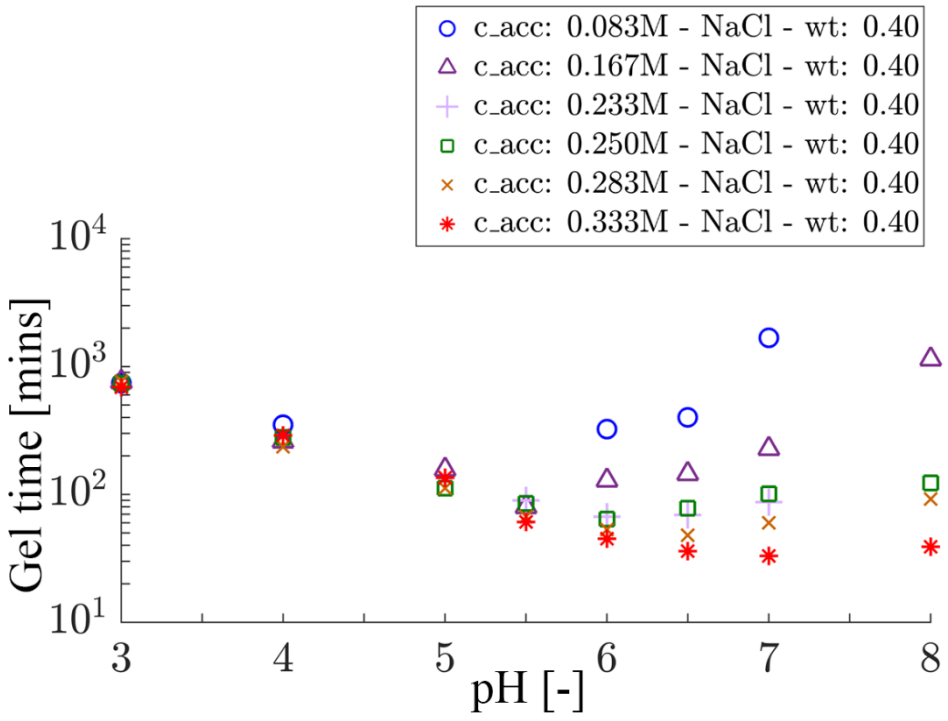

Figure 5-11 Experimental results for colloidal silica grout mixtures prepared with different NaCl concentration Gel time vs pH.

5.3.3. Influence of grout accelerator: Electrolyte valency

Figure 5-12 presents the gel time results of two series of colloidal silica grouts prepared using different accelerators NaCl and $CaCl_2$, at the same concentration (0.083 M). Similarly, Figure 5-13 presents the results for the same colloidal silica grouts prepared using 0.083 M $CaCl_2$ compared against grouts prepared using a NaCl accelerator at double the concentration 0.167 M. The colloidal silica grouts prepared using $CaCl_2$ resulted in faster gel times compared to the grout mixes prepared with NaCl even when double the accelerator concentration was used. It can be seen in Figures 5-12 and 5-13 that the greatest reduction in gel time occurs at pH 7. Whereas in acidic pH conditions between 3 to 5.5 results from the grout mixes prepared using the three different accelerators showed similar gel times. The results show in alkaline pH conditions the use of a $CaCl_2$ accelerator has a greater effect on destabilising colloidal silica than the use of a NaCl accelerator at twice the concentration.

The effect of increased gel time can be understood by the valency charge of the cations. Calcium (Ca^{2+}) are divalent ions within the $CaCl_2$ accelerator in contrast to the monovalent (Na^{+}) ions in NaCl. The divalent calcium cations have a greater effect depressing the diffuse double layer surrounding silica particles than the monovalent sodium cations. The negative surface charge of the silica particle is balanced out by the cation charge of Ca^{2+} and Na^{+} ions. Since calcium ion has a stronger charge than sodium ions, for the same accelerator concentration, divalent cations have a greater effect on reducing the electrostatic repulsion between particles illustrated in Figure 5-14 (Savarmand et al., 2003).

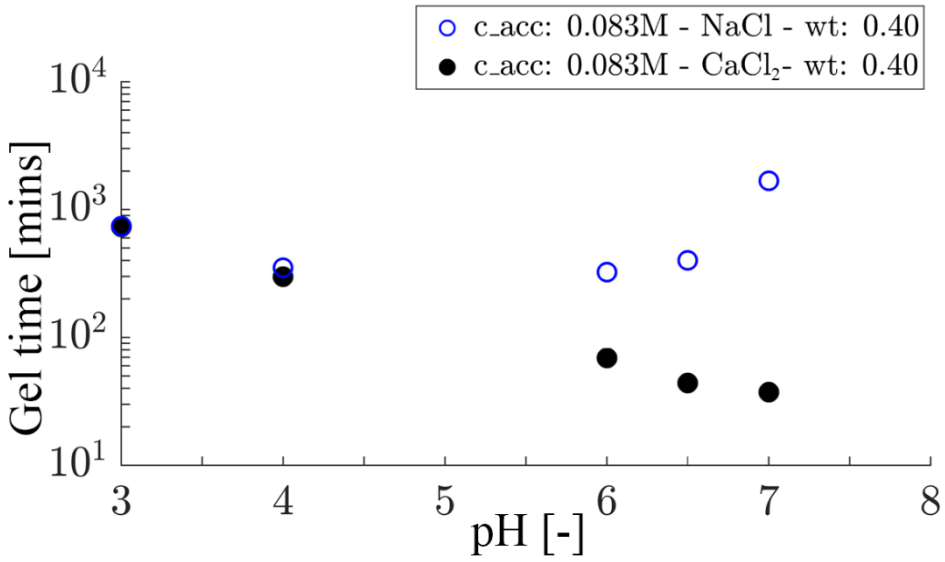

Figure 5-12 Gel time vs pH for colloidal silica grout mixtures with different accelerator cations of NaCl and $CaCl_2$ at the same electrolyte concentration 0.083M

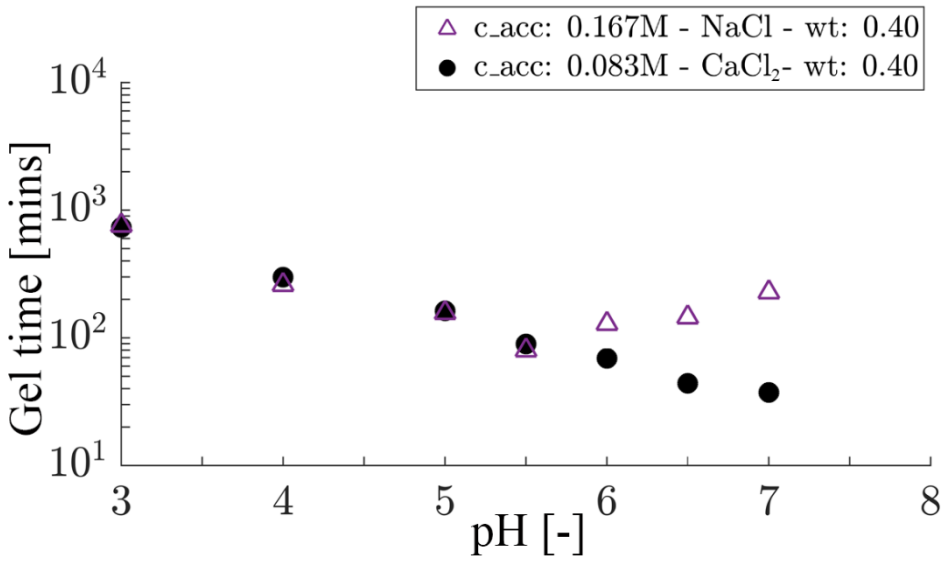

Figure 5-13 Gel time vs pH for colloidal silica grout mixtures with different accelerator cations of 0.167 M NaCl and 0.083 M $CaCl_2$

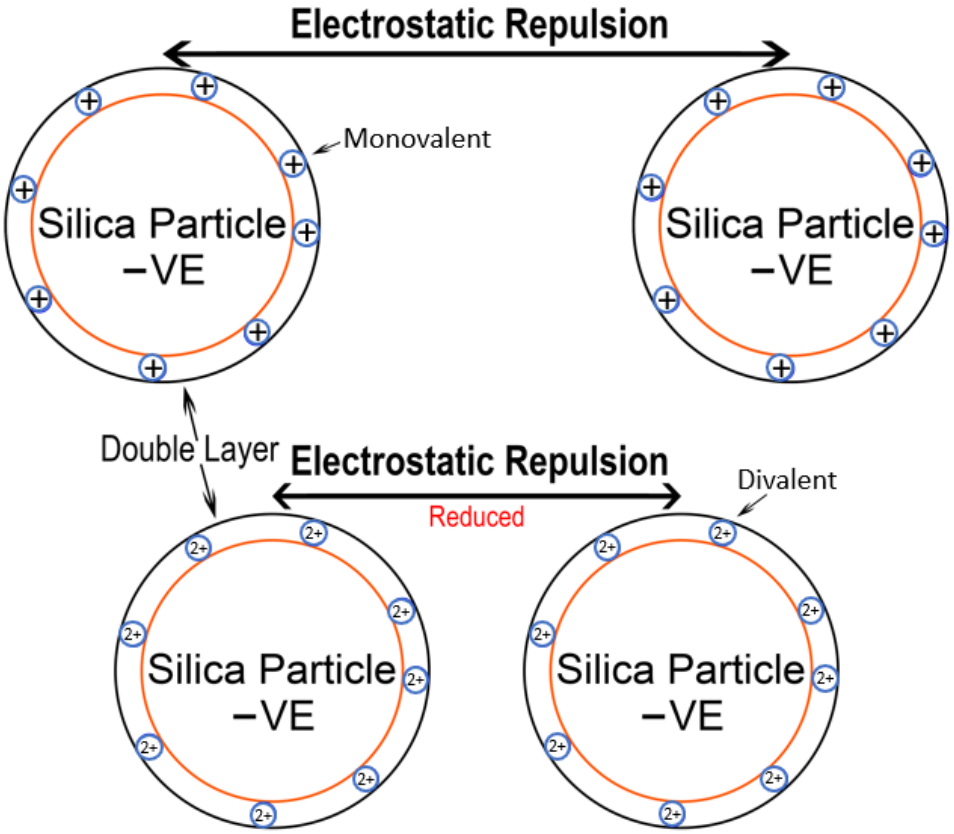

Figure 5-14 Conceptual images of the electrostatic repulsion between silica particles with monovalent and divalent cations.

5.3.4. Influence of grout accelerator: Molar mass

To investigate the effect of accelerator molar mass on grout gel times accelerators of the same valency were also investigated, a series of specimens were prepared using potassium chloride (KCl) accelerator (Table 5-3). Figure 5-15 presents the gel time results for colloidal silica grouts prepared using different accelerators NaCl and KCl, at the same concentration at pH conditions 8 to 5. Although sodium Na^+ and potassium K^+ ions are both monovalent ions and the molar concentration tested was the same (0.167M), the two sets of grout mixes showed different gel times under alkaline conditions. Colloidal silica specimens prepared using a KCl accelerator resulted in faster gel times. This is considered due to the larger size of the K^+ ions in comparison Na^+ ions, and its increased ability to reduce repulsion between silica particles to promote gelling. These results demonstrate that when considering the influence of electrolytes on gel times, it is important to not only consider molar concentration and valency but also molar mass.

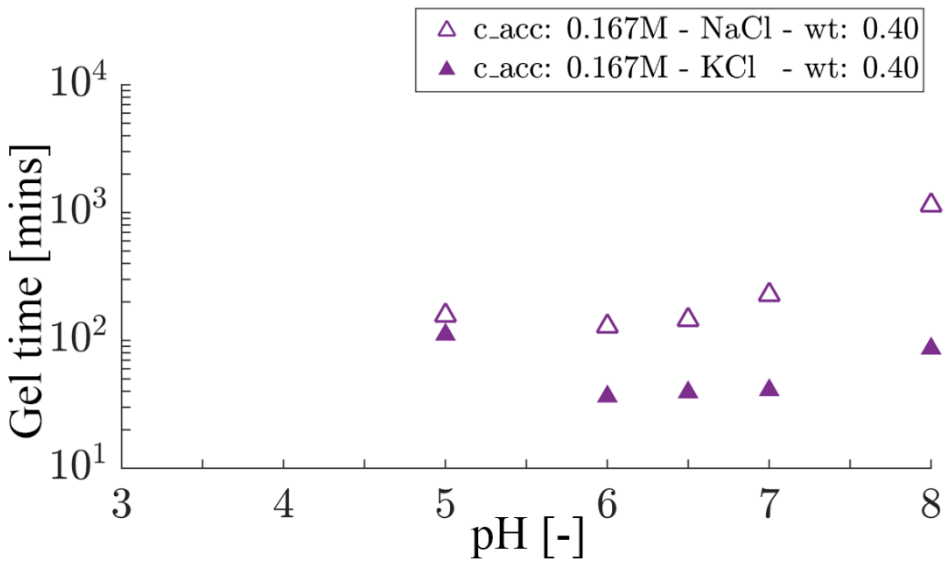

Figure 5-15 Gel time vs pH for CS gels prepared using 0.167 M monovalent accelerators of different molar mass cations: NaCl and KCl

5.3.5. Influence of silica concentration

To illustrate the effect of silica concentration on gel time, a series of grout specimens were prepared at a silica concentration of 37% by mass using a fixed accelerator concentration of 0.333 M NaCl and varying pH condition from 8 to 3. Table 5-3 shows the composition of colloidal silica grouts prepared with 37% silica concentration. Figure 5-16 shows the effect of silica concentration on gel time with colloidal silica specimens at varying pH. It can be seen that decreasing the silica concentration leads to a fairly consistent increase in gel time across the entire pH spectrum, i.e. in both acidic and alkaline pH conditions. A reduction in silica concentration leads to a reduced number of silica particles and thus reduced surface area where silanol bonds can form.

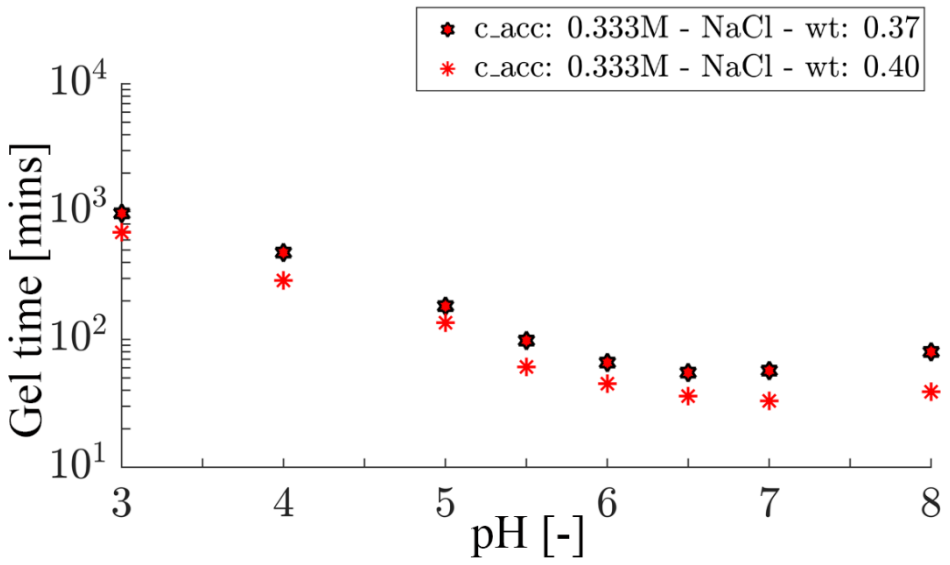

Figure 5-16 Gel time vs pH for colloidal silica grout mixtures with 0.333 M NaCl accelerator and different silica concentrations (0.37 and 0.40)

5.3.6. Influence of temperature

Figure 5-17 shows the comparison of gel times for grouts mixtures prepared using NaCl accelerator at a concentration of 0.333 M tested at temperature conditions ranging from 10°C to 30°C. Figure 5-18 presents the same for grouts mixtures prepared using NaCl accelerator at a concentration of 0.167M. The results in both Figure 5-17 and Figure 5-18 show that as temperature increases, the CS gel stability decreases, with shortest gel times occurring at highest temperature 30°C (open symbol line) and longest gel times at lowest temperature 10°C (closed symbol line). The rate of gelling increase with temperature can be understood by the kinetic energy increase. The induced silica particle

movement, and thus higher probability of silica particle collision promotes the gelation process and lowers the gel time (Iler, 1979, Verfel, 1989).

The influence of pH and electrolyte concentration identified in sections 5.3.2 can also be seen in the same temperature conditions test results by plotting data from Figure 5-17 and Figure 5-18 together in Figure 5-19. In the acidic pH range gel time is unaltered by variation in the accelerator concentration. Both the CS specimens prepared using 0.167 M and 0.333 M NaCl at pH 5 and tested at 10°C resulted in a similar gel time was. Likewise, at pH 5 at temperatures of 20°C and 30°C, similar gel times were observed demonstrating that in the acidic range gel time is independent of the electrolyte used.

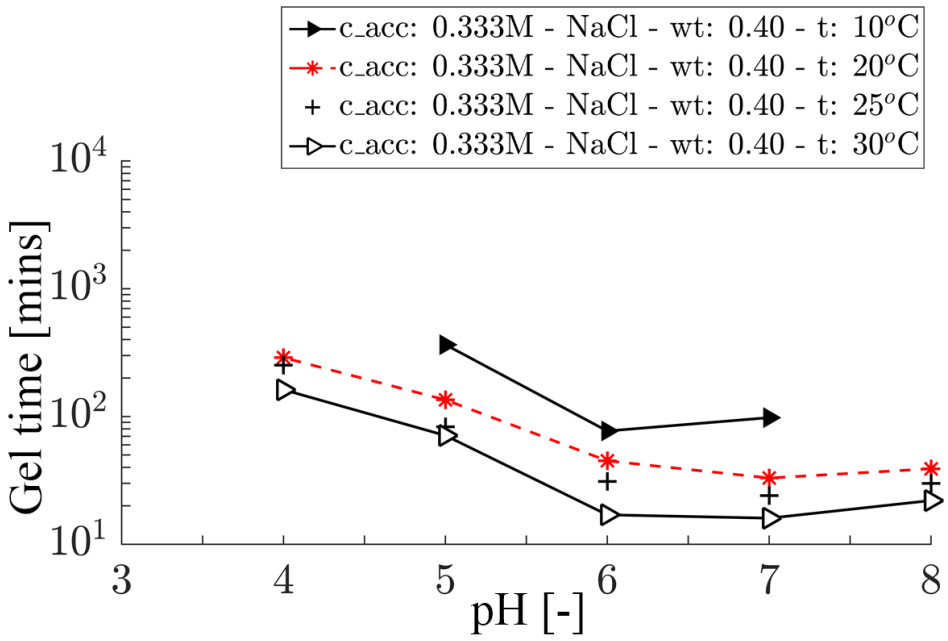

Figure 5-17 Gel time vs pH for CS gels prepared using 0.333 M NaCl tested at different temperatures

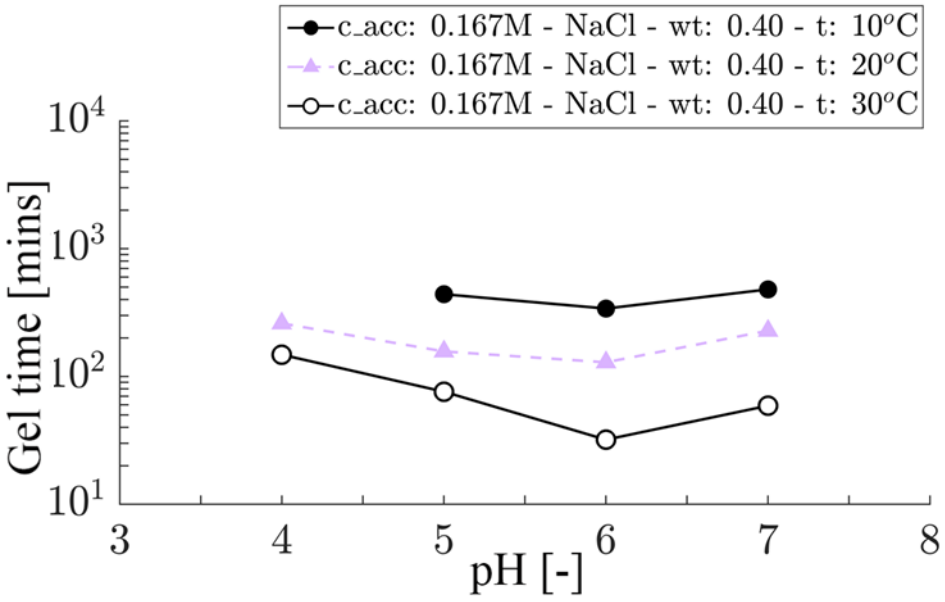

Figure 5-18 Gel time vs pH for CS gels prepared using 0.167 M NaCl tested at different temperatures

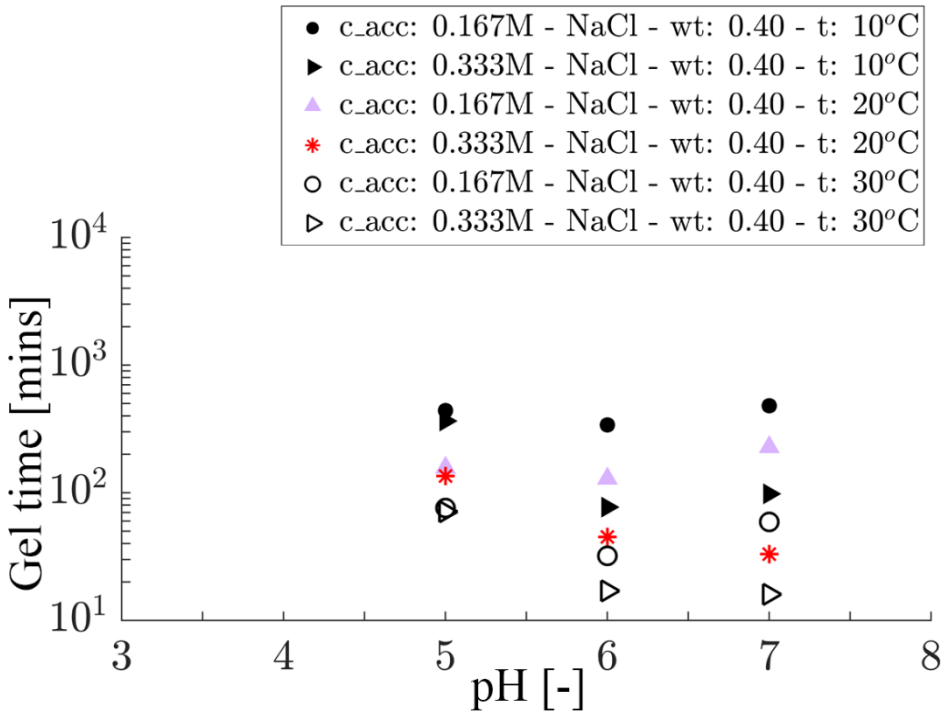

Figure 5-19 Gel time vs pH for CS gels prepared using 0.167 M & 0.333 M NaCl at different temperatures

5.4. Comparison of experimental methods

Figure 5-20 compares the results from the two test methods investigated, i.e. the time taken to achieve gel state 9 and the gel time determined from viscosity testing for the same colloidal silica grout mixture. Results across the six CS grouts prepared using NaCl accelerators at concentrations from 0.083 M to 0.333 M at varying pH conditions show that as expected gel time occurs before a rigid gel state 9 is reached, as these two conditions indicate different points of the gelation behaviour of colloidal silica grouts. Gel times determined from the viscosity testing is the point of rapid viscosity increase indicating the transition from a highly flowing gel into a non-flowing gel (this transition occurs over gel states 2 to 6, according to Table 5-2). Whereas gel state 9 corresponds to when a specimen becomes a rigid gel. Figure 5-21 shows a viscosity test colloidal silica specimen photo taken 20 mins after the test ended tilted at an angle >90^{o} to the horizontal demonstrating no gel movement.

The gel state test provides a useful low-cost tool for a preliminary assessment of grout mixture suitability for specific applications that may be useful for on site grout workability tests. The simplicity of the gel state test would enable the simultaneous assessment of several grout mixtures variations, for example grouts prepared with different concentrations of *in-situ* groundwater, with relative ease across a short period of time. To gain more precise information about grout gelation and viscosity behaviour, to aid in identifying suitable in situ grout mixtures additional viscosity testing could be conducted as required.

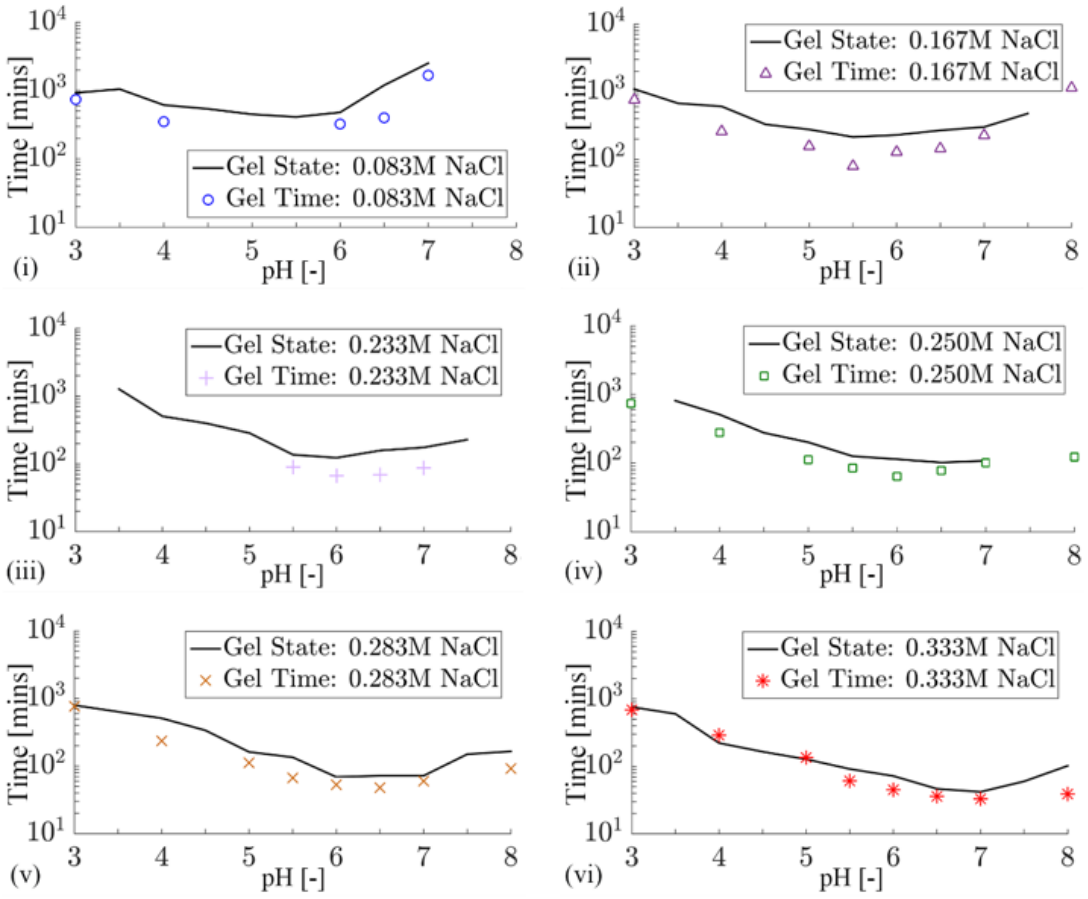

Figure 5-20 Comparison of gel state test (gel state 9) and viscosity test (gel time) results

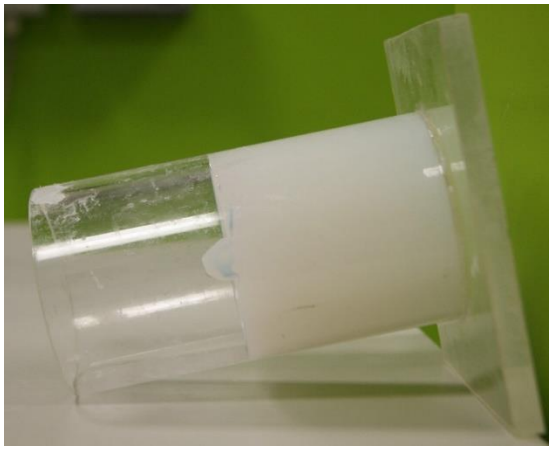

Figure 5-21 Photo of colloidal silica specimen taken after viscosity testing

5.5. Influence of clay soils

5.5.1. Material & method

This study investigates the influence of the presence of clay soils on the gelling behaviour of colloidal silica. Two clays were considered for testing kaolin and bentonite clay. The selection of clays used for the experimental testing was based on availability, but also provided comparisons between the influence of low swelling (kaolin) and high swelling (bentonite) clay on gelling. Initially, the intention was to conduct the gel state time and viscosity tests in the same manner as carried out in Sections 5.3 and 5.4. However, the introduction of clays (kaolin and bentonite) to the colloidal silica grouts resulted in the settlement of the clays to the bottom of the mixtures. Figure 5-22 shows a colloidal silica grout with bentonite clay settled at the bottom of the container after specimen preparation. Consequently, the influence of soils on the colloidal silica gelation behaviour is concentrated at the interface between colloidal silica grout and soil and thus may not be readily detectable by a viscometer located away from the interface.

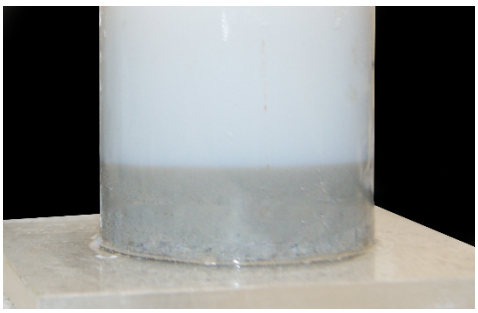

Figure 5-22 Viscosity testing of colloidal silica grout and bentonite clay

As such a modified gel state assessment test based on Persoff et al. (1999) was carried out using a magnetic stirrer to determine the time taken to reach gel state 9 for colloidal silica grout mixed with clays. The gel state time of the colloidal silica specimens with soils was tested to determine whether the presence of clays in situ can influence gelling behaviour. A standard colloidal silica mixture using a 0.283 M NaCl accelerator at a 5:1 ratio was used for testing. Two specimens of colloidal silica grout with different clay soils were prepared. In both specimens 10% kaolin clay or bentonite clay was added to the standard colloidal silica grout mixture. A third control specimen of grout only was prepared and tested.

In the modified gel state tests, the same gel state assessment scale was used (see section 5.2). A Stuart SM1 magnetic stirrer at a rate of 450 rpm was used to maintain suspension

of the clay within the grout mixture for the test duration. The use of the magnetic stirrer in these tests was to promote interaction between the clay particles and the colloidal silica grouts. Figure 5-23 shows the test set-up used for the modified gel state assessment. For the duration of testing specimens were periodically assessed every 5 minutes to determine gel state, with gel state 9 indicated by no horizontal movement in the specimen surface upon placement at 90°.

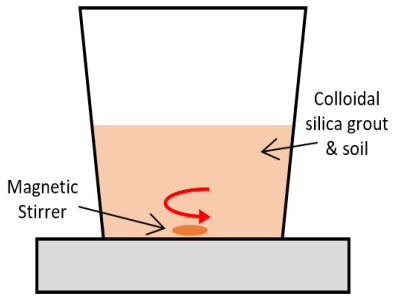

Figure 5-23 Modified gel state test setup

5.5.2. Results

Table 5-4 shows the results of the time taken to reach gel state 9 for colloidal silica grout specimens containing soils of bentonite clay and kaolin clay respectively. In the control specimen test, the observed gel state after 45 minutes as shown in Figure 5-24 indicates behaviours of a barely flowing gel (gel state 6) and a gel state 9 was reached after approximately 60 min, as expected for the standard colloidal silica mixture. The presence of both bentonite and kaolin accelerated the gelation process. In the bentonite clay & colloidal silica specimen it took only 20 mins to reach gel state 9, whereas it took 45 mins for the kaolin clay & colloidal silica specimen to reach a gel state 9. Figure 5-25 shows the specimens of clay and colloidal silica after testing with the clay soil mixed across the whole colloidal silica grout.

The influence of clays to the gelation behaviour of colloidal silica grout may be explained by considering the presence of cations adsorbed on net negatively charged clay particles and on the negatively charged end of clay mineral sheets. Bentonite contains predominantly the clay mineral montmorillonite, which typically has a much higher cation exchange capacity (CEC) than the clay mineral kaolinite, for example Mitchell & Soga, 2005 report a CEC value of 3meq/100g whereas they report a CEC value for smectite of 85meq/100g. It appears that the ability of clay particles to exchange cations

is accelerating the gelation process by the mechanisms previously discussed of electrolyte concentration (see section 5.3.2) and electrolyte valency (see section 5.3.3).

Table 5-4: Gel state times for specimens of soil and colloidal silica

Specimen	Gel state 9 (mins)
10% Bentonite clay & CS	20
10% Kaolin clay & CS	45
CS only	60

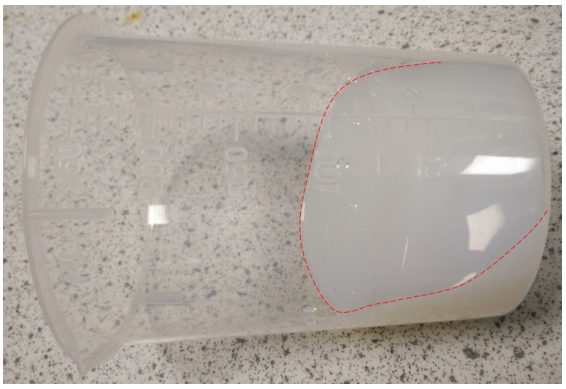

Figure 5-24 Modified gel state test control specimen following 45 mins of testing.

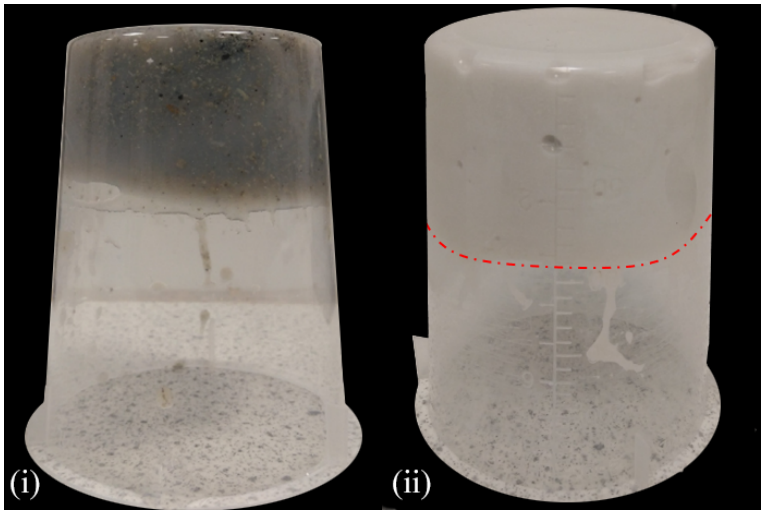

Figure 5-25 Modified gel state test specimens after gel state 9 (i) Bentonite clay & CS (ii) Kaolin clay & CS.

It should be noted that where clay is present within a permeable soil formation in the form of distinct clay lenses, then the presence of clay is likely only to induce premature gelling of a thin layer of the colloidal silica grout at the clay/grout interface, and as such may not greatly impact on the overall gelling of a grout plume/bulb. However, if there are clay particles well-mixed throughout a formation then this could impact on overall gelling

behaviour as demonstrated in Table 5-4. However, it should be noted that if a high clay content is present throughout the media ($\geq 10\%$), then perhaps colloidal silica grouting may not be necessary for the purpose of reducing hydraulic conductivity.

5.6. Case study

5.6.1. Electrochemical model development

The extensive experimental data determined in this chapter underpinned the development of an analytical model by Dr Matteo Pedrotti a PDRA working on the DISTINCTIVE project. The analytical model was developed to predict the gel time of colloidal silica grouts (5.1), taking into consideration variations in pH, electrolyte concentration, cation valency, cation molar mass, silica particle size and silica concentration.

$$t_{gel} = A \,.\, \frac{1}{S_s} \,.\, e^{(-pH)} + B \,.\, e^{(-CS_s C_{eq} + D).(pH - pH_{IEP})} \qquad (5.1)$$

where: t_{gel} is expressed in minutes, C_{eq} (equivalent molar concentration) in mol/L, S_S (specific surface) in 1/m, pH is dimensionless, pH_{IEP} is the pH at the isoelectric point. The parameters A (minutes/metre), B (minutes), C (the inverse of a molar concentration times metre, mL/mol) and D (dimensionless) are all constants.

5.6.2. Model calibration and validation

A subset of the data presented in Figure 5-11 were used to calibrate the model and determine parameters A, B, C and D (Figure 5-26). Subsequently the experimental data presented in Figures 5-12 to 5-16 were used to validate the model (Figure 5-27). In general, a good model fit is observed between experimental gel times and predicted gel times as shown in Figure 5-27.

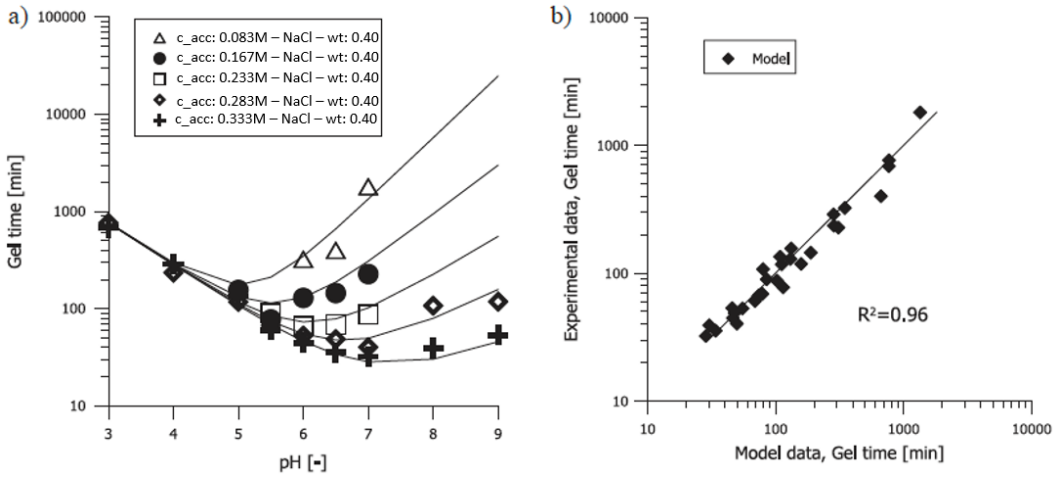

Figure 5-26 Model calibration based on experimental data of colloidal silica grout prepared with varying concentration of NaCl accelerator.

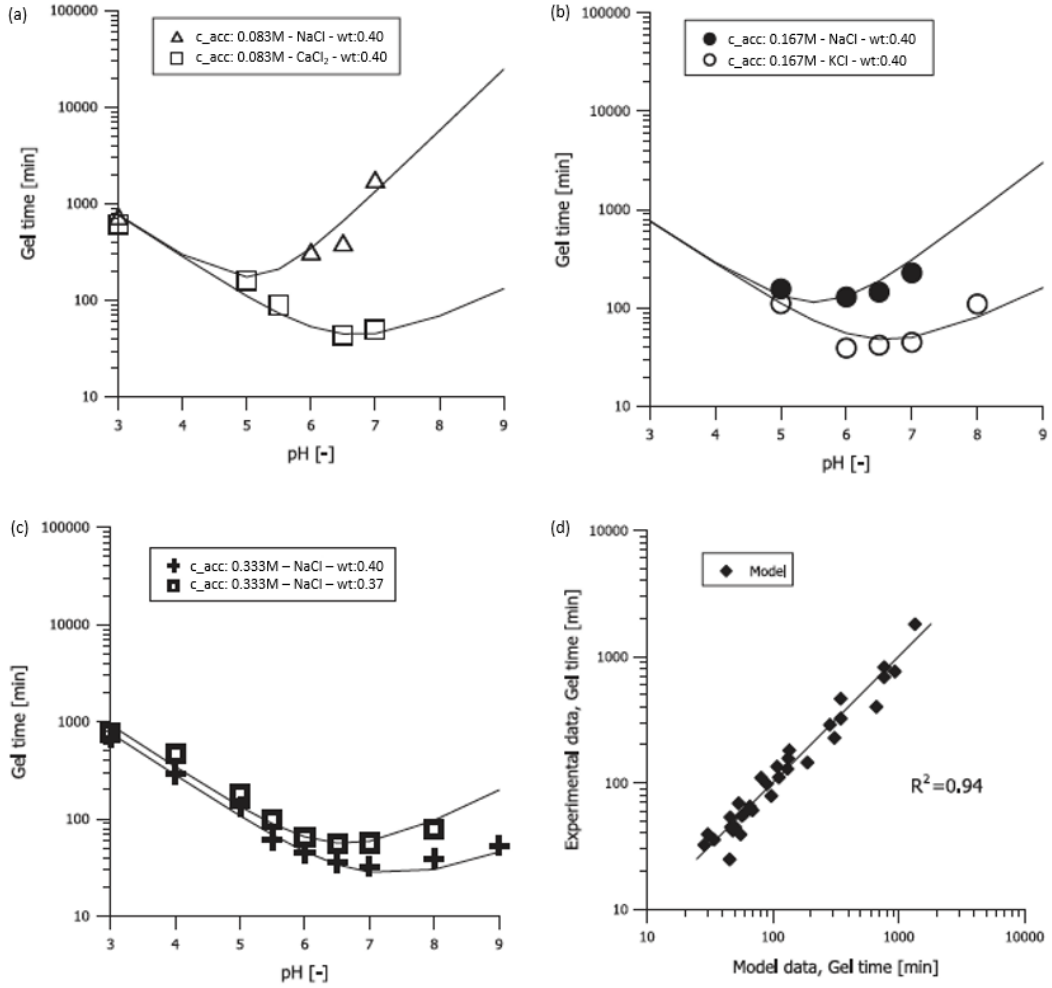

Figure 5-27 Model validation based on experimental data investigation influence of valency, molar mass and silica concentration

5.6.3. Model prediction with artificial groundwater

Using the analytical model developed an experimental case study was then conducted to demonstrate how the model could be used in a site specific context, for example to determine the appropriate accelerator concentration to use when preparing accelerator with in-situ groundwater. The groundwater composition selected for the tests were based upon published data for the Olkiluoto area; the site for disposal of spent nuclear fuel in Finland. The main composition of the groundwater has been well studied and was found to be 209 mM Na^{+}, 100 mm Ca^{2+} and 2.3 mM Mg^{2+} and average pH equal to 7 (Ollila, 1999).

For the grout design selection, a colloidal silica-accelerator ratio of 5:1 was used with MasterRoc MP320 as the chosen colloidal silica solution. A designated gel time for the simulation of 55 min was chosen; within the normal range of set times used in commercial grouting campaigns. To achieve this gel time, using the analytical model the required accelerator concentration was found to be 0.283 M NaCl when considering that the accelerator solution is prepared using distilled water is used, whereas only 0.183 M NaCl if the in situ groundwater at the Olkiluoto site were to be used in the preparation of the accelerator is considered. Three hypothetical cases were considered:

(i) 0.283 M NaCl accelerator concentration prepared with distilled water
(ii) 0.283 M NaCl accelerator concentration prepared with synthetic groundwater
(iii) 0.183 M NaCl accelerator concentration prepared with synthetic groundwater

The model prediction of viscosity evolution with time for a 55 min gel time is plotted alongside the experimental data for each case in Figure. 5-28. As expected, for case 2 the gelling is premature, since the cations already present in the in situ groundwater are ignored in the accelerator concentration calculation. This represents the current predicament of grouting contractors wishing to apply colloidal silica in saline or complex environments, where without having a tool to enable them to adjust their grout mixtures based on the local groundwater conditions, current practice may result in reduced control of colloidal silica gelling on site and thus impact grout penetration.

Figure 5-28 shows that the desired gel time and predicted viscosity evolution can be achieved within 3 min for both case 1 where the accelerator is prepared using distilled water only and case 3 where the accelerator is prepared taking into account the in situ groundwater cations present into the accelerator design calculations using the model.

These results support the use of the predictive gel time model for the design of grouting campaigns for injection at sites with saline or complex groundwater.

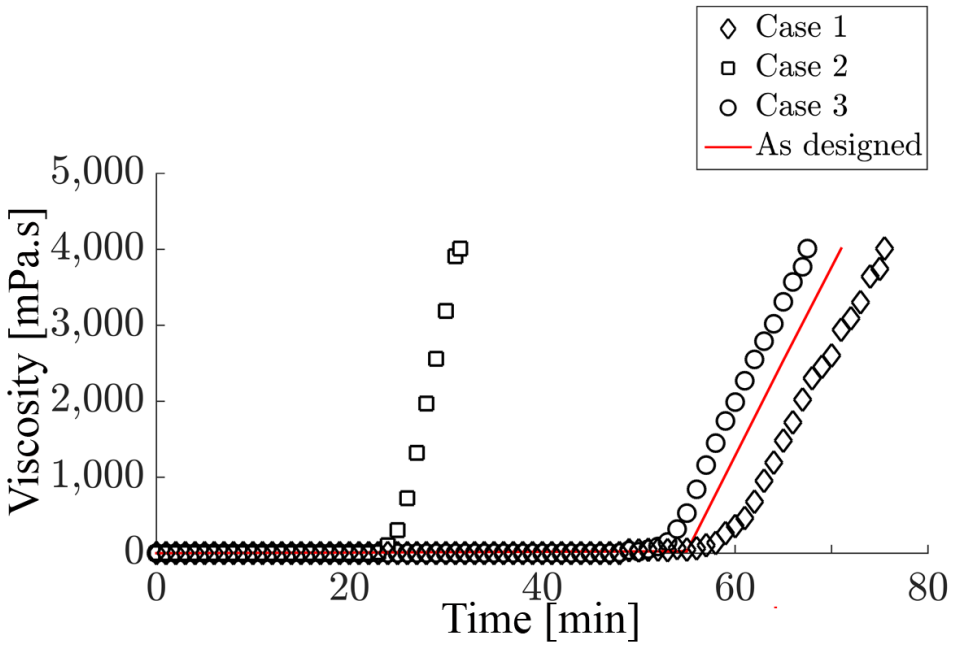

Figure 5-28 Experimental data for case 1, 2 and 3 compared with as "designed" viscosity prediction

5.7. Conclusion

This chapter presents the gel state and gel time behaviour of colloidal silica based grouts. Factors based on grout composition were investigated considering: accelerator concentration, electrolyte valency, molar mass of the electrolyte cation, and silica concentration. Furthermore, environmental factors influencing grout gelation behaviour including pH, temperature, and presence of sand and clays were also considered. The experimental results presented demonstrate that colloidal silica grout gel time can be controlled from minutes to >24hrs. Across the experimental study the following trends were identified:

- Reductions in gel time were observed with increasing accelerator concentration under alkaline conditions. Conversely, in acidic conditions gel times were unaltered by variations in the NaCl concentration.
- For each set of grout mixtures prepared using different NaCl accelerator concentrations, the gel time showed a non-monotonic trend when plotted against pH.

- Electrolyte containing divalent cations were shown to reduce gel times compared to monovalent cations at the same accelerator concentration in alkaline conditions.
- Electrolyte cations with a greater molar mass, resulted in faster gel times in alkaline conditions.
- In highly acidic pH conditions, neither electrolyte concentration nor molar mass had a minimal influence on gelling behaviour.
- Decreasing the silica concentration of grout specimens increased gel time in both acidic and alkaline pH conditions.
- Increasing temperature was shown to reduce CS grout gel times.
- The presence of sands were shown to have no influence on gelling behaviour, whereas the presence of kaolin or bentonite clays resulted in reduced gel times.

The experimental data in this chapter underpinned the development of an analytical model by Pedrotti et al. (2017) for predicting gel times of colloidal silica based grouts considering pH, electrolyte concentration, cation valency, cation molar mass, silica particle size and silica concentration for the gel time.

The development of this model will enable the bespoke design of grouting campaigns to optimizing grouting strategies using specific grout mixtures of colloidal silica solution and accelerators to achieve desired gelation behaviour and gel times relevant to specific applications. Grout mixtures could therefore be tailored to utilising existing resources such as in-situ groundwater and available electrolyte solutions. Furthermore, for the implementation of horizontal hydraulic barriers in situ, a long gel time would be required to allow the grout to be injected and penetrate a permeable formation prior to gelling occurring. Use of colloidal silica in this way has to date been prevented by a lack of knowledge on how to design and control gelling behaviour.

Chapter 6. Conclusions and recommendations

This thesis was aimed at investigating the performance of colloidal silica grout, as a geomaterial for deployment in the construction of hydraulic barriers. In the application as a hydraulic barrier factors influencing the deployment of colloidal silica grout were considered including the wetting-drying, mechanical and gelling behaviour of the colloidal silica and colloidal silica grouted soils under varying environmental conditions and groundwater composition and differing in-situ soil conditions.

The specific research objectives of this thesis were to:

- Determine the soil water retention behaviour of colloidal silica and colloidal silica grouted soils, given that for *in situ* application variations to the water table may result in variable saturation conditions.
- Determine the hydro-mechanical behaviour (1D compression and shearing behaviour) of colloidal silica gel and colloidal silica grouted soils under different curing times and curing conditions using industry standard geotechnical tests.
- Determine the influence of pH, electrolyte concentration and temperature on the gelling behaviour of colloidal silica, in order, to design controllable gel times considering *in-situ* environmental conditions.

6.1. Summary of findings

6.1.1. Soil water retention behaviour of colloidal silica grout

Reported in *Chapter 3* are the results of a detailed investigation of the water retention behaviour of colloidal silica grout and soils specimens mixed with colloidal silica grout using the chilled-mirror dew-point technique (WP4-C).

This research has determined for the first time the soil water retention behaviour of colloidal silica and colloidal-silica grouted soils. This research demonstrates the potential

application in locations of temperate climate conditions and varying degrees of saturation dependant on the groundwater table level. The increased water retention capacity associated with sandy soils grouted with colloidal silica, indicates that in temperate climates, i.e. where the water table <20m below the ground surface, the barrier formed should remain saturated and retain its function as a low hydraulic conductivity barrier.

6.1.2. Hydromechanical behaviour of colloidal silica grout

In *Chapter 4* the mechanical and hydraulic behaviour of colloidal silica grouts and soils specimens mixed with colloidal silica grout under different environmental conditions were investigated. A series of one-dimensional consolidation and direct shear tests were performed on specimens prepared under different environmental conditions (water, 2.5% NaCl saline solution, and 90% relative humidity) and varying curing periods (1, 2, 4, and 8 weeks). Three colloidal silica grouted soil mixtures were investigated: sand, kaolin clay, and sand-10%kaolin.

Research in this thesis on the mechanical and hydraulic behaviour of colloidal silica grout illustrates the mechanical improvement of soils treated with colloidal silica under drained conditions using industry standard geotechnical tests. Deployment of colloidal silica grout could be adopted in environments where not only hydraulic containment is critical but where reduced deformation and enhanced resistance to shearing would be beneficial, for example in landfill capping, lining of contaminant storage trenches, or in the outer fill layers of embankments in order to minimise internal seepage and infiltration.

6.1.3. Gelation behaviour of colloidal silica grout

In *Chapter 5* the gelation behaviour of colloidal silica grout was examined through an extensive laboratory campaign considering grout composition and environmental factors. Grout compositions of different accelerator concentration, electrolyte valency, molar mass of the electrolyte cation, and silica concentration were investigated. Likewise, environmental factors including pH, temperature, and presence of sand and clays were considered.

This research supports the development of bespoke colloidal silica grouts using tailored grout mixtures of colloidal silica solution and accelerators to achieve desired gelation behaviour and gel times relevant to specific site applications. For example the predictive model would enable use of in situ groundwater at coastal sites, and would allow colloidal

silica to be used in new ways for example to create in situ horizontal hydraulic barriers using longer gel times than is currently achievable using commercial grout mixtures.

6.2. Implications for legacy nuclear sites

In this section the implications of this research for the use of colloidal silica grout as a hydraulic barrier for in-situ containment at legacy nuclear sites are discussed. Colloidal silica grout has been considered as a promising material in the in situ installation of injectable hydraulic barriers due to its initial low viscosity, negligible toxicity, small particle size, and low achievable hydraulic conductivity.

Figure 6-1 presents a cross-section through a silo at the Magnox Swarf Storage Silo (MSSS) facility at Sellafield, UK. This facility was constructed in 1962 and comprises a reinforced concrete structure with a 1.5m thick concrete base and 1.4m thick external walls (Hollmen, 2013). The base of the facility lies approximately 6m below the ground. In the 1970s there was a confirmed leak at this facility with contamination entering the ground at this location, with the pathway eventually becoming plugged, it is thought with the sludge material from the silo. In November 2019, Sellafield reported an increase in leakage rate from MSSS (Kirby, 2004). Current leakage rates are estimated to be ~1.5-2.5 m^3/day (Hollmen, 2013). Due to the facility being embedded in the ground, it is currently unknown where leakage is occurring, and if this leakage is occurring through a single or multiple cracks.

The research presented in this thesis has shown that by controlling gel time it would be possible to use colloidal silica in novel ways to prevent release of the radionuclide contaminated liquor from the silos migrating away from the immediate vicinity of the facility. Ultimately in this example colloidal silica could potentially be used to form vertical barriers around the structure, but also to form an underlying horizontal barrier using a grout mixture with a relatively long gel time and potentially a pump and extract technique to pull the grout along underneath the structure. This could therefore form a secondary containment structure around this existing facility. To prevent this filling up with rainwater, a capping layer would be required at the ground surface, again this could be potentially created with colloidal silica by using a grout mixture with a very short gel time or another capping technique. At the Sellafield site, the maximum depth of the water table is ~12m below ground level (NDA, 2016) based on the water retention results

presented in this thesis, it should be possible to maintain the colloidal silica barrier system in a saturated state if it intersects the water table and as such desiccation cracking should not be a concern. Finally, as decommissioning works proceeds additional loading will be placed on the structure (upwards of 50 tonnes in the next few years) and retrieval of material from these silos will commence within the next 10 years (Hollmen, 2013). The research in this thesis, demonstrates that grouting of soils with colloidal silica can reduce soil compressibility and thus reduce settlements under loading and minimise heave upon unloading, this could be beneficial in protecting already fragile structures from further deterioration during decommissioning. At Sellafield, it is anticipated that decommissioning works will take >100 years.

This is just one example of a complex situation at an existing nuclear facility where colloidal silica could potentially be deployed. Of course, further studies would be required to investigate the interaction with Sellafield specific variables (e.g. Sellafield soil composition, elevated radioactivity in groundwater and in soils). There are other potential applications for colloidal silica both within nuclear contexts including for example the containment of contamination which has been stored within shallow burial unlined trenches and in non-nuclear contexts for example development of novel clay-colloidal silica mixtures for use in landfill capping or the outer layers of embankments to reduce seepage and also potentially erosion.

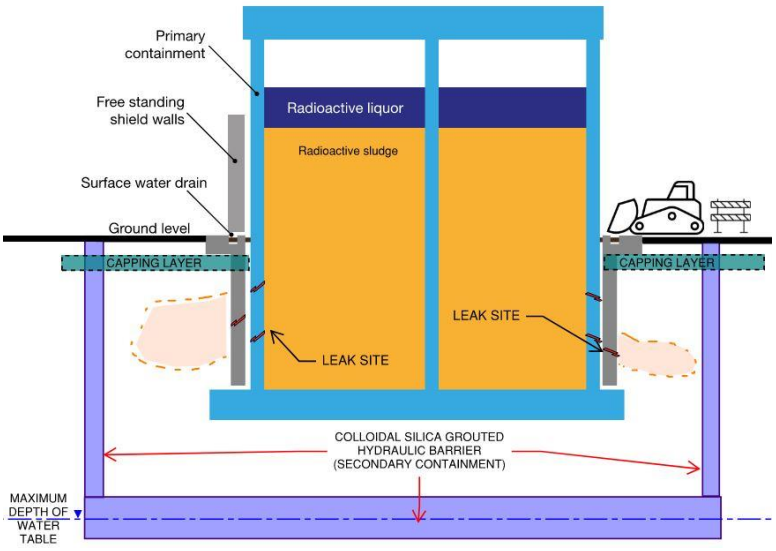

Figure 6-1 Secondary containment colloidal silica grouted hydraulic barrier.

6.3. Recommendations for future work

Following on from the work undertaken in this thesis there are several areas recommended for further research.

As part of this thesis, water retention curves of soil specimens with colloidal silica and SEM, X-CT and photographic images showed that macropores were filled with colloidal silica. To further understand the interactions between clay particles and the colloidal silica, further micro- scale testing should be conducted. The use of mercury intrusion porosimetry, could not be successfully implemented in this study due to the specimen collapse during the freeze-drying process. Testing using a higher concentration colloidal silica solution or identification of alternative drying pathways could enable successful specimen preparation to further investigate the particle configuration of colloidal silica test specimens within the matrix of a geomaterials. Furthermore, alternative microscale techniques should be investigated including e.g. Transmission Electron Microscopy which can enable resolution at the nano-scale.

The analytical model for predicting the gel time of the colloidal silica grout should be further developed to incorporate the influence of temperature and the influence of clay content and clay mineralogy to widen the in situ conditions in which it can be applied.

In order to further enhance confidence in the deployment of colloidal silica in situ where complex environmental conditions exist, and to ensure the integrity of a hydraulic barrier (i.e. to avoid gaps in formation of a grout curtain), an ability to monitor grout penetration in situ is desirable. Preliminary research is on-going at Strathclyde into potential monitoring techniques, including the use of Electrical-resistivity tomography, which can detect the high saline content (i.e. accelerator) of the grout mixture relative to the existing groundwater.

To further investigate the application of colloidal silica grouts as a hydraulic barrier to prevent contamination transports at nuclear legacy sites the effect of colloidal silica grout on the mobility of radionuclides is required, this is critical to ensure that any grout injected does not act to enhance mobility of radionuclides currently sorbed onto clays in situ. To this end, Gustafson (2000) investigated the leaching behaviour of Strontium (Sr) and Caesium (Cs) contaminated soils grouted with colloidal silica. They demonstrated that grouting with colloidal silica acts to enhance the retention behaviour (with respect to

radionuclides) compared to ungrouted soils. Future experiments should investigate a wider range of radionuclides that may be expected at legacy nuclear waste sites including for example Uranium and Plutonium isotopes.

This thesis demonstrated the mechanical and hydraulic improvements achieved by grouting soils with colloidal silica via small-scale laboratory tests. To further understand the practical implementation of colloidal silica grouting trials at both large laboratory and field scales need to be conducted. Large scale testing of colloidal silica grouting should incorporate standard ground investigation testing methods such as pressuremeter testing, dynamic probing, plate load testing or hand shear vane alongside subsequent sample collection and laboratory analysis to further investigate mechanical and hydraulic performance.

Increasing global emphasis towards the climate environment agenda, highlights further work into evaluating and quantifying the environmental impact of utilising colloidal silica grouts is required. An embodied carbon assessment of colloidal silica grout should be carried out which compares the impacts of the formation of a colloidal silica hydraulic barrier with other traditional methods of forming hydraulic barriers, e.g. the use of bentonite slurry trench cut-off wall.

References

ADLER, J. J., RABINOVICH, Y. I. & MOUDGIL, B. M. 2001. Origins of the non-DLVO force between glass surfaces in aqueous solution. *Journal of Colloid and Interface Science,* 237**,** 249-258.

AGUS, S. S. & SCHANZ, T. 2005. Comparison of four methods for measuring total suction. *Vadose Zone Journal,* 4**,** 1087-1095.

AHMED, S., LOVELL JR, C. W. & DIAMOND, S. 1974. PORE SIZES AND STRENGTH OF COMPACTED CLAY. *ASCE J Geotech Eng Div,* 100**,** 407-425.

AITCHISON, G. D. 1965. Engineering concepts of moisture equilibria and moisture changes in soils. *Moisture Equilibria and Moisture Changes in Soils Beneath Covered Areas: A Symposium in Print***,** 7-21.

ALLEN, L. H. & MATIJEVIĆ, E. 1969. Stability of colloidal silica: I. Effect of simple electrolytes. *Journal of Colloid and Interface Science,* 31**,** 287-296.

ALLISON, J. D., PURKAPLE, J. D. & SUMMERS, L. E. LABORATORY EVALUATION OF CROSSLINKED POLYMER GELS FOR WATER DIVERSION. Polymeric Materials Science and Engineering, Proceedings of the ACS Division of Polymeric Material, 1986. 784-790.

ANGEL, S., BRADSHAW, K., CLEAR, C., JOHNSON, D., KENNY, M., PRICE, B. & SOUTHALL, M. 2005. *The Essential Guide to the Remediation of Brownfield Land*, MPA The Concrete Centre.

APPS, J. A., PERSOFF, P., MORIDIS, G. & PRUESS, K. 1998. Method for formation of subsurface barriers using viscous colloids. Google Patents.

ASSOCIATION FRANÇAISE DES TRAVAUX EN, S. 1991. Recommendations on grouting for underground works. *Tunnelling and Underground Space Technology incorporating Trenchless,* 6**,** 383-461.

ASTM 2010. Standard Test Method for Measurement of Soil Potential (Suction) Using Filter Paper. ASTM International.

ASTM 2014. D4016 - Standard Test Method for Viscosity of Chemical Grouts by Brookfield Viscometer (Laboratory Method).

ATANGANA NJOCK, P. G., SHEN, J. S., MODONI, G. & ARULRAJAH, A. 2018. Recent Advances in Horizontal Jet Grouting (HJG): An Overview. *Arabian Journal for Science and Engineering,* 43**,** 1543-1560.

AXELSSON, M. 2006. Mechanical tests on a new non-cementitious grout , silica sol: A laboratory study of the material characteristics. *Tunnelling and Underground Space Technology,* 21**,** 554-560.

BALDYGA, J., JASIŃSKA, M., JODKO, K. & PETELSKI, P. 2012. Precipitation of amorphous colloidal silica from aqueous solutions—Aggregation problem. *Chemical Engineering Science,* 77**,** 207-216.

BALLESTEROS, A., SANDA, R., PEINADOR, M., ZERGER, B., NEGRI, P. & WENKE, R. 2014. Analysis of events related to cracks and leaks in the reactor coolant pressure boundary. *Nuclear Engineering and Design,* 275**,** 163-167.

BASF 2014. MasterRoc MP 320. Zurich, Switzerland.

BEAVERS, J. A., SRIDHAR, N. & BOOMER, K. D. 2014. Corrosion Management of the Hanford High-Level Nuclear Waste Tanks. *Jom,* 66**,** 491-502.

BERGNA, H. E. & ROBERTS, W. O. 2005. *Colloidal Silica Fundamentals and Applications*.

BIRD, P. G. 1941. *Colloidal solutions of inorganic oxides*. US patent application.

BOWLES, J. E. 1968. *Foundation analysis and design,* New York, New York : McGraw-Hill.
BRUCE, D. A., LITTLEJOHN, G. S. & NAUDTS, A. M. C. 1997. Grouting materials for ground treatment: A practitioner's guide. *Geotechnical Special Publication*, 306-334.
BSI 1990. BS1377-7:1990. *Methods of Test for Soils for Civil Engineering Purposes: Shear strength tests (total stress).* London: BSI: British Standards Institution.
BSI 2000. BS EN 12715:2000 *Execution of special geotechnical work - Grouting.* London: BSI.
BSI 2017. *BS EN ISO 17892-5:2017 - Geotechnical investigation and testing. Laboratory testing of soil. Incremental loading oedometer test*.
BULUT, R. & LEONG, E. C. 2009. Indirect measurement of suction. *Laboratory and Field Testing of Unsaturated Soils.*
BURGER, C. A. & SHACKELFORD, C. D. 2001. Soil-water characteristic curves and dual porosity of sand-diatomaceous earth mixtures. *Journal of Geotechnical and Geoenvironmental Engineering,* 127, 790-800.
BUTRÓN, C., AXELSSON, M. & GUSTAFSON, G. 2007. Silica Sol for Rock Grouting – Tests on Mechanical Properties. Göteborg: Chalmers University of Technology.
BUTRÓN, C., AXELSSON, M. & GUSTAFSON, G. 2009. Silica sol for rock grouting: Laboratory testing of strength, fracture behaviour and hydraulic conductivity. *Tunnelling and Underground Space Technology,* 24, 603-607.
CAMBEFORT, H. 1977. The principles and applications of grouting. *Quarterly Journal of Engineering Geology,* 10, 57-95.
CARUSO, M. & TARANTINO, A. 2004. A shearbox for testing unsaturated soils at medium to high degrees of saturation. *Geotechnique,* 54, 281-284.
CERATO, A. B., MILLER, G. A. & HAJJAT, J. A. 2009. Influence of clod-size and structure on wetting-induced volume change of compacted soil. *Journal of Geotechnical and Geoenvironmental Engineering,* 135, 1620-1628.
CHANG, S. Y., LIU, L. & ASHER, S. A. 1994. PREPARATION AND PROPERTIES OF TAILORED MORPHOLOGY, MONODISPERSE COLLOIDAL SILICA CADMIUM-SULFIDE NANOCOMPOSITES. *Journal of the American Chemical Society,* 116, 6739-6744.
CHANGIZI, F. & HADDAD, A. 2017. Improving the geotechnical properties of soft clay with nano-silica particles. *Proceedings of the Institution of Civil Engineers - Ground Improvement,* 170, 62-71.
COLLINS, K. & MCGOWN, A. 1974. FORM AND FUNCTION OF MICROFABRIC FEATURES IN A VARIETY OF NATURAL SOILS. *Geotechnique,* 24, 223-254.
CONLEE, C. T. 2010. *Dynamic Propertiies of Colloidal Silica Soils using Centrifuge Model Tests and Full-Scale Field Test.* PhD, Drexel University.
CONLEE, C. T., GALLAGHER, P. M., BOULANGER, R. W. & KAMAI, R. 2012. Centrifuge modeling for liquefaction mitigation using colloidal silica stabilizer. *Journal of Geotechnical and Geoenvironmental Engineering,* 138, 1334-1345.
CRAIG, R. F. 2004. *Craig's Soil Mechanics, Seventh Edition*, Taylor & Francis.
CRONEY, D. & COLEMAN, J. D. Soil thermodynamics applied to the movement of moisture in road foundations. Seventh International Congress for Applied Mechanics, 1948 London. 163-177.
DAS, B. M. 2009. *Principles of Geotechnical Engineering*, Cengage Learning.
DAS, B. M. 2010. *Principles of geotechnical engineering,* Stamford, Conn., Stamford, Conn. : Cengage Learning.

DECAGON DEVICES INC 2010. WP4C Dewpoint PotentiaMeter Operator's Manual, Version 2. *Decagon Devices, Inc.* Pullman, WA.
DEFRA 2010. SP1001 Contaminated Land Remediation. *CL:AIRE*.
DEFRA 2012. Environmental Protection Act 1990: Part 2A Contaminated Land Statutory Guidance. *In:* AFFAIRS, D. F. E. F. R. (ed.). HM Government.
DELAGE, P., TESSIER, D. & MARCEL-AUDIGUIER, M. 1982. Use of the Cryoscan apparatus for observation of freeze-fractured planes of a sensitive Quebec clay in scanning electron microscopy. *Canadian Geotechnical Journal,* 19**,** 111-114.
DERJAGUIN, B. V. & LANADAU, L. 1941. Acta Physiochim. *USSR,* 14**,** 633.
DURMUSOGLU, E. & YAVUZ CORAPCIOGLU, M. 2000. Experimental Study of Horizontal Barrier Formation by Colloidal Silica. *Journal of Environmental Engineering,* 126**,** 833-841.
ENVIRONMENT AGENCY 2005. Indicators for land contamination. *Environment Agency Report SC030039/SR.* Almondsbury,.
FERRARI, A., FAVERO, V. & LALOUI, L. Experimental analysis of the retention behavior of shales. 47th US Rock Mechanics / Geomechanics Symposium 2013, 2013. 653-657.
FINSTERLE, S., MORIDIS, G. J., PRUESS, K. & PERSOFF, P. 1994. Physical barriers formed from gelling liquids: 1. numerical design of laboratory and field experiments. *Other Information: PBD: Jan 1994.*
FREDLUND, D. G. 2014. The emergence of unsaturated soil mechanics. *Canadian Geotechnical Journal,* 51**,** IX-X.
FREDLUND, D. G. & RAHARDJO, H. 1993. *Soil mechanics for unsaturated soils*, Wiley-Interscience.
FREDLUND, D. G., RAHARDJO, H. & FREDLUND, M. D. 2012. *Unsaturated Soil Mechanics in Engineering Practice*, John Wiley and Sons.
FUNEHAG, J. & AXELSSON, M. 2003. Hydrogeological characterisation and sealing of narrow fractures in hard rock-A case study. *Materials and Geoenvironment*.
FUNEHAG, J. & FRANSSON, Å. 2006. Sealing narrow fractures with a Newtonian fluid: Model prediction for grouting verified by field study. *Tunnelling and Underground Space Technology,* 21**,** 492-498.
FUNEHAG, J. & GUSTAFSON, G. 2008. Design of grouting with silica sol in hard rock – New methods for calculation of penetration length, Part I. *Tunnelling and Underground Space Technology,* 23**,** 1-8.
GALLAGHER, P. M. 2000. *Passive Site Remediation for Mitigation of Liquefaction Risk.* PhD, Virginia Polytechnic Institute and State University.
GALLAGHER, P. M., CONLEE, C. T. & ROLLINS, K. M. 2007a. Full-Scale Field Testing of Colloidal Silica Grouting for Mitigation of Liquefaction Risk. *Journal of Geotechnical and Geoenvironmental Engineering,* 133**,** 186-196.
GALLAGHER, P. M. & MITCHELL, J. K. 2002. Influence of colloidal silica grout on liquefaction potential and cyclic undrained behavior of loose sand. *Soil Dynamics and Earthquake Engineering,* 22**,** 1017-1026.
GALLAGHER, P. M., PAMUK, A. & ABDOUN, T. 2007b. Stabilization of liquefiable soils using colloidal silica grout. *Journal of Materials in Civil Engineering,* 19**,** 33-40.
GALLAGHER, P. M., SPATARI, S. & CUCURA, J. 2013. Hybrid life cycle assessment comparison of colloidal silica and cement grouted soil barrier remediation technologies. *Journal of Hazardous Materials,* 250**,** 421-430.
GALVANI, A. 2003. *Resistenza a taglio di un argilla non satura ricostituita in laboratorio.* MEng, University of Trento.

GEE, G. W., CAMPBELL, M. D., CAMPBELL, G. S. & CAMPBELL, J. H. 1992. Rapid measurement of low soil-water potentials using a water activity meter. *Soil Science Society of America Journal,* 56**,** 1068-1070.
GENS, A. 2010. Soil-environment interactions in geotechnical engineering. *Geotechnique,* 60**,** 3-74.
GLAMHEDEN, R. F., B; JACOBSSON, L; HARRSTROM, J; BERGLUND, J; BERGKVIST, L 2010. Counterforce applied to prevent spalling.
GRACE 2007. LUDOX Colloidal Silica in Coatings Lithium Polysilicate in Coatings Technical Information. United States.
GRANATA, R., VANNI, D. & MAURO, M. 2015. New experience in ground treatment by permeation grouting. *Proceedings of the Institution of Civil Engineers - Ground Improvement,* 168**,** 122-129.
GUSTAFSON, J. M., P; JOKINEN, M; ROSENHOLM, J 2000. The influence of pH and NaCl on the zeta potential and rheology of anatase dispersions. *Colloids and Surfaces*.
HAMDERI, M. & GALLAGHER, P. M. 2015. Pilot-scale modeling of colloidal silica delivery to liquefiable sands. *Soils and Foundations,* 55**,** 143-153.
HEAD, K. H. 1992. *Manual of soil laboratory testing,* London, London : Pentech Press ;.
HELAL, M. & KRIZEK, R. J. Preferred orientation of pore structure in cement-grouted sand. Geotechnical Special Publication, 1992. 526-540.
HEMPHILL, G. 2012. *Practical Tunnel Construction*, Wiley.
HERNQVIST, L., KVARTSBERG, S., FRANSSON, Å. & GUSTAFSON, G. A swedish grouting design concept: Decision method for hard rock tunneling. Geotechnical Special Publication, 2012. 816-825.
HOLLMEN, K., SIEVANEN, U., FUNEHAG, J., GRANBERG, N., LYYTINEN, T. & SYRJANEN, P. 2013. Working Report Colloidal Silica Grouting in Demonstration Tunnel 2 in ONKALO.
HOLLMEN, K. S., U; FUNEHAG, J; GRANBERG, N; LYYTINEN, T; SYRJANEN, P 2013. Working Report Colloidal Silica Grouting in Demonstration Tunnel 2 in ONKALO.
HOLTZ, R. D. & KOVACS, W. D. 1981. *An introduction to geotechnical engineering*.
HUNT, J. D., EZZEDINE, S. M., BOURCIER, W. & ROBERTS, S. 2013. *Kinetics of the Gelation of Colloidal Silica at Geothermal Conditions, and Implications for Reservoir Modification and Management*, ; Lawrence Livermore National Laboratory (LLNL), Livermore, CA.
HUSSIN, J. D. 2013. Methods of Soft Ground Improvement. *The Foundation Engineering Handbook, Second Edition.* CRC Press.
ILER, R. K. 1979. *The Chemistry of Silica: Solublity, Polymerization, Colloid and Surface Properties, and Biochemistry*, John Wiley & Sons.
JUNG, K., PARK, S., GEONG, G., LEE, K., CHUNG, U. & PAIK, S. Radioactive waste management plan during the triga mark II and III decommissioning.
JURINAK, J. J. & SUMMERS, L. E. 1991. Oilfield applications of colloidal silica gel. *SPE Production Engineering,* 6**,** 406-412.
KAROL, R. 2003. *Chemical Grouting and Soil Stabilization*.
KIRBY, B. H., E 2004. Zeta potential of microfilmed substrates: 1. Theory, experimental techniques, and effects on separations. *Electrophoresis,* 25**,** 187-202.
KOBAYASHI, M., JUILLERAT, F., GALLETTO, P., BOWEN, P. & BORKOVEC, M. 2005. Aggregation and charging of colloidal silica particles: Effect of particle size. *Langmuir,* 21**,** 5761-5769.

KOBAYASHI, S., SOYA, M., TAKEUCHI, N., NOBUTO, J., NAKAYA, A., OKUNO, T., SHIMADA, S., KANETO, T. & MAEJIMA, T. 2014. Rock grouting and durability experiments of colloidal silica at Kurashiki underground LPG storage base. *Rock Engineering and Rock Mechanics: Structures in and on Rock Masses.* CRC Press.

LALOUI, L., NUTH, M., FRANÇOIS, B. & LALOUI, L. 2013. Mechanics of Unsaturated Soils. *Mechanics of Unsaturated Geomaterials.* John Wiley & Sons, Inc.

LANDMAN, J., PAINEAU, E., DAVIDSON, P., BIHANNIC, I., MICHOT, L. J., PHILIPPE, A.-M., PETUKHOV, A. V. & LEKKERKERKER, H. N. W. 2014. Effects of Added Silica Nanoparticles on the Nematic Liquid Crystal Phase Formation in Beidellite Suspensions. *The Journal of Physical Chemistry B,* 118**,** 4913-4919.

LEONG, E. C. & RAHARDJO, H. 1997. Review of soil-water characteristic curve equations. *Journal of Geotechnical and Geoenvironmental Engineering,* 123**,** 1106-1117.

LEONG, E. C., TRIPATHY, S. & RAHARDJO, H. 2003. Total suction measurement of unsaturated soils with a device using the chilled-mirror dew-point technique. *Geotechnique,* 53**,** 173-182.

LI, M., FU, Q.-L., ZHANG, Q., ACHAL, V. & KAWASAKI, S. 2015. Bio-grout based on microbially induced sand solidification by means of asparaginase activity. *Scientific reports,* 5**,** 16128-16128.

LI, S., LIU, R., ZHANG, Q. & ZHANG, X. 2016. Protection against water or mud inrush in tunnels by grouting: A review. *Journal of Rock Mechanics and Geotechnical Engineering,* 8**,** 753-766.

LIAO, H. J., HUANG, C. C. & CHAO, B. S. Liquefaction resistance of a colloid silica grouted sand. Geotechnical Special Publication, 2003. 1305-1313.

LIM, H. M., LEE, J., JEONG, J.-H., OH, S.-G. & LEE, S.-H. 2010. Comparative Study of Various Preparation Methods of Colloidal Silica. *Engineering,* 02**,** 998-1005.

LOMBARDI, G. The role of cohesion in cement grouting of rock. Proceedings, Quinzième Congrès des Grands Barrages, 1985 Lausanne, Switzerland. 235–261.

LU, N. & KHORSHIDI, M. 2015. Mechanisms for Soil-Water Retention and Hysteresis at High Suction Range. *Journal of Geotechnical and Geoenvironmental Engineering,* 141.

LU, N. & LIKOS, W. J. 2004. *Unsaturated soil mechanics,* New York, Wiley.

MAHER, M. H., RO, K. S. & WELSH, J. P. 1994. High strain dynamic modulus and damping of chemically grouted sand. *Soil Dynamics and Earthquake Engineering,* 13**,** 131-138.

MCKIE, R. 2009. *Sellafield: the most hazardous place in Europe* [Online]. https://www.theguardian.com/environment/2009/apr/19/sellafield-nuclear-plant-cumbria-hazards: The Guardian. [Accessed 24 August 2020].

MILLER, E. A. & ROYCROFT, G. A. 2004. Seismic Performance and Deformation of Levees: Four Case Studies. *Journal of Geotechnical and Geoenvironmental Engineering,* 130**,** 344-354.

MITCHELL, J. K. 1976. *Fundamentals of soil behavior*, Wiley.

MITCHELL, J. K. & SOGA, K. 2005. *Fundamentals of soil behavior,* Hoboken, N.J, John Wiley & Sons.

MOLLAMAHMUTOGLU, M. & YILMAZ, Y. 2010. Pre- and post-cyclic loading strength of silica-grouted sand. *Proceedings of the Institution of Civil Engineers - Geotechnical Engineering,* 163**,** 343-348.

MONGILARDI, E. & TORNAGHI, R. Construction of larger underground openings and use of grouts. 1986 Beijing.
MORGENSTERN, N. R. & TCHALENKO, J. S. 1967. Microscopic Structures in Kaolin Subjected to Direct Shear. *Géotechnique,* 17**,** 309-328.
MORIDIS, G., APPS, J., PERSOFF, P., MYER, L., MULLER, S., PRUESS, K. & YEN, P. A field test of a waste containment technology using a new generation of injectable barrier liquids. Spectrum, 1996 Seattle. Medium: ED; Size: 16 p.
MORIDIS, G., PERSOFF, P., APPS, J., MYER, L., PRUESS, K. & YEN, P. 1995a. A field test of permeation grouting in heterogeneous soils using a new generation of barrier liquids. *Committed To Results: Barriers for Long-Term Isolation. ER,* 95.
MORIDIS, G., PRUESS, K., PERSOFF, P. & APPS, J. Performance and properties of colloidal silica and polysiloxane grouts. Proc., Int. Containment Technology Workshop, 1995b.
MORIDIS, G. J., FINSTERLE, S. & HEISER, J. 1999. Evaluation of alternative designs for an injectable subsurface barrier at the Brookhaven National Laboratory site, Long Island, New York. *Water Resources Research,* 35**,** 2937-2953.
MULLIGAN, C. N., YONG, R. N. & GIBBS, B. F. 2001. Remediation technologies for metal-contaminated soils and groundwater: an evaluation. *Engineering Geology,* 60**,** 193-207.
NAO 2018. The Nuclear Decommissioning Authority: progress with reducing risk at Sellafield. The Nuclear Decommissioning Authority.
NATHANAIL, J., BARDOS, P. & NATHANAIL, P. 2007. Contaminated Land Management: Ready Reference.
NDA 2016. Draft Business Plan Financial year beginning April 2017 to financial year ending March 2020.
NOLL, M. R., BARTLETT, C. L. & DOCHAT, T. M. In situ permeability reduction and chemical fixation using colloidal silica. Proceedings of the Sixth National Outdoor Action Conference, 1992. 443-57.
NONVEILLER, E. 1989. *Grouting, theory and practice,* Amsterdam, Elsevier.
NORAMBUENA-CONTRERAS, J. 2015. Water retention curve of soil-cement composite material. *Ingeniare,* 23**,** 647-654.
NORTHCROFT, I. W. 2006. Innovative materials and methods for ground support, consolidation and water sealing for the mining industry. *Journal of the South African Institute of Mining and Metallurgy,* 106**,** 835-843.
OLLILA, K. 1999. Dissolution of unirradiated UO2 fuel in synthetic groundwater – Final report (1996–1998). Posiva Rep.
ONR 2016. LC34: LEAKAGE AND ESCAPE OF RADIOACTIVE MATERIAL AND RADIOACTIVE WASTE. *Nuclear Safety Technical Inspection Guide.* Office for Nuclear Regulation.
PEDROTTI, M. 2015. *An experimental investigation on the micromechanics of non-active clays in saturated and partially saturated states.* PhD thesis, University of Strathclyde.
PERON, H., LALOUI, L., HUECKEL, T. & HU, L. B. 2009. Desiccation cracking of soils. *European Journal of Environmental and Civil Engineering,* 13**,** 869-888.
PERSOFF, P., APPS, J., MORIDIS, G. & WHANG, J. M. 1999. Effect of dilution and contaminants on sand grouted with colloidal silica. *Journal of Geotechnical and Geoenvironmental Engineering,* 125**,** 461-469.
PERSOFF, P., FINSTERLE, S., MORIDIS, G. J., APPS, J., PRUESS, K. & MULLER, S. J. 1995. Injectable barriers for waste isolation. *Heat Transfer - Portland 1995,* 91**,** 58-67.

PERSOFF, P., MORIDIS, G. J., APPS, J., PRUESS, K. & MULLER, S. J. 1994. Designing Injectable Colloidal Silica Barriers for Waste Isolation at the Hanford Site. *In Situ Remediation: Scientific Basis for Current and Future Technologies, Pts 1 and 2*, 87-101.

PERSOFF, P., MORIDIS, G. J., APPS, J. A. & PRUESS, K. 1998. Evaluation tests for colloidal silica for use in grouting applications. *Geotechnical Testing Journal,* 21, 264-269.

PETRY, T. M. & JIANG, C. P. 2007. Soil suction and behavior of chemically treated clays. *Transportation Research Record*, 30-38.

POWRIE, W. 2014. *Soil mechanics : concepts and applications,* Boca Raton, [Florida], Boca Raton, Florida : CRC Press/Taylor & Francis.

RAWLINGS, C. G. 2000. *Grouting for ground engineering,* London, London : CIRIA.

REZAEE, L., SHABANPOUR, M. & DAVATGAR, N. 2011. Estimating the soil water retention curve from soil particle size distribution using the Arya and Paris model for Iranian soils. *Turkish Journal of Agriculture and Forestry,* 35, 649-657.

RICHARDS, B. G. 1965. Measurement of the free energy of soil moisture by the psychrometric technique using thermistors. *Moisture Equilibria and Moisture Changes in Soils Beneath Covered Areas*, 39-46.

RISÖ, K. 2011. *Gelation of colloidal silica sols.* Msc, Chalmers university of technology.

RIVETT, M. O., PETTS, J., BUTLER, B. & MARTIN, I. 2002. Remediation of contaminated land and groundwater: experience in England and Wales. *Journal of Environmental Management,* 65, 251-268.

SAVARMAND, S., CARREAU, P. J., BERTRAND, F., VIDAL, D. J. E. & MOAN, M. 2003. Rheological properties of concentrated aqueous silica suspensions: Effects of pH and ions content. *Journal of Rheology,* 47, 1133-1149.

SCANLON, B. R., ANDRASKI, B. J. & BILSKIE, J. 2002. *Water potential: miscellaneous methods for measuring matric or water potential,* Madison, WI, Soil Science Society of America.

SCHOLFIELD, R. K. The pF of the water in the soil. Third international congress of soil science, 1935. 38-48.

SEPA 2017. Land remediation and waste management guidelines.

SIBELCO 2015. Product Specification: CH DSG. SIBELCO, UK.

SKEMPTON, A. W. & JONES, O. T. 1944. Notes on the compressibility of clays. *Quarterly Journal of the Geological Society,* 100, 119-135.

SMETTEM, K. R. J. & KIRKBY, C. 1990. Measuring the hydraulic properties of a stable aggregated soil. *Journal of Hydrology,* 117, 1-13.

SOBTI, J. & SINGH, S. K. 2017. Hydraulic conductivity and compressibility characteristics of bentonite enriched soils as a barrier material for landfills. *Innovative Infrastructure Solutions,* 2, 12.

SPENCER, L., RIX, G. J. & GALLAGHER, P. M. Dynamic Properties of Collodial Silica Gel and Sand Mixtures. 4th International Conference on Earthquake Geotechnical Engineering, 2007.

SRIDHARAN, A. & NAGARAJ, H. B. 2000. Compressibility behaviour of remoulded, fine-grained soils and correlation with index properties. *Canadian Geotechnical Journal,* 37, 712-722.

SRIDHARAN, A. & RAO, G. V. 1973. Mechanisms controlling volume change of saturated clays and the role of the effective stress concept. *Géotechnique,* 23, 359-382.

SYDANSK, R. D. 1990. A Newly Developed Chromium(III) Gel Technology. *SPE*, 346-352.

TARANTINO, A. 2009. A water retention model for deformable soils. *Geotechnique,* 59**,** 751-762.
TARANTINO, A. 2010. Basic concepts in the mechanics and hydraulics of unsaturated geomaterials. *Mechanics of unsaturated geomaterials.*
TARANTINO, A. & TOMBOLATO, S. 2005. Coupling of hydraulic and mechanical behaviour in unsaturated compacted clay. *Géotechnique,* 55**,** 307-317.
TOMIOLO, A. 1982. Principles of Grouting. Short Course on Soil & Rock Improvement, Techniques Including Geotextiles. Reinforced Earth and Modern Piling Method: Asian Institute of Technology, Thailand.
TROMPETTE, J. L. & CLIFTON, M. J. 2004. Influence of ionic specificity on the microstructure and the strength of gelled colloidal silica suspensions. *Journal of Colloid and Interface Science,* 276**,** 475-482.
TRUEX, M. J., PIERCE, E. M., NIMMONS, M. J. & MATTIGOD, S. 2011. Evaluation of In Situ Grouting as a Potential Remediation Method for the Hanford Central Plateau Deep Vadose Zone. *Pacific Northwest National Laboratory*.
TSUJI, M., FUNEHAG, J., KOBAYASHI, S., SATO, T. & MIKAKE, S. Comparison of grouting with silica sol in the Äspö Hard Rock Laboratory in Sweden and Mizunami underground research laboratory in Japan. ISRM International Symposium - 8th Asian Rock Mechanics Symposium, ARMS 2014, 2014. 1237-1246.
U.S. ARMY CORP OF ENGINEERS 1995. Engineering and design chemical grouting. *EM 1110-1-3500 Manual 1110-1-3500.* Washington, D. C.
UYGAR, E. & DOVEN, A. G. 2006. Monotonic and cyclic oedometer tests on sand at high stress levels. *Granular Matter,* 8**,** 19-26.
VAN GENUCHTEN, M. T. 1980. CLOSED-FORM EQUATION FOR PREDICTING THE HYDRAULIC CONDUCTIVITY OF UNSATURATED SOILS. *Soil Science Society of America Journal,* 44**,** 892-898.
VANAPALLI, S. K. 1994. *Simple Test Procedures and Their Interpretation in Evaluating the Shear Strength of an Unsaturated Soil.* PhD thesis, University of Saskatchewan.
VANAPALLI, S. K., FREDLUND, D. G. & PUFAHL, D. E. 1999. The influence of soil structure and stress history on the soil-water characteristics of a compacted till. *Geotechnique,* 49**,** 143-159.
VANAPALLI, S. K., FREDLUND, D. G., PUFAHL, D. E. & CLIFTON, A. W. 1996. Model for the prediction of shear strength with respect to soil suction. *Canadian Geotechnical Journal,* 33**,** 379-392.
VERFEL, J. 1989. *Rock grouting and diaphragm wall construction / by Jaroslav Verfel,* Amsterdam ; New York : New York, Elsevier ; Distribution for the USA and Canada, Elsvier Science Pub. Co.
VERWEY, E. J. & OVERBEEK, J. T. G. 1948. *Theory of the Stability of Lyophobic Colloids,* Amsterdam.
WANG, Z. F., SHEN, S. L., HO, C. E. & KIM, Y. H. 2013. Investigation of field-installation effects of horizontal twin-jet grouting in Shanghai soft soil deposits. *Canadian Geotechnical Journal,* 50**,** 288-297.
WARNER, J. 2004. *Practical Handbook of Grouting: Soil, Rock, and Structures*.
WHANG, J. M. Chemical-based barrier materials. Assessment of barrier containment technologies: A comprehensive treatment for environmental remediation applications. International Containment Technology Workshop, 1995 Baltimore, MD, USA.

WILLIAMS, P. J. 1982. The surface of the earth: an introduction to geotechnical science. *The surface of the earth: an introduction to geotechnical science.*

WITHERSPOON, P. A., WANG, J. S. Y., IWAI, K. & GALE, J. E. 1980. Validity of Cubic Law for fluid flow in a deformable rock fracture. *Water Resources Research,* 16**,** 1016-1024.

WOODWARD, J. 2005. *An introduction to geotechnical processes,* London ; New York, London ; New York : Spon Press.

YONEKURA, R. & KAGA, M. Current chemical grout engineering in Japan. Geotechnical Special Publication, 1992. 725-736.

YOSSAPOL, N. 2002. *Remediation of Chromium Contaminated Soils with Colloidal Silica.* PhD, New Jersey Institute of Technology.

YOSSAPOL, N. & MEEGODA, J. N. Physical Mechanisms of Colloidal Silica Grouting in Remediation of Chromium Contaminated Soil. HAZARDOUS AND INDUSTRIAL WASTES, 2001.

YOTSUMOTO, H. & YOON, R. H. 1993. Application of Extended DLVO Theory. II. Stability of Silica Suspensions. *Journal of Colloid And Interface Science,* 157**,** 434-441.

ZALUSKI, M. H., MANCHESTER, K., NORTH-ABBOTT, M. A. & WRAITH, J. Performance of the Colloidal Silica Barrier Installed at Brookhaven National Laboratory, a Computer Modeling Study. 2001.

ZEBOVITZ, S., KRIZEK, R. J. & ATMATZIDIS, D. K. 1989. Injection of fine sands with very fine cement grout. *Journal of Geotechnical Engineering,* 115**,** 1717-1733.

List of Tables

List of Figures